Fall 2021

Application of Digital Transformation in the Water Desalination Industry to Develop Smart Desalination Plants

Ibrahim Yousif

APPLICATION OF DIGITAL TRANSFORMATION IN THE WATER DESALINATION INDUSTRY TO DEVELOP SMART DESALINATION PLANTS

by

Ibrahim Yousif

Bachelor of Engineering
The British University in Egypt / London South Bank University, 2018

Submitted in Partial Fulfillment of the Requirements

For the Degree of Master of Science in

Mechanical Engineering

College of Engineering and Computing

University of South Carolina

2021

Accepted by:

Abdel-Moez E. Bayoumi, Director of Thesis

Lang Yuan, Reader

Rhea Matthews, Reader

Tracey L. Weldon, Interim Vice Provost and Dean of the Graduate School

ACKNOWLEDGEMENTS

I would like to express my gratitude by thanking my advisor Prof. Abdel Bayoumi. He has provided me the opportunity to be a part of his research team at the McNair Center, guidance not only professionally but personally, and unconditional support and monitoring throughout six years of my master's and my undergraduate studies. Also, I would like to thank his family members for always making me feel home.

I would also like to thank my committee member Mrs. Rhea Matthews who has provided me with such a phenomenal support, knowledge, and guidance since day one I started my graduate degree. I would like to extend my thanks to my undergraduate school, The British university in Egypt for helping me being ready for this opportunity and my undergraduate advisors Prof. Attia Attia, Dr. Atef Abdelhadi, Dr. Ziad Khalifa and Dr. Mohamed Balaha. Also, I would like to thank the center of predictive maintenance team in the BUE for their time, and support.

Grateful acknowledgment, to my fellow researchers who have provided be with advice, assistance, and feedback. This work would not be possible without the great team that I have had the chance to be a part of and contribute to. Special thanks to Clint Saidy, Kaishu Xia, Mohammed Hassan, Andre Calderon, Mustafa Hassan, Chase Murray, Rhiannon Bullard, and Evan Barnett.

Last but not least, my deepest appreciation for my family and friends for their unconditional love and support specially Ahmed Saied, Seif Hisham, Liudas Panavas, Anil

Kircaliali, Roudy Wehbe, Alex Brasington, Darby Nugent, Maggie Kindsvater, Joshua Halbritter, and Omar Baraghet.

ABSTRACT

Fresh water shortage threatens the development and prosperity of many countries including several areas in the United States. Sea and ground water reverse osmosis desalination is rapidly becoming a dominant technology for overcoming water shortage threats by providing cost-effective freshwater production. Digital transformation can be used to help facilitate and advance water treatment technologies by reducing costs and minimizing downtime. Digital transformation is a process that encapsulates digital tools and technologies such as cloud computing, machine learning, artificial intelligence, the internet of things, and virtual/augmented reality. It is a process where objects in the physical world are given virtual replicas established via collected real-time data that is exchanged from sensors attached to the physical system to create a virtual digital twin. These virtual replicates represent the same behaviors that govern the physical object throughout its life development and operation.

Utilizing digital transformation technology in the water desalination industry is essential for multiple benefits such as optimization, control, fault detection, health monitoring, reducing capital and operation costs by reducing maintenance operations and downtime, and improving the design and manufacturing process.

This thesis develops a proof of concept for utilizing digital transformation in water desalination by building digital twins for two components within a water desalination system. A three-piston high-pressure pump energy recovery device (HPP - ERD) along with a three-stage reverse osmosis digital membrane model have been built and integrated

into a digital twin that can be used to evaluate the system's behaviors under normal and abnormal conditions, predict future failures, and improve the overall system design. The developed digital twin was validated with real-time data collected from a physical water desalination system. This digital transformation proof of concept, including all algorithms, models, and techniques developed in this thesis, can be expanded to the remaining components and subsystems of a water desalination plant for further optimization.

TABLE OF CONTENTS

LIST OF FIGURES

CHAPTER 1

INTRODUCTION

1.1 WATER SHORTAGE BACKGROUND AND HISTORY

Drinking water is considered a gift from the nature to many countries. As the world population grows and consequently the demand for freshwater for urban, agricultural, and industrial use increases, so do the challenges arising from the need to meet global market demand with innovative technologies. An effective water treatment known as Water Sanitation and Hygiene (WASH) was recommended by the World Health Organization (WHO) to filter [1], to achieve a safe, clean drinkable water. The United Nations Environment Program (UNEP) mentioned that one-third of the world's population lives in countries with not enough permeate water to sustain the world population demand [2]. Extracting fresh water from the sea is not new Nature played always that role by using the sun effect, sea water such as oceans and seas evaporates, which yields clouds to form causes precipitation of rain or snow as soon as the masses of humid air reach colder regions. The precipitation water is pure because the salt in the sea is not volatile; only the water evaporates.

Two-thirds of the world population will face water scarcity by 2025 [2] [3]. As over a billion of people will suffer from clean water shortage. Most of these people are living rural areas with low density human population which will make it harder to install water alternative systems [4]. In addition, water demand will rise, and several factors such as

manufacturing rises, climate changes, urbanization, and population development. In several regions and countries, their primary source of drinking water is water with variable salinity, such as seawater and brackish water. Water distillation was more common for producing clean water; however, nowadays, membranes proved their technology in the market and became a more efficient, more cost-effective candidate. The total water reservoirs amount is about 1.4 billion cubic kilometers, just 2.5% of the total amount is freshwater [5]. This freshwater portion is divided into the water, which presents in the groundwater, polar ice, and atmosphere. The drinkable water directly available out of this 2.5%, for human and another organism is only 0.014%. while the rest 97.5% of the total amount are oceans (Saline water) [6].

1.2 DRINKING WATER PROPERTIES

Table 1.1:Water Classification According to Salinity [7]

Designation	**Total dissolved salts (ppm)**	**Category**
Fresh water	<500	Using for drinking and irrigation.
Slightly brackish	500-1000	Irrigation.
brackish	1000-2000	Using for irrigation with caution.
Moderately saline	2000-5000	Primary drainage.
Saline	5000-10000	Secondary drainage and saline ground water
Highly saline	1000-35000	Very saline ground water source
Brine	>35000	Sea

1.3 WATER DESALINATION INTRODUCTION

Freshwater production is not considered the only problem. Process energy is also considered one of the big problems during the desalination process. As water desalination process requiring a critical amount of energy. A study estimated that to produce 1 million

m3/day of water demands 10 million tons of oil per year due to the conventional energy high cost and its harmful effect on the environment [7]. Therefore, renewable energy sources start gaining attraction in the market in particularly solar energy. Using of renewable energy is effective because it reduces the pollution of the environment, its free supplying sources and continuous, low maintenance energy cost and keep the conventional energy resources for other purposes.

The water desalination process for both brackish and seawater has become the first solution to solve this water crisis and is implemented as a leading water resource in many countries [8], as shown in figure 1.1. Among desalination processes, solar desalination has proved it is the most practical and clean energy source. Especially in the arid and semi-arid areas like the middle east, where there are many water resources with lack and high power/energy supply costs.

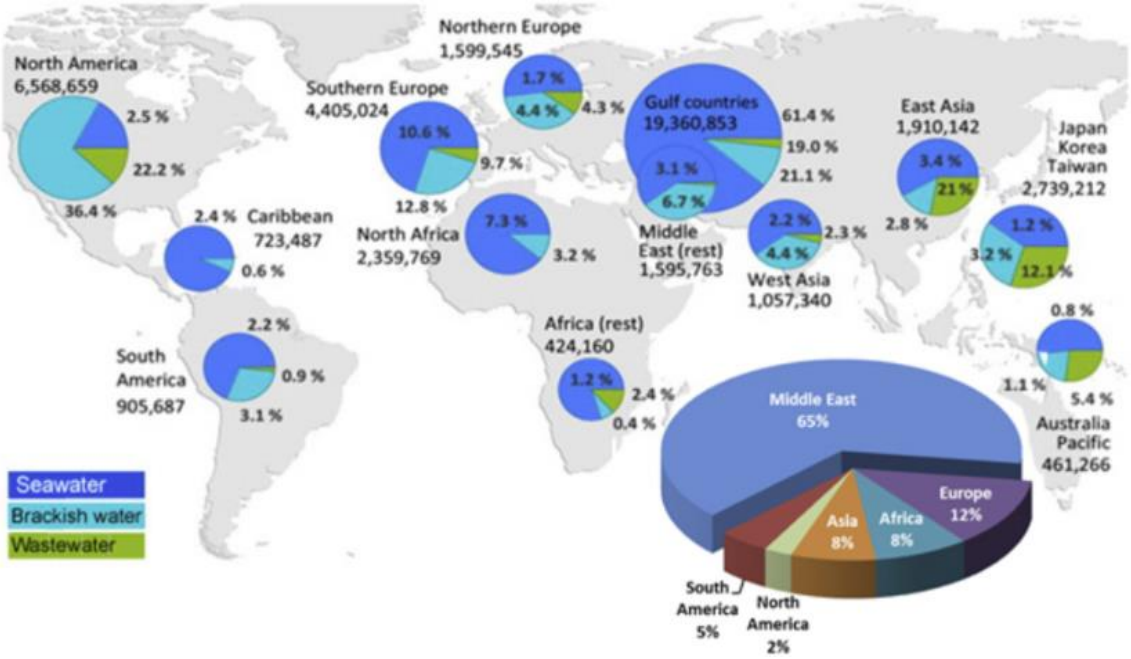

Figure 1.1: Water Desalination World Share [10]

1.4 POBLEM DEFINITION

Due to rapidly increasing world populations, the demand for freshwater is also growing. This 2.5% of freshwater is not distributed equally as 30% of these freshwater resources constitute groundwater [9]. However, in arid and semi-arid areas like most of the middle east countries, it is difficult and expensive to obtain underground water also to ship. Therefore, developing alternatives to produce permeate water from saltwater as permeate water is required for several industrial applications, domestic uses and in agricultural. Fresh water shortage is an essential factor in economic development. The percentage of 97.5% of the earth's water exists in the oceans [3] The desalination of the seawater considered to be the best alternative to meet globally demands of freshwater. Water desalination effect different industries with the rapid growth in the pharmaceutical industry [10] [11], desalinated water is used for drug testing and diluting certain solutions, and in the oil and gas industry, fresh and low salinity water supplies are essential for enhanced oil recovery (EOR) applications [12] [13] [14]. Offshore and onshore petroleum platforms in remote areas require gallons of freshwater every day, while shipping to these platforms is costly and inefficient. Furthermore, low salinity water injection is required to maintain reservoir pressure and stabilize the production rate. Consequently, on-site water desalination technology can benefit the oil and gas industry as it is efficient and less expensive. Years ago, the membrane was purposely used for water treatment such as desalination and micro-filtration processes. The reverse osmosis separation process got invented 30 years ago. Reverse osmosis has become a standard unit operation in chemical engineering, with development of the membrane technology that expanded to be used in a wider variety of industry and complicated industry applications instead of being confined only in the water

industry. Such as recovery of protein in the dairy industry, the concentration of food, urban communities water treatment and industrial wastes, sea and brackish water desalination, which yields for freshwater production in several applications, including the semiconductor industry, and also in chemical and petrochemical applications [15] [16] [17] [18] [19]. The membrane technology is basically separate the water and salt to two different zones according to their concentration. Membranes are made of a wide variety of materials, such as polymeric and non-polymeric materials. The most famous successful membranes used to desalinate seawater and brackish water are spiral wound and hollow fine fiber (HFF) [20] [21].

As the world population grows and consequently the demand for freshwater for urban, agricultural, and industrial use increases, so do the challenges arising from the need to meet global market demand with innovative technologies. Maintaining the water desalination system running under healthy condition [22] [23], which keeps the sea water reverse osmosis plant running. insures not only the implementation of sustainable development and prosperity, but sometimes it is very vital to maintain human lives. In the last 10 years identifying the fault in time was a challenge not just in the mechanical components but in several industrial components such as electrical and hydraulic components [24] [25]. Because they are subjected to different uncertain environmental conditions and damage caused by acoustic emissions, misbalance, misalignment, occasional shocks, poor power quality, supply imbalance, and vibrations, and the way it is handled. Health monitoring the water desalination plants become a must as many humans' lives are depending on these plants as their only source of water. Identifying the fault occurrence in time is not enough as it won't solve the problem of water supply especially

if these plants are in remote areas where maintenance operators for these plants may be not qualified enough to solve the problem on time [23]. Nowadays with the development of the predictive maintenance and digital transformation improves the diagnostic abilities in the health monitoring area because of the enhancement of the sensor's technologies, data driven techniques, big data analytics, data preprocessing, machine learning, signal processing algorithms, smart control, artificial intelligence, and the development of the computational power.

This research is joint research between two universities the University of South Carolina and the British University in Egypt as the Egyptian government is seeking to build new communities in selected desserts by reclaiming to them 1.5 million acres. The government aims for these communities a high sustainable life quality while promoting agriculture. These communities are expected to face freshwater shortage as the salinity of the underground water reaches 7,000 ppm in some of these desert areas and up to 32,000 ppm in seas.

This approach is conducted by a joint team from the Center of Excellence in Predictive Maintenance (CPM) at the British University of Egypt (BUE) and the Center for Predictive Maintenance (CPM) at the University of South Carolina (USC), USA. The Egyptian team leads the part of designing and manufacturing and full integration of the small RO water desalination system equipped with onboard monitoring, data extraction and control system. Having the physical system in Egypt supported both teams with a solid understanding of the system's physical behavior and properties, by monitoring the system under healthy and generated harsh conditions, collecting real-world data by employing adequate sensors and a data acquisition system that sensing and extracting the pump

parameters such as static and dynamic pressure, flow rate, salinity, and vibration data. The US team develops an Industry 4.0 framework, including a digital twin of the system that will allow for self-diagnosis and system decision making to ensure optimal performance. These features enable remote monitoring and control of the desalination plant. The digital twin (DT) health monitoring system (HMS) receives data from onboard sensor monitoring critical variables of the plant in Egypt, train and compare these extracted measurements to the plant's historical and theoretical models' output. This enables the system to optimize its performance to achieve prolonged life predictions and better efficiency. The current health of the system will be updated in real-time and will be shared with a remote decision-making authority. If there is an anomaly in the readings, corrective action will be initiated, and responsible personnel would be alerted to the new state of the system. The Internet of Things (IoT) enables this interconnected network of machines and people and will enable the existence of a reliable, remotely operated, automated, decentralized SWRO water treatment plant in the desert.

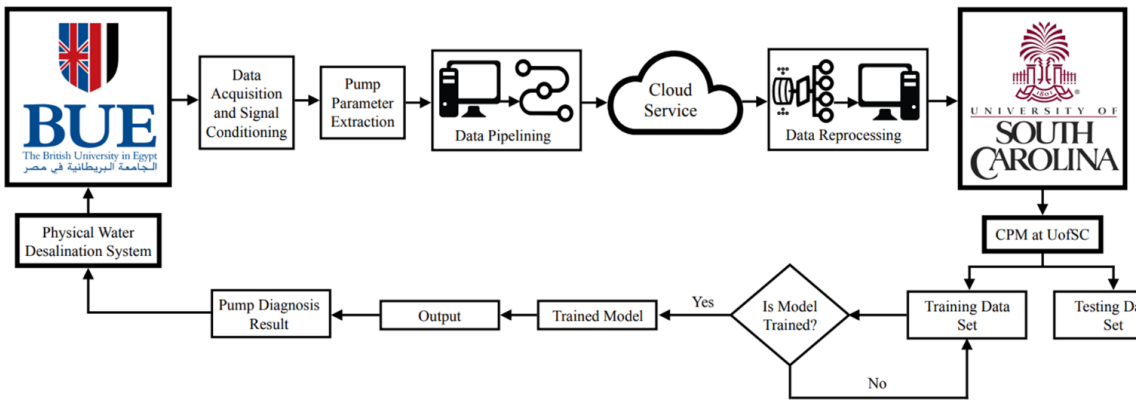

Figure 1.2: Implemented water desalination system status monitoring scheme for fault prediction

1.5 RESEARCH OBJECTIVES

This research project aims to build Digital Twin for a smart water desalination system which focused on building a reciprocating 3-piston high-pressure pump energy recovery device (HPP - ERD) digital model using Amesim software. Moreover, we construct a three-stage reverse osmosis digital membrane model using C language. The HPP – ERD and digital membrane model are integrated to achieve the water desalination system digital twin and then use to implement an effective condition monitoring algorithm. This is achieved by blending and correlating real-time streaming IoT data with simulation data. The second step is applying advanced signal processing, artificial intelligence, machine learning, and advanced techniques for modeling to create a virtual dynamic representation of the whole system and precise estimation of its current and future health conditions.

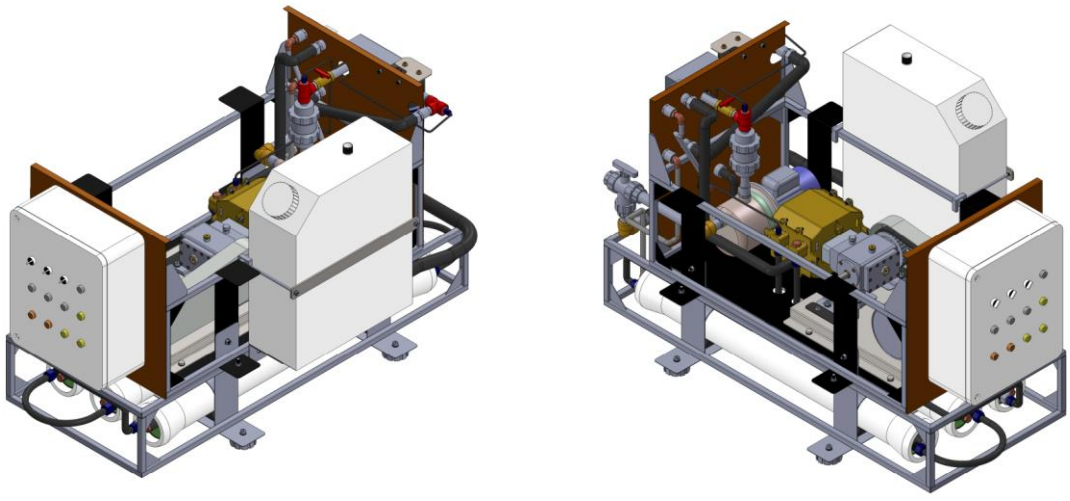

Figure 1.3: System Digital Twin Design

When the digital twin representation for the physical system is built, it can be simulated the physical system under different operating conditions. While studying the

system under normal operating conditions it is also allowed to start simulating it under harsh conditions. When the fault is diagnosed, the digital twins' algorithms will recommend the corrective action so it can be applied on the digital system before applying it on the physical system. Figure 18 shows the digital twin capabilities in fault correction and detection. Another usable digital twin application in predictive maintenance and fault detection is simulating the system's performance under harsh and destructive operating conditions (which cannot be physically tested) to estimate the remaining useful life of the system.

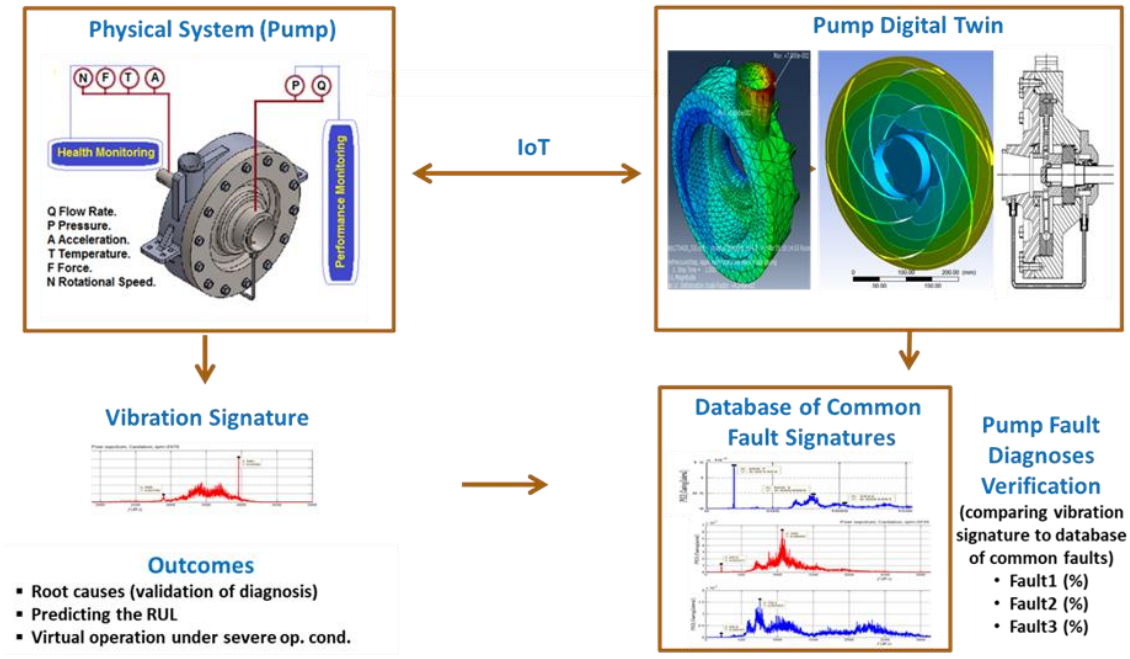

Figure 1.4: Illustration of Using Digital Twin for Fault Detection and Correction.

1.6 THESIS OUTLINE

Chapter 2 Presents a literature review of the water desalination major processes, water desalination methods, comparison of different membranes technologies, water desalination system main

components, digital transformation, digital twin, IoT, smart systems, predictive maintenance, condition-based maintenance, HPP and RO membrane mathematical equations, and finally, a brief description of health monitoring and dashboards.

Chapter 3 This chapter shows the research plan, in both theoretically and a roadmap showing the how the research started and what was the final goal of this research, a brief introduction on the used software's methodologies.

Chapter 4 The is chapter describe the real-world physical system components, attached sensors, data acquisition systems, the frequent occurring failures, and each team role.

Chapter 5 Introducing the digital models that is used in the thesis, from Amesim model which is modeling and simulating the HPP-ERD, the 3-stage RO membrane digital model constructed in C-script, how both models were integrated together, developed machine learning algorithms and digital models for fault detection and design improvements.

Chapter 6 Represents the digital models simulations, results, and discussion, comparison of the real-world data and the digital twin generated data.

Chapter 7 Concludes the presented work with recommendations and future research opportunities.

Appendix A Shows the derivation, modeling, validation, and the simulations of the 3-stage reverse osmosis membrane.

CHAPTER 2

LITERATURE REVIEW

This literature review chapter starts by discussing the water desalination technology, and a comparison between water desalination and distillation. Then, an overview of water desalination components, digital transformation, digital twin, IoT, smart systems, predictive maintenance, monitoring, dashboards and condition-based maintenance history and previous used cases in industry. Finally, the geometric aspect behind the high-pressure reciprocating pumps and reverse osmosis membrane mathematical models.

2.1 WATER DESALINATION TECHNOLOGIES.

Desalination is the process which is separating saline water into two different paths of water forms using energy in different forms [26]. One of the water paths is the permeate/freshwater, drinkable water with a low salt concentration. The other path has more salinity concentration, even greater than the salinity which exists in the feed water stream concentration [26]. Brackish water and seawater can be called saline water depending on the water sources and salinity. Water desalination started been industrialized over the years ago to start being the most optimum and successful solution. However, desalination involves expensive infrastructure [27]. The way of separating system that is applied into physical, thermal, and chemical processes can classify the desalination process. Thermal processes and membrane processes are the two most usable and capable

types of water desalination processes [28]. Although, freezing and ion exchange technologies are desalination alternatives as well, as shown in the figure below. However, they are not being used on a wide scale. Most of the desalination plants are either operated with conventional or renewable energy sources for permeate water production [29]. International Desalination Association (IDA) mentioned that the market share of water desalination operative plants is 92.5 million of m3/day, however the capacity of the water desalination plants cumulative estimated to be 99.8 million m3/day worldwide as this percentage includes the installed plants since 1965 [8]. Nowadays, desalination is playing an important life role for at least 1% of people around the world depends on the water desalination technologies as their fresh water supply. However, according to United Nations, by 2025 there will be 14% of the people around the world suffering from water scarcity [9].

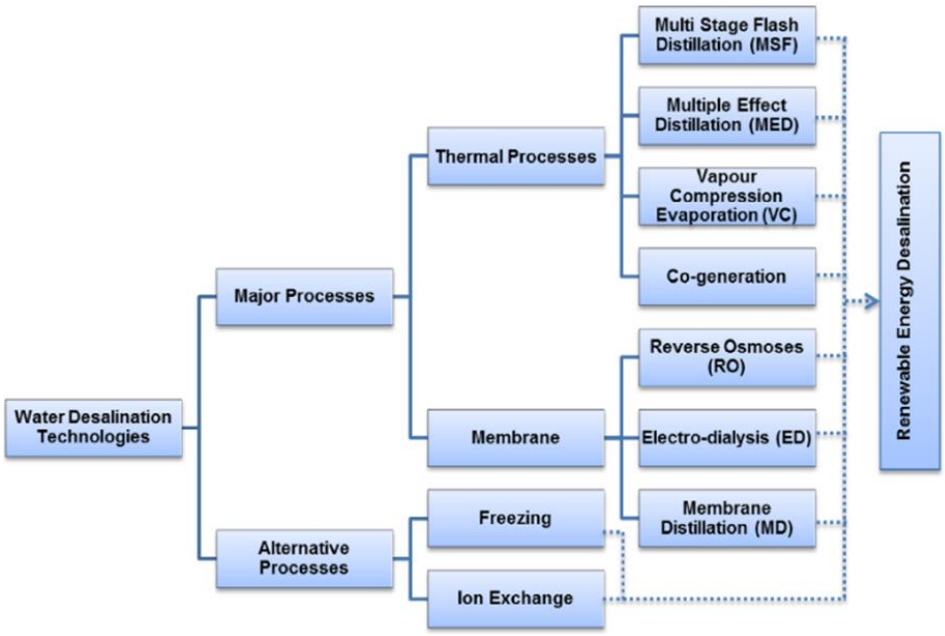

Figure 2.1: Water Desalination Technologies [30]

2.2 MAJOR PROCESSES:

2.2.1 Thermal Desalination

Evaporation and condensation principles are the thermal desalination process keys where the water temperature increases until it achieves the saturation temperature, where evaporation take place if the water temperature increased than the saturation temperature. The separation process starts by taking the vapor to another heat exchanger and leaving the salt behind to produce freshwater. Using the steam generators, and the back pressure steam extraction from the turbines in power stations, etc. are all techniques used to produce thermal energy [30] [31]. Thermal desalination technologies used often with seawater and rarely used with brackish water due to its high cost. It's also the most and oldest desalination technique that have been used Thermal desalination most common processes are [32]:

- Multiple-effect distillation (MED)
- Multi-stage flash distillation (MSF)
- Solar water desalination.
- Vapor-compression evaporation (VC)

MED and MSF processes use evaporators that work in vacuum conditions to achieve the best performance standard. In all cases, the vacuum is created by making use of multi-stage steam jet vacuum pumps. Together with the relative condensers, these vacuum pumps are an integral part of the evaporation system, and for this reason, they are becoming more and more a cause for attention [2].

2.2.2 Multiple-effect distillation

Multiple-effect distillation is still used and considered to be the oldest water distillation technique as they started using this technique over 100 years. Where MED and MSF have very close techniques that use series of effects of the evaporative technique. The water vapor of the first vessel or effect serves as the heating medium for the second, and so on. The more vessels or effects there are, the higher the performance ratio [33]. The evaporators in the desalination units were provided by steam from these plants. Then that steam ends up being the fresh water which got produced as a water vapor condensation from each vessel [34] [35].

2.2.3 Multi-stage flash distillation

Since the 1950s the multi-stage flash distillation (MSF) has been used. multi-stage flash distillation is considered one of the most in-use technology types regarding thermal desalination. The process occurs after heating the feed water under high pressure and heading to the first chamber, the pressure is released which rushing the water boiling phase and yields to a sudden evaporation. The distillation processes are producing 3.4billion gpd of freshwater which is 50% of the water desalination production, Where MSF plants are representing 84% out of the distillation process market share. [2].

2.2.4 Solar water desalination:

Is transferring the salt water into drinkable fresh water is a process to be done by using direct or indirect methods by converting the sun’s energy to heath energy. Solar stills are the first method used to convert water contamination into a permeate form on a large scale [36].

2.2.5 Vapor-compression evaporation (VC):

The VC distillation technology usually utilized by combined other technology process with it as multiple-effect distillation, or itself. VCD is commonly used for medium-scale and minor units like big commercial buildings, resorts, hotels, and industrial applications. As they are generally small incapacity, the idea behind VCD is to reduce the pressure which yields to decrease the water boiling point temperature [37]. The heat source used to evaporate the feed water comes from compressing the vapor, as shown in the figure below. Mechanical compression systems and steam jets are purposely used to evaporate the incoming feedwater by condensing the steam to produce sufficient energy to do this evaporation process [38].

2.2.6 Nonconventional solar sources:

Solar desalination technique is satisfying the requested water needs in several regions. This technique is one of the most convenient freshwater alternatives to several world regions. Solar desalination is suitable for small communities where sources of electricity are not available, and there is plenty of solar radiation. Furthermore, solar energy is considered a clean energy source, and it is an environmentally friendly and highly promising technology [2] [39] [40]. Solar desalination has characterized as a cost savings method since solar energy is easy to access in many regions and its endless source of energy [2]. This energy be able to either used for water desalination directly through solar stills or indirect ways where the distilled units is getting supplied with power from the solar energy device system. methods for solar-powered desalination techniques are:

- Getting enough energy to heat the feedwater using the photovoltaic cells.
- Solar cells

2.2.6.1 Photovoltaic cells (PV):

The photovoltaic cell's structure is an uncomplicated approach that involves the photovoltaic cells generating enough electricity to provide the needed power to the responsible heating source for feed water heating [41]. Photovoltaic cells are taking advantage of solar energy as an indirect energy source. it uses solar energy heat the feedwater after converting the electricity generated to heat, furthermore these photovoltaic cells can be attached with storage batteries [42].

2.2.6.1 Solar stills:

Solar still is considered as a direct method of solar distillation where direct sun radiation to evaporate feedwater using solar stills. Solar stills are used for distilled water from saltwater. It can be used with large and medium systems even it can be designed to meet the water needs of just one family. Solar stills are relatively inexpensive, predominantly when used for a small group [43].

2.3 WATER DESALINATION METHODS AND COMPONENTS.

2.3.1 Membrane desalination:

Water desalination using membranes is the salts and mineral separation process from water. when water passes through a semipermeable membrane. Membrane desalination processes are classified into subcategories [44]:

- Reverse osmosis (RO)
- Electrodialysis (ED)
- Membrane distillation (MD)

2.3.1.1 Electrodialysis (ED)

Electrodialysis is a membrane voltage driven process that the salts removed using electrical potential through membranes and leaves the freshwater behind. ED and ion

exchange has many mechanism similarities [45]. ED and RO are similar as both require a pump to build pressure and push the water through the membranes to start the desalination process; however, the pumps required for the ED process are more expensive [46]. ED was commercialized in the 1960s and preferable to be used with brackish water desalination [11]. Principles ED process depends on:

- Cations are the positively charged ions of salts dissolved in water, they called anions if they are negatively charged.
- Suitable membranes can be assembled to permit selective passage of either anions or cations. As the ions get attracted to the electrodes with opposite electric charge [47].

2.3.1.2 Membrane distillation (MD) and Reverse osmosis (RO)

Professor Samuel T. Yuster in the early 1950s, started the idea which led to reverse osmosis at the University of California at Los Angeles (UCLA). Prof. Yuster conceived the idea of using Gibb's adsorption equation as a guideline to find techniques for producing freshwater from saline water (sea and brackish water) [48] (Sourirajan, 1970). The first successful test was performed in 1958 using a flat plastic film, supported by a porous plate at UCLA [49] [50] (Sourirajan, 1986). Independently at the University of Florida, Breton and Reid did the first successful RO test at the same time using cellulose acetate membranes and seawater [51] [52] (Breton, 1957; Reid and Breton,1959). In 1958 the breakthrough that made RO commercially attractive happened when Loeb and Sourirajan test the first asymmetric cellulose acetate membrane [53]. Nowadays, RO technology has been flourished from research lab scale to large industrial plants, and more different

applications are being discovered each year involves RO academic, industrial and research centers throughout the world [26].

Reverse osmoses are simple, economically competitive, and do not require phase change, which is particularly important for heat solutions sensitivity, such as pharmaceutical materials and food products. The RO is a pressure driven separation method. Reverse osmosis operating pressure is in range of 3.4 to 68 bar [12]. RO has been commercialized since the 1970s and has become the most used primary desalination method in the United States. Reverse osmosis capable for desalinating feed water with more than 30,000 ppm salt concentration [11]. Reverse osmosis is a scientific procedure that reverses the natural process of osmosis. It is sufficient to apply pressure greater than the osmotic pressure to the concentrated solution to cause a reverse flow through the membrane, obtaining the salts' separation in the water. The advantages of reverse osmosis are considerable:

1. Capable to waters with any saline content, from groundwater to seawater.
2. No use of chemicals that must be discharged after use
3. Relatively low operating costs compared to resin plants, especially in the presence of influential high salinity.
4. The simplicity of operation is a process that does not require periodic regeneration as occurs in resin plants.

The osmosis system cannot constantly be fed with water as it is, as some elements present in it (free chlorine, turbidity, hardness, iron) would interfere with the osmotic process, sometimes irreversibly damaging the membranes. Therefore, a softening pre-treatment or chemical conditioning may be necessary, depending on desired water

characterization. Furthermore, the water temperature must never exceed 35 ° C. According to the amount of removed impurities the membrane filtration family is divided into four types:

- Microfiltration
- Ultrafiltration
- Nanofiltration
- Hyperfiltration [reverse osmosis]

Microfiltration

Filtration down to 1 μm to remove suspended particles. The main application is for pre-treatment before hyperfiltration [reverse osmosis systems] and filtration of fresh water to make it drinkable [54].

Ultrafiltration

Ultrafiltration devices are applied to remove the water turbidity, suspended solids, and microbiological contamination in treatment drinkable water, and the food and beverage industry [55].

Nanofiltration

Removes ninety-nine percent of bacteria exists in water and from eighty to eighty-five percent of soluble mineral salts. Nanofiltration principle is the same as that of RO. Nanofiltration devices are used as an alternative to traditional water softening. The cost of operating a nanofiltration plant is much lower since the need to regenerate the softener with a large amount of salt is entirely different removed. Installations are used to eliminate divalent [Fe ++, Ca, Mg] ions from water. They are mainly used in treatment of water for

water food and beverage processing, boiler cleaning, water heating systems, and the preparation and application of water in high-power cooling towers [56].

Hyperfiltration [reverse osmosis]

Reverse osmosis removes ninety-nine percent of bacteria exists in water and from ninety-five to ninety-nine percent of soluble mineral salts. Natural osmosis that transpires in nature is the opposite of RO. Feed water, that must be purified from salts, which supplied under high pressure to a container separated by a semi-permeable membrane. The membrane permits just clean water to flow across it, however it does not allow ions of dissolved substances. Are deposited upon the membrane. Thus, pure demineralized water [permeate] is obtained from a part of the supplied water, while in the remaining part, on the contrary, the concentration of salts (concentrate) increases [57].

- RO devices to desalinate fresh water.
- RO devices to desalinate brackish water.
- RO devices to desalinate seawater.

Reverse osmosis cannot remove the well gasses molecules because of its small size; However, it removes all the dissolved and particulate solids of any size. This kind of membranes can remove more than ninety percent of solid compounds with the size of two hundred Daltons or even more than this number. $1.666054 \times 10{-}24$ g is equal to 1 Dalton this means reverse osmosis membranes can reject all attached bacteria, solids, other human pathogens, viruses, and protozoa that exists in the feed water. [26]

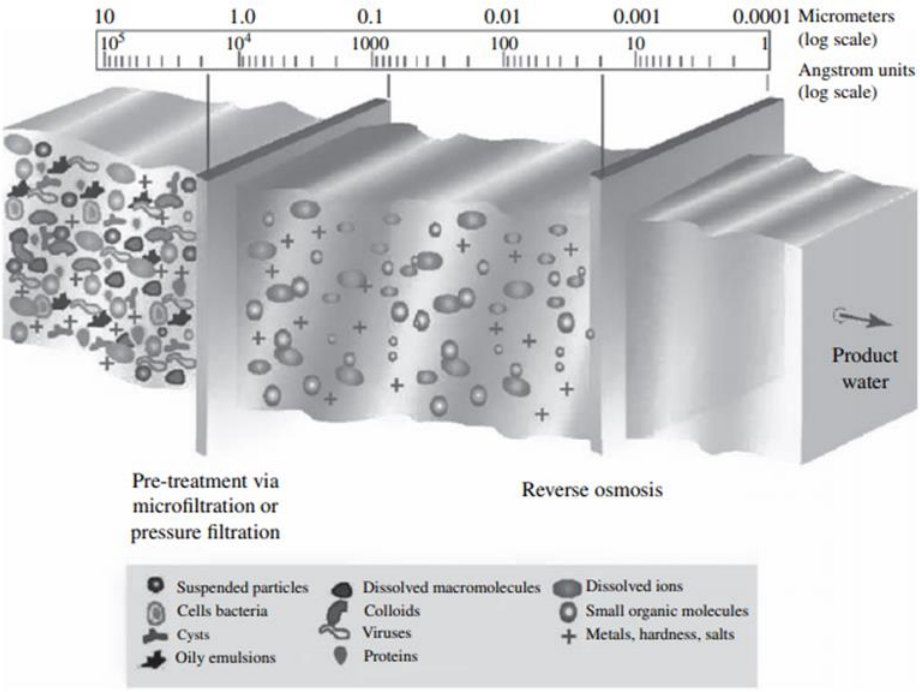

Figure 2.2: Contaminant Removal by Reverse Osmosis Membrane [26]

2.4 WATER DESALINATION SYSTEM USING REVERSE OSMOSIS MEMBRANE

MAJOR COMPONENTS

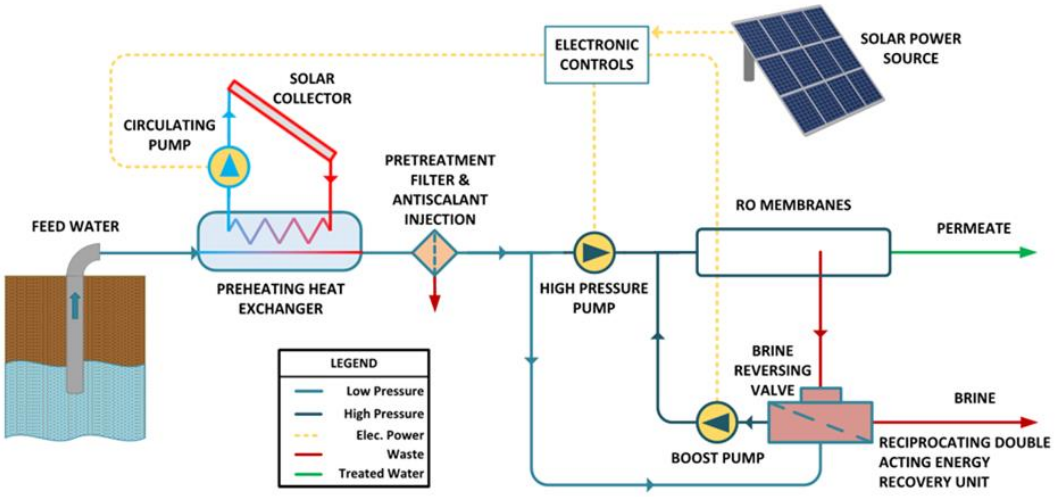

Figure 2.3: Key Components & Systems of a Water Desalination Plant

2.3.2 Pretreatment system

Pretreatment takes a vital role in the reverse osmosis system as it is a must to clean the membrane surface from the suspended solids all the time**.** It is essential to pretreat the water to make sure that microbial growth and salt precipitation is not taking place on the membranes. Pretreatment can include chemical feed followed by sand filtration, sedimentation, flocculation, and coagulation as conventional methods [58]. The plant's pretreatment technique depends on several factors which are space availability, the characterization quality of the feedwater, and other requirements for the reverse osmosis membrane.

2.3.3 High-pressure pump (HPP)

Pumps are mechanical devices that converts mechanical energy into hydraulic energy. They are divided into two main types of the positive displacement pumps such as piston pumps with industry market share of 27% and rotodynamic pumps such as centrifugal pumps with industry market share of 73%. RO is a pressure driven separation process as required feed pressure must go beyond the built osmotic pressure, increasing directly with water salinity. The heart of the water desalination system using reverse osmosis membrane is the high-pressure pump, since it is role is generating the pressure of the feed water to permit the permeation process to occur across the reverse osmosis. the pressures for sea water reverse osmosis are in the range of 600-1200 psi and 150 psi for slightly brackish water [59]. The materials of the selected pump must meet the seawater corrosion requirement. Pump Metallic materials and corrosion-resistant materials must adhere to electrochemical series Due to sea water’s strong electrochemical corrosion and high electrical conductivity. HPP supplies the water with the needed pressure to pass across

the RO membranes and reject salt. Accordingly, high-pressure pump is the essential mechanical element in the SWRO desalination plant. Maintaining the HPP working under healthy conditions, which keeps the SWRO desalinating plant running, ensures sustainable development and prosperity, as sometimes it is vital to maintain human lives. Pumps are divided into two types:

- Positive displacement pumps (PDP):

  They force the fluid to move by cornering a fixed amount of the fluid then forcing this fluid to flow out to the outlet manifold. In other words, the fluid is pressed to a predetermined space encircled by mechanical parts then settled in it using few mechanical methods. Then using this mechanical methods and parts to force the fluid out of this finite space [60]. These types of pumps are getting classified regarding to the move of the fluid mechanism. PDP types are:

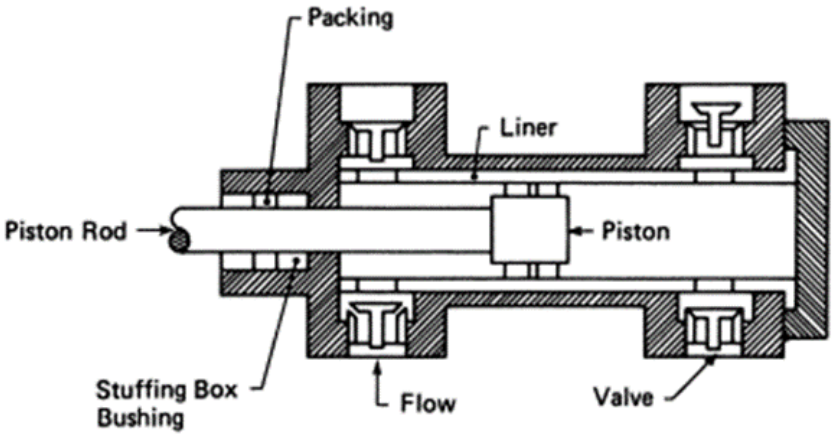

Figure 2.4: Positive Displacement Pump (Piston pump) [60]

Rotary type: these types of pumps are requiring a small clearance between the outer pump edge and the rotary pump to make the rotor rotates at steady slow speed as if it operates in high speed it yields to erosion. eventually it will lead the liquid to pass through

because of the enlarged clearances, which yield to an efficiency reduction. Rotary pump types:

(1) Gear pumps: the simplest type of rotary pumps where there are two gears responsible for pushing the liquid.

(2) Screw pump: there are two screws rotating against each other where they are responsible to push the fluid.

(3) Rotary vane pumps these pumps are trapping the fluid between the pump casing and the vane's rotor.

Reciprocating pumps: it forces the fluid to get in the cylinder during the suction process when the pressure difference between the cylinder and the inlet manifold/pipe the suction phase start and the fluid getting in the cylinder and settle until it builds pressure difference between the cylinder and the outlet manifold to start the discharging phase [61].

2.3.4 Membrane systems

The membrane housing called pressure vessel where the membrane is getting assemble, and inside it is the semipermeable membrane so the feed water will be allowed to pass across it. There are two famous/common RO membrane types for water desalination: Spiral wound and hollow fiber [62].

2.3.4.1 Spiral wound:

Spiral wounds membranes are constructed as flat membrane sheets that have three layers of structure. The cellulose acetate or a thin film of other types of composite polymers is usually made from polyamide, poly-sulphone, or polyurea polymers [26].

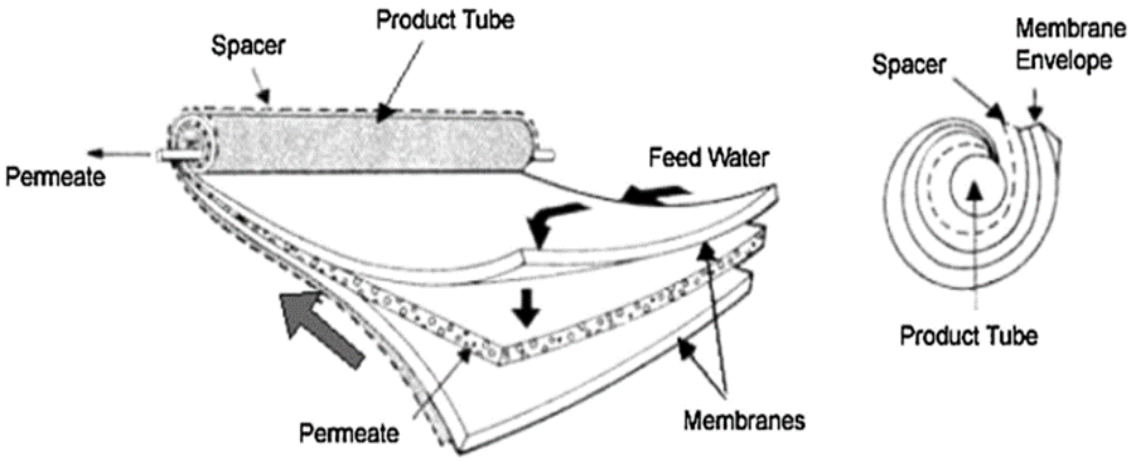

Figure 2.5:Spiral Wound Membrane Cross Section View [26].

Spiral wound reverse osmosis membrane is the most commercially used membrane. It includes 40 to 42 flat membrane sheets for typical 8-inch diameter membrane [book]. A central collecting tube which is wrapped by an envelope is the spiral wound membrane design. The feed water flows in a spiral path inside the membrane envelope, and while the central tube is gathering the permeate water under the pressure effect. the perforated permeate collector tube is surrounded by separating spacers and sheet membrane leaf's[book]. The minor amount of the feed water flow across the membrane and called the permeate portion the major portion of the feedwater does not flow across the membrane and increase its salinity concentration also there is a feedwater portion is discharging without passing across the membrane [11]. Increasing of the salinity concentration occurs due to super salts concentration without feed water get discharged under the required pressure. the feed water flowrate that gets discharged as a higher salinity water is fifty percent in the case of seawater and twenty percent for brackish water.

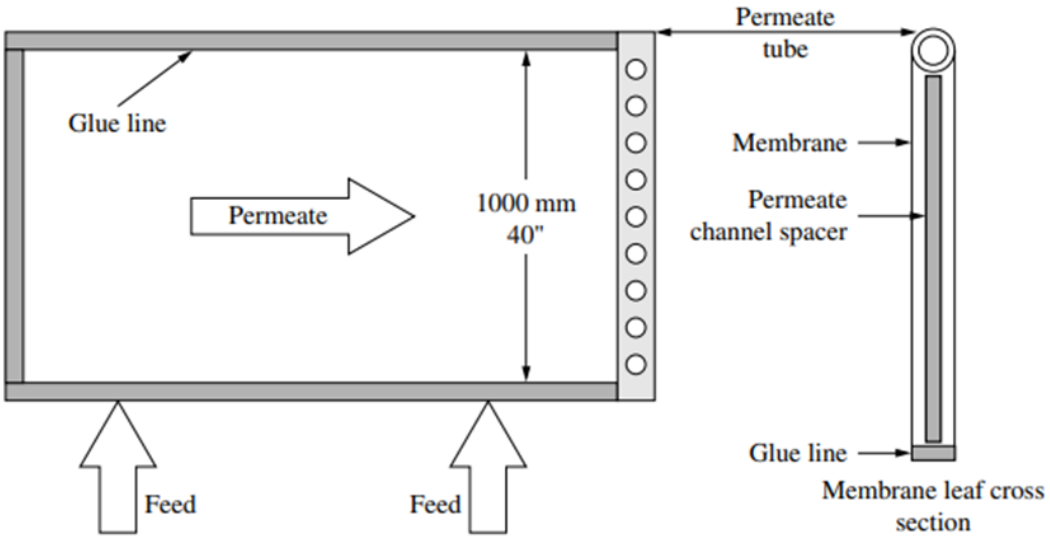

Figure 2.6: Flat-Sheet Membrane Envelope [26].

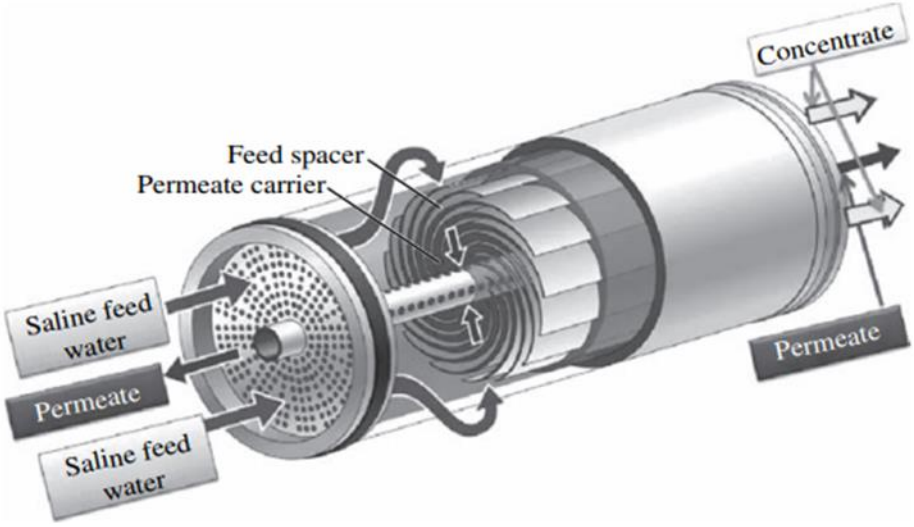

Figure 2.7: Spiral Wound Membrane Element [26].

2.4.3.2 Hollow fiber

This type is designed to have several hollow fiber membranes in the pressure vessel. Have a U-shaped bundle designed to be accommodated in a pressure vessel. polyamide and cellulose triacetate are the membrane materials. Permeate water under pressure passes

through fiber walls and flows in the hollow fibers for collection, while the saline water under pressure flows along the outside of hollow fibers. Hollow fiber the spiral wound membrane is widely used in desalination more than the hollow fiber membrane.

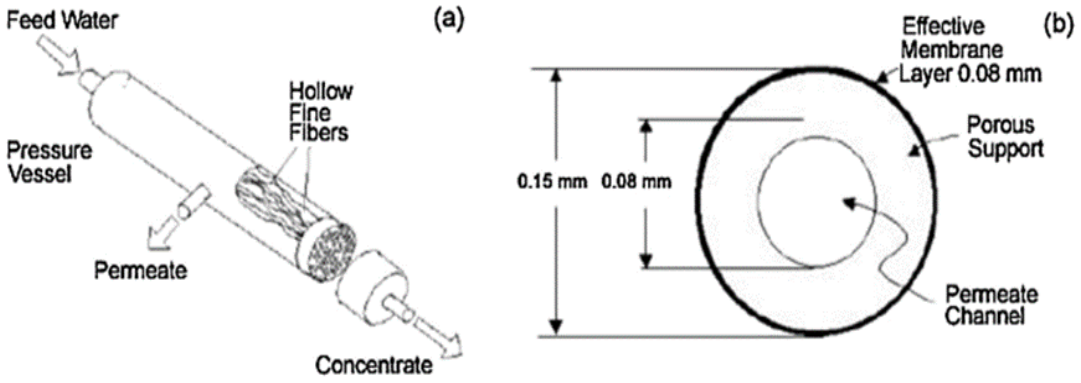

Figure 2.8: Hollow fiber membrane [26]

2.3.4 Post-treatment:

At this level, water is getting to stabilize and getting to prepare for distribution. Disinfection and adjusting the alkalinity, hardness, and pH are necessary if combined with other water supply sources to meet up with the drinking water standards and prevent any corrosion effect in the distribution network [63].

2.5 DIGITAL TRANSFORMATION, DIGITAL TWIN ITS IMPLEMENTATION IN THE PREDICTIVE MAINTENANCE AREA

2.5.1 Digital Transformation

Digital transformation has been the most attractive word in this century; it has become the future theme that is not just affecting the economy. It affects the whole society. The notion of digital transformation first started appearing in literature around 1968 in nuclear spectroscopy [64] and computer analysis of microscopic images [65]. However, this concept has evolved since then. Digital transformation integrates and uses digital

technologies into business and industrial processes to enable significant improvements [66] [67]. Digital transformation has different definitions for every company and industry. Even the digital transformation product will look different from one industry to another and from a company to another. However, in general terms, digital transformation or digitalization definition is a game-changer of the century as it is the conversion of manual or non-digital services, solutions, and businesses by integrating the newer digital technology instead of the non-digital technology in all areas. The changes that the digital models and technologies can bring to company's business model results as change in the company structure, the process automation, and the business model product [68]. Digital transformation aims to make the digital customers more effectively engaged with the customer experience life cycle. Digital transformation area of research now is focusing more on the successful digital transformation cases and showing the improvements in this area and its capabilities. Also focusing on the electronic data, products, and service accessibility to build a better customer relationship [69].

Industry 4.0, the implementation of digital transformation in the industry which aims integrated smart factories. Discrete products are mass-produced sustainably to fulfill consumer demand in global competition. Smart manufacturing focuses on end-to-end digitalization process and integrating ecosystems solution. By seeking completely integrated solutions, and is characterized by connectivity, automation, digitalization, and decentralization [70]. Most prominently, the United States has more interest in the smart manufacturing area, while Germany has more interest in applying and developing programs for "Industrie 4.0" [71]. Industries and engineering applications worldwide start applying the digital transformation in the designing, product life management

manufacturing, monitoring the physical systems during operations. Digitalization process supports better interaction and connection between the users, systems, and the machines, which yields to increasing the productivity, faster decision making, reducing the friction and less downtime, leading to elevating profitability and improving customer experience [69].

Digitalization means using more IT to enable and take advantage of digital technology and data. Digitalization become the future of the future products and production engineering. Driven by the need for mobility and supported by the cloud, AI, and IOT, customers want a digital experience in everything. A study shows that 87% of business leaders consider digitalization as a top priority. Digital Transformation makes organizations and government agencies perform in creating more capable products and services. It can be done more quickly and effectively. The pandemic/crises of COVID 19 proved that digital transformation is a must as it forced many organizations to start the digitalization process and try to achieve their digitalization goals. Whether by establishing secure platforms for working remotely or making supply chains and manufacturing ecosystems more agile.

2.5.2 Digital Twin

The Predictive maintenance has been developed and got a lot of research interest in the previous few years. The development of the diagnostic abilities of the predictive maintenance area because of the enhancement of the sensor's technologies, data analytics, machine learning, signal processing algorithms, artificial intelligence, and the development of the computational power [22]. The new era of digital transformation and industry 4.0 has introduced the new model of a digital twin to the field of predictive maintenance.

Digital twin is the virtual representation for the physical systems, this virtual representation can be representing the physical system dynamics, the products, the conditions, and attributes. Incorporating simulation data collected from digital models with sensors' data collected from the physical twin helps decision-makers better understand the system. This, in turn, helps to improve and optimize the operation and maintenance plans, means less downtime, less operating and maintenance cost, and ultimately more profit. The digital twin is assisted in improving the ability to track the systems performance, control system efficiency, and take the proper maintenance decisions at the ideal time regarding performance versus part life [72].

Digital twin described in many ways in both academia and industry [73]. However, all definitions agreed that the digital twin is an organized collection of physical models. A multiscale probabilistic ultra-realistic simulation of systems or products reflects a real model time data of its parallel physical twin using historical data and real-time data [74]. Digital twin models include all aspects of physical systems, including mechanical, hydraulic, chemical, material, thermal, and statistical models. The mentioned models represent accurate real-time data representation, including the properties, condition, and performance for the system regards many variations related to the operating conditions [75]. Using the new digital twin models' concepts are helpful for predicting further accurate outcomes such as reliability, performance, flexibility, wear and tear, and maintainability. These models are supported by data getting from the integrated sensors to give the ability to predict system performance, predict failures, evaluate different scenarios, and enhance efficiency by reducing the cost.

The aerospace industry was the first industry to use digital twins. Tuegel et al. (2011) [105] described that digital twin as it was not representing the manufacturing process it used on individual aircraft as that digital twin was be updated by data from actual aircraft using big data analysis to improve lifespan and prediction maintenance. Tuegel did describe that the Multiphysics modeling challenge was a solution method of stressors such as physical forces and temperature are modeled together. Glaessgen and Stargel (2012) [36] mentioned that maintenance prediction intervals and damage analysis are based on some factors such as factors of safety, similitude, among others, and heuristics. The accuracy of this model was based on experiments and experimentations; however, each aircraft and damage are unique in its type and behavior that why the analyses and predictions must be preservative, which ends up using more materials and weight. The digital twin's safety and reliability should be connected/linked with the actual/physical aircraft through onboard sensors. Digital twin variations are based on the data transfer flow and direction. The digital model is an informational model of the physical system updated by changes in the physical system but without any data interchange as the digital shadow does not influence the physical system Kritzinger et al. (2018) [56].

Digital twin outcomes: monitor and optimization the system, start operational flexibility by creating faster and more predictable objects, economic dispatch by long term planning for improved economics while respecting systems operation boundaries, system availability, and reliability by proactive monitoring to the system and the system parts life through optimization and controls to drive the desired outage target and reducing the unplanned outcomes through online monitoring and prognostics which improves both system availability and enterprise-level performance, and inventory control by tracking the

operations and maintenance history of production assets which play a role in maintenance cost reduction as its maximize the parts/components lifetime, improve capital management decisions with more accurate assets operations, monitoring system spare parts schedule and forecasting, and repair history.

Digital twin converted from being just a descriptive model that feeds the users with data to be an actionable and interactable model that allows the users to design and test the virtual version to discover manufacturability and modes of failures [70]. The digital twin has proved its importance to industry 4.0 through simulation to all phases of product life cycles like the real-life data Alcacer and Cruz-Machado (2019) [64]. They defined the digital twin as an ultra-high-fidelity simulation [64]. A digital twin is defined as the ultra-high synchronization between the physical product and the digital twin. Which also includes multi-physics modeling Tao et al. (2018) [101]. Padovan et al. (2019) [79] described that digital twin could also be used as a knowledge service as it can be an online help service that is helping according to the historical and real-world data gathered. There was an argument that digital twins can replace physical resources and reduce the energy, material, and time waste as simulations will reduce the try and error time Greives (2005) [68].

2.5.3 Internet of things (IoT)

IoT is a network of physical properties that are digitally connected and can sense, monitor, and control/interact with business and between business and supply chain [69]. IoT enables information/data to be collected and transferred accurately in real-time through the network [76]. This enables agility, visibility, tracking, and data/info sharing to expedite well-timed planning, control, and coordination [77]. Internet of things is a transforming

based service for the industry sector. IoT cannot be working in isolation environment as these technology needs interactive business models, capabilities and new organizational structure that must be coupled with original product and customer experience.

Internet of things is not an easy task to be implemented. Seventy-five manufacturing companies attempt IoT transformation. IoT is a technologically very complex task to achieve. Three years was the duration that most of these companies took to complete this transformation project and the results were poor. With all these significant attempts, only 5% of IoT adopters achieved significant business outcomes. Some of these companies did not achieve their goal as they struggled with processing and storing the new data. While the other companies realized that their significant effort were not precious towards their business models. Even the most established companies that achieved their IoT transformation goal underestimated the complexity of this technology. It will motivate cooperate with additional companies. This transformation will require new softwares with new capabilities in developments and analytics. It will change pricing schemes and approaches. These were the reasons why the companies failed to proceed with this transition, as they underestimated the complexity and the organizational impact of the challenge. However, the successful companies adopting this technology are driving better business handling efficiency.

2.5.4 Smart systems:

Both in academia and industry are seeking to the key and product of the digital transformation is the smart system. Using digital twin and physical systems together creates a smart system, which are helpful in several areas, such as improving the design, manufacturing process, validation, verification, improving productivity, and monitoring.

There are many ways for the smart system to displaying the data depends on the need. One of the most visualization types for smart systems is dashboards. Dashboards are easy and fast to understand format, which has a good effect on making decisions according to more knowledge, which yields better results. Dashboards can store, process, and calculate conducted data in one location. virtual or augmented reality are another type of data visualization. These types of visualizations help in transferring the knowledge study the behavior of systems through simulating hands-on experience [78].

2.5.5 Predictive Maintenance

Pumps are playing an essential role in a wide range of industry applications [22]. Pumps must be continuously monitored to maximize the plant's profit and operate with maximum reliability, capacity, and efficiency. Also, to avoid mechanical and hydraulic pumps failure, as it is considered a big loss of time, money, and maintenance efforts to until the system will be operating again [22]. Predictive maintenance programs aiming to prevent unexpected faults from occurring in the mechanical systems. The fault prediction is based on the data which is gathered from the sensors that is plugged to the physical system [22]. Digital models can study the dynamic behavior of the pump. When the digital twin is constructed, they can simulate the pump performance under different operating conditions. There are many exciting applications of using these digital models, one of these applications is predictive maintenance by simulating the pump under harsh and destructive operating conditions. To observe and study the behavior of the systems under these harsh conditions and the remaining useful life of the system, which is not recommended to be physically tested as it will cost money, time, and maintaining efforts. Another exciting digital models' application is fault correction and detection, as shown in the figure below.

This concept is working on diagnosing the faults then applying the recommended action which will be tested on the digital system before the physical system [22]. This paper focused on 3D fully turbulent CFD model showing cavitation condition and vapor formation. Second simulation of the casing vibration under cavitation conditions. The rig tests experimental results, and it is set up. Mohammed A. Hassan and Amr A. Abdel Fatah used the two digital models in predictive maintenance by simulating the cavitation fault causes in the centrifugal pump. By simulating the dynamic performance of the pump casing with the pressure pulsation, they compared the CFD model with the model of 'Gaussian pressure pulsation'. This model identified the cavitation by studying the pump casing vibration level with a frequency relative to the impeller blades. Due to cavitation, the radial vibration magnitude did increase by 2.6 times more than the healthy operating conditions.

2.5.6 High-pressure pump mathematical equations and physical behavior

Reciprocating pumps are widely used in hydraulic drive systems. The reciprocating pump system anatomy is consisting of Outlet manifold, input manifold, an accumulator, and few cylinders which contains pistons and these pistons connected to the crankshaft via connecting rods. Fluid flowing in each cylinder at low pressure is compressed and discharged through a discharge port. Discharging process take place whenever the existing cylinder's pressure exceeds the exists pressure in the outlet manifold. The outlet valves which responsible for the discharging process in the cylinders keep their opening order.

A simplified schematic of the single-piston pump is shown in Figure 2.10 [79]. The working principle of the pump is the reciprocating suction and discharge actions inside the cylinder during the suction phase the suction valve open and discharge valve close while the operating fluid entering the cylinder from the input manifold due to pressure drops

inside the cylinder. This operation is reversed during the discharge phase. while the pressure inside the cylinder builds to exceed the discharge manifold and discharge valve opens to allow operating fluid to exit the cylinder. There is a connecting rod that receives drive from the crankshaft and connected with the piston which is made to reciprocate. Figure 2.9 shows a simplified schematic for a three-piston pump. This schematic explains the suction valves are open regarding the difference of the pressure among the suction pipes and the cylinders. the discharge process take place when there is a pressure difference between the outlet manifold and the cylinders which yields discharge valves to open.

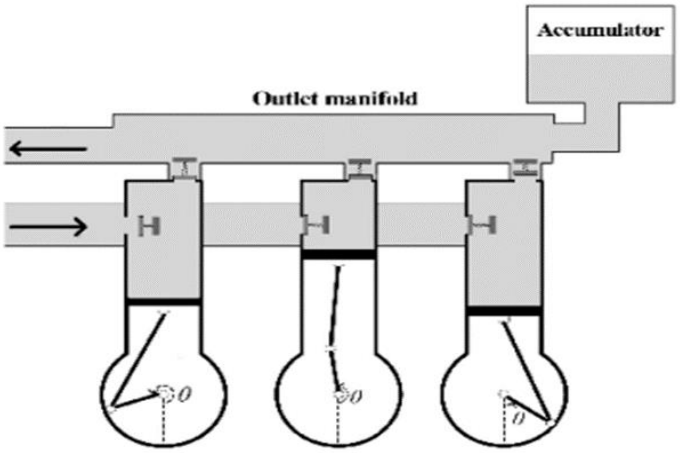

Figure 2.9: Schematic Diagram of
Reciprocating Pump [79]

As shown in Figure 2.9, the crank shaft is rotating constantly while the piston in each single cylinder moves downward and upward among the (TDC) top dead center and the (BDC) bottom dead center. Using the Reynolds transport theorem, the volume flow rate inside the cylinder Q_c is calculated using Eq. (1) [16 of Lee2015]:

$$Q_c = Q_p - Q_s + Q_d \quad (1)$$

Where:

Q_p is the volume flow rate attributed to piston displacement.

Q_s is the volume flow rate of the fluid flowing in through the suction port.

Q_d is the volume flow rate of the fluid flowing through the discharge port.

θ the crankshaft rotational angle and all the volume flowrates are function of θ

Q_p is defined as in Eq. (2), Eq. (3), and Eq. (4):

$$Q_p = \frac{dV_p}{dt} \tag{2}$$

$$V_p = A_p x_p + V_c \tag{3}$$

$$x_p = r(1 + cos\theta) + l(1 - \sqrt{1 - r^2/l^2 sin^2\theta}), \tag{4}$$

$$V_p = V_c + A_p \left(\left(r(1 - \cos(\theta))\right) + e\left(1 - \sqrt{1 - \left(\left(\frac{r}{e}\right) sin(\theta)\right)^2}\right)\right) \;\&\; \theta = \omega t \tag{5}$$

$$Q_p = -\omega\, A_p\, r\, sin(\omega t) \left(1 + \frac{\left(\frac{r}{e}\right) cos(\omega t)}{\sqrt{1 - \left(\left(\frac{r}{e}\right) sin(\omega t)\right)^2}} \right) \tag{6}$$

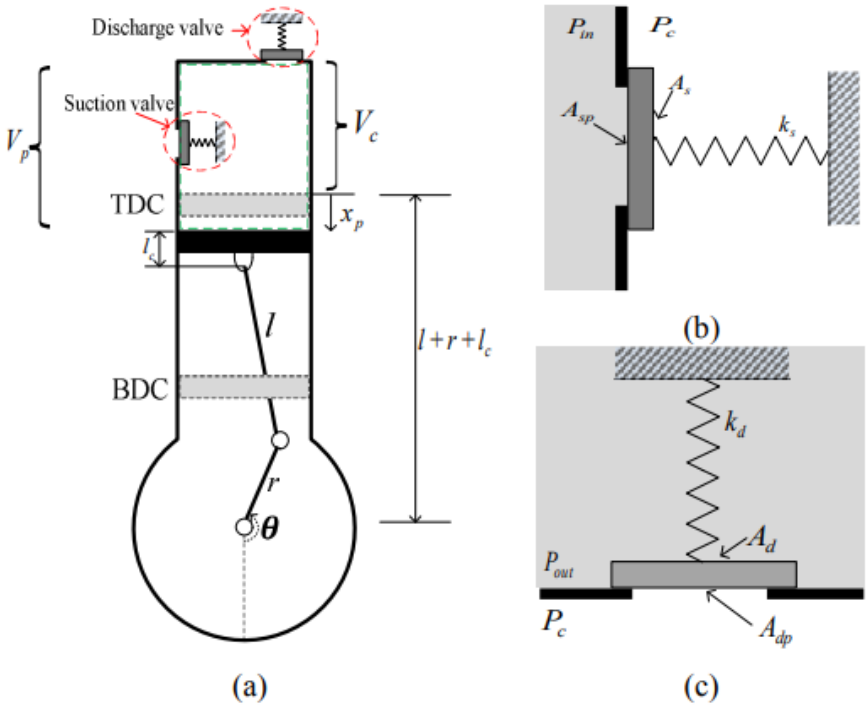

Figure 2.10: Single cylinder reciprocating pump [79]:
(a) Schematic diagram; (b)suction valve; (c) discharge valve.

Where:

- V_p *is the cylinder volume changing with the piston displacement*
- l *connecting rods*
- r *crank radius*
- $\theta = \omega t$ *the rotation angle of the crankshaft* [79].
- A_p *denote the cross − sectional area of the piston*
- V_c *the clearance volume*

The volume flow rates through the valve port ($Q_s$and Q_d) are expressed as Eq. (7) and Eq. (8), respectively [79]:

$$Q_s = A_{sp}\, C_{in} \sqrt{\frac{2(P_{in} - P_c)}{\rho}}, \tag{7}$$

$$Q_d = A_{dp}\, C_{out} \sqrt{\frac{2(P_c - P_{out})}{\rho}}, \tag{8}$$

Where:

- $A_{sp}\ is\ cross-sectional\ areas\ of\ the\ suction\ valve.$
- $A_{dp}\ is\ the\ cross-sectional\ areas\ of\ the\ discharge\ valve.$
- C_{in} & $C_{out}\ are\ flow\ coefficients.$
- $P_{in}\ is\ denote\ pressure\ in\ the\ suction\ pipe.$
- $P_{out}\ is\ denote\ pressure\ in\ the\ outlet\ pipe.$
- $P_c\ is\ denote\ the\ pressure\ in\ the\ cylinder.$
- $\rho\ is$ the fluid density.

$The\ elastic\ bulk\ modulus\ \beta$ in Eq. (9, 10), which correlates the volume and pressure inside the cylinder changing with the rotation angle of the crankshaft:

$$\beta = -V_p \frac{dP_c}{dV_p} \tag{9}$$

$$\frac{dP_c}{dt} = -\beta \frac{Q_c}{V_p} \tag{10}$$

During the suction phase:

(x_s) is the displacement.

(u_s) is the velocity.

($\dot{u}_s$) is the acceleration of the suction valve.

They are calculated by solving the second order differential Eq. (11) governing the spring-mass system shown in Figure 2. 1. Similarly, during the discharge phase, Eq. (12). governs the dynamic behavior of the discharge valve.

$$\dot{U}_s = (P_{in} - P_c)\left(\frac{A_{sp}}{m_s}\right) - \left(\frac{F_{si}}{m_d}\right) - X_s\left(\frac{K_s}{m_s}\right) - U_s\left(\frac{C_{vs}}{m_s}\right) \quad \text{during suction phase} \quad (11)$$

$$\dot{U}_d = (P_c - P_{out})\left(\frac{A_{dp}}{m_d}\right) - \left(\frac{F_{si}}{m_d}\right) - X_d\left(\frac{K_d}{m_d}\right) - U_d\left(\frac{C_{vd}}{m_d}\right) \quad \text{during discharge phase} \quad (12)$$

Where:

K_s *The initial compression of suction valve spring*

K_d *The initial compression of discharge valve spring*

X_s^{ini} *Spring constant of suction valve spring*

X_d^{ini} *spring constant of discharge valve spring*

P_c *when it reaches the satisfaction in the equation. below the suction valve open*

P_{out} *reaches the satisfaction in the equation below the discharge valve open*

While equations (13) and (14) shows the opening angles (θ_3 and θ_1) of the suction and discharge valves.

$$P_{in}A_{sp} \geq P_cA_s + \Delta F_s + k_s x_s^{ini} \quad (13)$$

$$P_cA_{dp} \geq P_{out}A_d + \Delta F_d + k_s x_d^{ini}, \quad At\theta = \theta_3, \quad (14)$$

$$P_c = \frac{\varepsilon_s A_{sp}}{A_s} P_{in} - \frac{k_s x_d^{ini}}{A_s}, \varepsilon_s = 1 - \frac{\Delta F_s}{A_{sp}} \frac{1}{P_{in}} \quad At\theta = \theta_1, \quad (15)$$

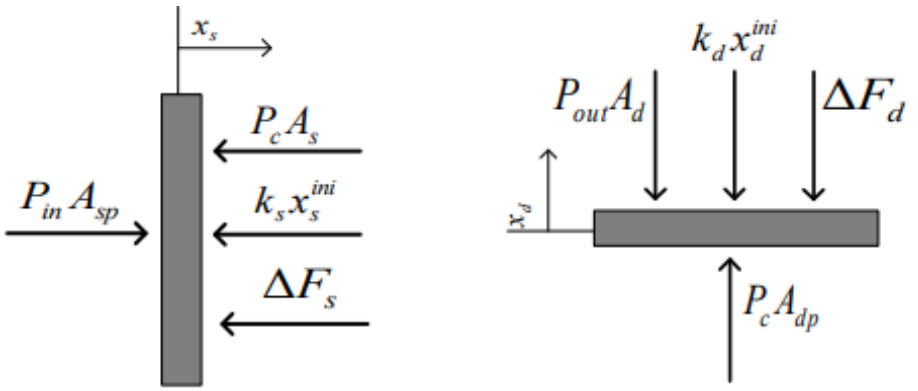

Figure 2.11: (A) Free body diagram for suction valve.
(B) Free body diagram for discharge valve [79].

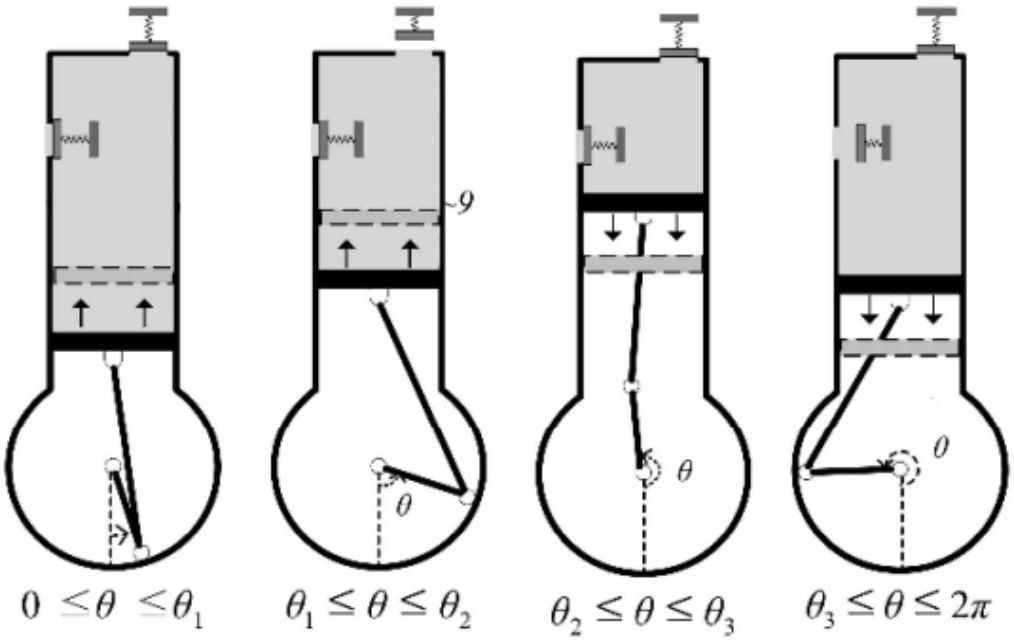

Figure 2.12: The four operating modes of
one cylinder in reciprocating pump [79].

Four different operating modes are describing the reciprocating pump kinematics behaviors. These four operating modes are depending on the discharge and suction valves opening and closing positions which relates also to the piston displacement as shown in Fig. 2.12. depending on these four operating modes the volume flow rate in each cylinder is specified differently. Where these four modes are:

(a) compression mode.
(b) discharge mode.
(c) expansion mode.
(d) suction mode.

$$Compression\ mode = \ Q_c = Q_p \tag{16}$$

$$Q_c = Q_p + Q_d \tag{17}$$

$$Q_c = Q_p \tag{18}$$

$$Q_c = Q_p - Q_s \tag{19}$$

(a) suction valve dynamic forces (b) discharge valve dynamic forces

Figure 2.13: Dynamics of Discharge & Suction Valves [79]

2.5.7 Reverse osmosis membrane mathematical equations to model the system feed pressure.

[80] Used forward osmosis to reduce the system energy consumption with 50% ~1.5 kWh/m³) (2.5–4 kWh/m³) is the energy used to produces high quality water from high pressure sea water reverse osmosis. Reducing system energy consumption yields to reducing costs. The experiments were for a long term over 14 days, although forward osmosis membranes fouling was not a main issue. The initial flux declined by 28% after continuous operation of ten days. However, the initial FO membranes flux recovered by 98.8% after cleaning it with clean water and air scouring.

Spiral wound membrane is the most common commercial used membrane in industry due to its high membrane area to volume ratio (specific surface area), and

high permeation rate, and ease of operation [22]. Clean water spirals to the central collection tube through the permeate envelope while the saline water passes along the length of the module. When the feed water portion is passing through the membrane this portion become more concentrated at the end of the brine channel, which yields to an increase in the osmotic pressure. Both the feed and the permeate are transported through the module in fluid-conductive spacer material [23]. To enhance the effective velocities and reduce the void volumes spacers are placed in both brine and permeate channels [24].

The RO membrane mathematical derivation model below is used to determine the system(feed) pressure and system flowrates at given actuator conditions. The model was tested, and the simulated dynamics of the digital model system are modeled based on the use of mass and energy balances with respect to time [81].

To determine the effect of the valve actuator position on the flow rates and pressures of the system, a macroscopic mechanical energy balance is taken around the brine stream valve (control volume 2) and can be written as [19]:

$$\frac{d}{dt}(K_{tot} + \emptyset_{tot}) = -\Delta\left(\frac{1}{2}\frac{< v^3 >}{< v >} + \hat{\phi} + \frac{p}{\rho}\right)w + W_m - E_C - E_V \qquad (20)$$

Where:

Δ represents the balance of kinetic energy entering and leaving the control volume.

(< v >) is the average fluid velocity over the pipe cross-section ($in.m/s$),

φˆ is the potential energy difference between the inlet and outlet ($in.J/s$)

p is the pressure difference between the inlet and outlet ($in\ Pa$),

ρ is the density of the fluid ($in\ kg/m3$),

w is the fluid mass flow rate ($in\ kg/s$),

(Wm) is the rate of doing work on the fluid by moving surfaces in the control volume ($in\ J/s$),

(Ec) is the compression term ($in\ J/s$),

E_V is the viscous dissipation (or friction loss) term ($in\ J/s$).

Several assumptions invoked to simplify the problem. These assumptions are listed in mathematical terms below:

Assumptions:

1. Incompressible fluid ($E_c = 0$) which is reasonable for the liquid system in question
2. at zero elevation ($\emptyset_{tot}, \hat{\phi} = 0$). all components of the system are in the same horizontal plane and neglecting the gravity.
3. no work done on system ($W_m = 0$). containing only the pipe and valve.
4. constant density $\rho 1 = \rho 2$. This assumption yield to assumption 5.
5. $\Delta v = 0\ at\ plane\ 1\ and\ plane\ 2$. velocity at the entrance and exit planes of the boundary are equal which is reasonable as all the mass entering the pipe before the valve exiting it after the valve.
6. Estimate $E_v as\ \frac{1}{2} < v^2 > e_v w$. is a common simplification of this energy balance [19].
7. Estimate $\frac{<v^3>}{<v>}\ as\ v^2$

Using assumption 1 to 3 in equation 1 reduces to:

(21)

$$\frac{d}{dt}(K_{tot}) = -\Delta\left(\frac{1}{2}\frac{< v^3 >}{< v >} + \frac{p}{\rho}\right)w - E_V$$

Using assumption 5, Eq. 2 yields to:

$$\frac{d}{dt}(K_{tot}) = -\left(\frac{\Delta p}{\rho}\right)w - E_V \tag{22}$$

Using assumption 6, $K_{tot} = \int \frac{1}{2}\rho v^2 dV$, and the chain rule $\frac{dv^2}{dt} = 2v\frac{dv}{dt}$, Eq. 3 yields:

$$\frac{d}{dt}\left(\int \frac{1}{2}\rho v^2 dV\right) = -\frac{\Delta p}{p}w - \frac{1}{2}v^2 e_v w \tag{23}$$

$$\frac{1}{2}\rho\left(\int dV\right)\frac{dv^2}{dt} = -\frac{\Delta p}{p}w - \frac{1}{2}v^2 e_v w \tag{24}$$

Using the fact that $w = \rho v A p$ and dividing through by v:

$$\rho V\frac{dv}{dt} = -\Delta p A_p - \frac{1}{2}v^2 e_v \rho A_p \tag{25}$$

Where:

$\Delta p = p1 - p2 = Psys = Pretentate = Pfeed$ is assumed to be equal to system feed pressure after neglecting the pressure drop in the membrane module. as is the case in the following derivation. Thus, Eq. 7 yields:

$$\rho V\frac{dv}{dt} = P_{sys}A_p - \frac{1}{2}v^2 e_v \rho A_p \tag{26}$$

Which is essentially a momentum balance around control volume 2, and can be simplified to yield:

$$\frac{dv}{dt} = \frac{P_{sys}A_p}{\rho V} - \frac{1}{2}\frac{A_p e_v v^2}{V} \tag{27}$$

Equation 9 shows the velocity from the valve to the valve resistance. this valve resistance is a dimensionless as it can be equal to zero when there is no resistance existence and equal to infinity when the valve is completely closed.

2.5.7.1 Overall mass balance:

The mass balance around control volume 1 can be represented as follows:

$$0 = [A_p^f \upsilon_f \rho] - [A_p^r \upsilon_r \rho + A_p^p \upsilon_p \rho] \quad (28)$$

Where:

- υ_f is the feed stream velocity in m/s,
- vr is the retentate stream velocity in m/s,
- υ_p is the permeate stream velocity in m/s,
- A_p^f is the cross-sectional area of the feed line,
- A_p^r is the cross-sectional area of the retentate line,
- A_p^p is the cross-sectional area of the permeate line (all cross-sectional areas in m2).

Approximating the water density as being concentration invariant, Eq. 10 can be expressed as:

$$0 = A_p^f . \upsilon_f - A_p^r . \upsilon_r + A_p^p . \upsilon_p \quad (29)$$

Using the algebraic relation relating transmembrane pressure to the permeate velocity, $\upsilon_p = k(P_{sys} - \Delta\pi)$ Eq. 11 yields:

$$0 = \upsilon_f A_p^f - \upsilon_r A_p^r - k A_p^p (\Delta P_m - \Delta\pi) \quad (30)$$

$k = \frac{A_m K_m}{\rho A_p^p}$ (Or more commonly represented as $k = \frac{L_p A_m}{A_p^p}$) and $\Delta P_m = P_{sys} - P_p$ (P_p is taken to be the same as the pressure of the raw feed). Solving Eq. 3.12 for P_{sys} results in:

$$P_{sys} = \frac{\rho A_p^p}{A_m K_m} (A_p^f \upsilon_f - A_p^r \upsilon_r) + \Delta\pi \quad (31)$$

$$A_p^p = A_p^f = A_p^r = A_p \tag{32}$$

$$P_{sys} = \frac{\rho A_p}{A_m K_m}(A_p(\upsilon_f - \upsilon_r)) + \Delta\pi \tag{33}$$

Where:

- K_m *is the overall feed − side mass transfer coefficient* $(in\ m/s)$,
- A_m *is the effective membrane area* $(in\ m^2)$, and
- Lp *is the membrane permeability* $(in\ m\ s^{-1}Pa^{-1})$.

Substituting Eq. 31 into the energy balance (Eq. 27) yields:

$$\frac{d\upsilon}{dt} = \frac{A_p^p}{A_m K_m V}(A_p^f \upsilon_f - A_p^r \upsilon_r) + \frac{A_p^r}{\rho V}\Delta\pi - \frac{1}{2}\frac{A_p^r e_\upsilon \upsilon^2}{V} \tag{34}$$

The Δπ term represents the osmotic pressure difference across the reverse osmosis membrane. Δπ is function of salt concentration (Salinity) and the temperature of the solution. A mathematical relation is needed to estimate the overall osmotic pressure.

$$\Delta\pi = \delta C_{eff}(T + 273) \tag{35}$$

Where:

- $\boldsymbol{\delta}$ = 0.2641,
- The osmotic pressure, π, is in Pascals,
- $Ceffective$ is in ppm, and
- T is in ◦C.
- $Ceffective$ is the value for the effective overall concentration

Average value should provide accurate results for low recovery operations $(0.5(C_{renetate} + C_{feed}))$, but for high recovery, this assumption fails to consider the non-linearity of the salt concentration profile with respect to the distance from the entrance of the membrane. Work using the log-mean average [95].

$$C_{effective} = aC_{feed} + (1 - a)C_{renetate} \quad (36)$$

Where:

- C_{feed} is the amount of total dissolved solids (TDS)in the feed stream (in ppm or mg/L).
- a is a dimensionless effective concentration weighting coefficient (a = 0.5 as an assumption).
- $C_{renetate}$ is the salt concentration in the retentate (or concentrate) stream (in ppm or mg/L).

An equation directly relating the feed concentration to axially average osmotic pressure difference is used:

$$\Delta\pi = f_{os}C_{feed}\frac{ln(\frac{1}{1-Y})}{Y} \quad (37)$$

$f_{os}$is a dimensionless empirically obtained constant (f_{os}= 78.7) [95], and Y is the overall system recovery:

$$Y = \frac{Q_p}{Q_f} \quad (38)$$

Q_p is the permeate stream flow rate and $Q_f$is the feed stream flow rate.

2.5.8 Condition-based maintenance and predictive maintenance case studies

Condition-based maintenance (Scheduling maintenance), which applies according to continuous machine measurements, is one of the most effective and applicable methods [82]mentioned. The International Foundation for Research in Maintenance and its abbreviation (IFIRM) mentioned condition-based maintenance is employed to 80% of the

maintenance operations as its cost-effective. Using the time and frequency domain in the vibration analysis to detect the centrifugal pump impeller crack. This paper [83] measured pump vibration under healthy conditions first. Then they did generate nine different artificial cracks in the pump impeller. As an indicator for failure severity, increasing the impeller amplitude passing time and frequency vibration index. Every machine generates a warning when there is a failure based on continuous machine measurements using a specific transducer to diagnose and detect that fault [8]. Centrifugal pump volute casing failure detection and optimization have been studied by [84]. They did present volute casing fatigue life expected for both real failed and optimized. (University of Strathclyde) has observed a high vibration level at impeller blade passing frequency and its harmonics. They designed a fault analysis and diagnosis simulation (FADS) computer-based system. The pump vibration effect on the unbalance and misalignment have been studied by [85] The pump overall vibration level was extremely high compared with ISO 10816-1.

Zouari et al. [86] used artificial neural networks to build a diagnosis system for centrifugal pumps based on fault classifier for different fault conditions and pattern recognition such as (misalignment, cavitation, partial flow, and air injection). While developed rotor crack and wear detection, and diagnosis in a centrifugal pump built-in software-based system's output measurements by Rainer Nordmann and Martin Aenis [87]. Carsten et al. [88] developed a fault detection and isolation algorithm in a centrifugal pump using structural analysis. [81] used vibrations frequency spectrums and sound pressure levels to develop a centrifugal pumps faults diagnosis method. Based on power signatures/signals and motor current. Centrifugal pump faults (cavitation and impeller degradation) a diagnostic approach has been developed by Hernandez-Solis and Carlsson

[89]. Process controls take essential place in the desalination industry for it is responsibility in increases the plant lifetime also decreases downtime and maintenance cost [80] as shown in the figure below. Proposed controlling water treatment plants in a smart environment by gathering data and analyzing these data to achieve water desalination most efficient approach operations. They integrated new-age technologies with the desalination plants such as IoT, Network communication, Cloud Portal, Sensors powered by solar energy. Were essential for effective and efficient desalination system operations. Saudi Arabia is developing a smart city along the northern red seacoast to be the first country with desalination solar parabolic mirrors dome [Saudi Neom Smart cities, 2020].

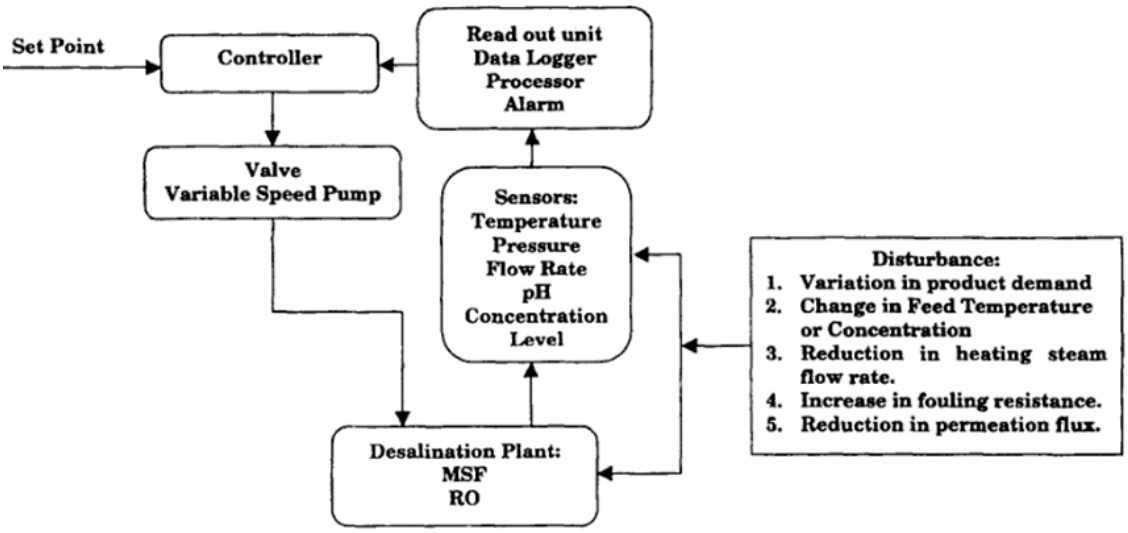

Figure 2.14: Desalination System Process Control

2.5.9 Monitoring

In the last decade identifying fault occurrence in time was a challenge not only in mechanical components but in several industrial components. These industrial components are subjected to different uncertain environmental conditions and damage caused by acoustic emissions, misbalance, misalignment, occasional shocks, poor power quality,

supply imbalance, and vibrations, and the way it is handled, which can lead to unscheduled maintenance interventions which is difficult to perform and expensive [5, 8]. Nowadays with the development of the diagnostic abilities in the health monitoring area because of the enhancement of the sensor's technologies, data driven techniques, big data analytics, data preprocessing, machine learning, signal processing algorithms, smart control, artificial intelligence, and the development of the computational power. Health monitoring advancing the evaluating and monitoring of the industrial systems by improving the systems reliability and life cycle management and avoiding machines shutdown for more periodic maintenance and breakdown time.

2.5.10 Dashboards

Dashboards allow for all processing, storage, and calculations to be conducted in one location. They also present the necessary information quickly and in an easy-to-understand format so that decisions are made with more knowledge and can yield better results. Once the fault detection models have been implemented, the analysis and results will need to be presented to allow users to quickly understand any problems and inform their decisions. Additional benefits of these dashboards are the ability to enhance training and facilitate knowledge transfer through simulating hands-on experience. A key part of these dashboards is that the information presented is customized and tailored to fit the needs of different users. Two sample views are shown in Figure 15. The left side shows a user the health status of the multiple water desalination plants they are overseeing, an executive might use this view to make decisions. The right side shows the health and status of a specific system and the fault detection analysis.

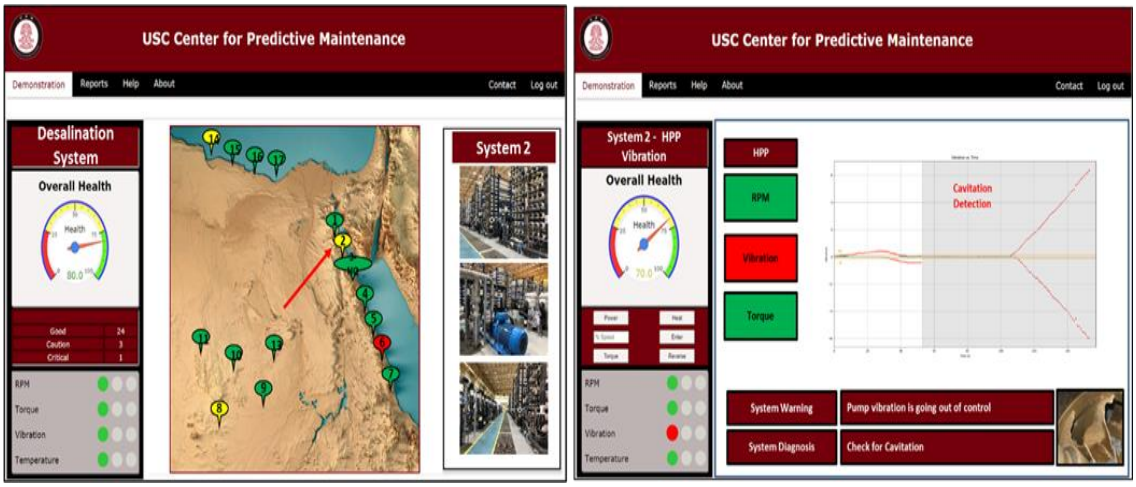

Figure 2.15: Dashboard Views

CHAPTER 3

APPROACH

This chapter represents the research plan, in both theoretically and a roadmap showing the how the research started and what was the final goal of this research, a brief introduction on Amesim methodology and why we are using this software to build the digital twin. A RO membrane digital model roadmap and how tests was applied for validating the digital model and how the digital model was integrated with Amesim software.

3. APPROACH:

1. Build an Amesim model for a 1-piston pump, including suction and discharge check valves.
2. Construct a one-stage reverse osmosis membrane digital model using C-language.
3. Validate the dynamic behavior of the two-models using P, Q, valve displacement waveforms.
4. Extend the HPP-model to include 3-pistons.
5. Extend the RO membrane model to be a three-stage membranes digital model.
6. Integrate the three-piston pump with energy recovery device.
7. Validate the dynamic behavior of the 3-pistons pump energy recovery device model and the three-stage membrane digital model.

8. Integrate the HPP – ERD and digital membrane model to achieve a water desalination digital twin.
9. Validate the HPP – ERD and digital membrane model to achieve a water desalination digital twin.
10. Cross-validate the whole model using dynamic simulation data from Amesim using real-world data from physical system.
11. Using Ameism model for design improvements and achieve a water desalination smart system.
12. Using various digital models and machine learning models for monitoring and fault detection different systems components.

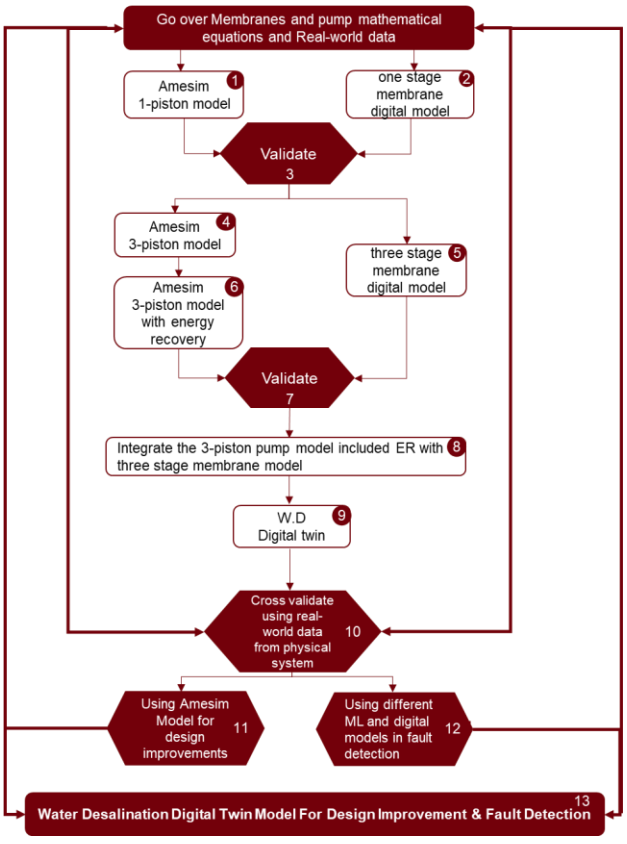

Figure 3.1: Digital Twin Construction Plan

3.1 BUILDING PHYSICS-BASED DIGITAL TWIN OF THE HIGH-PRESSURE PUMP (HPP):

Digital twin is the virtual representation for the physical systems. This virtual representation can be representing the physical system dynamics and the products [12]. The digital twin can achieve based on one digital model or combination of digital and mathematical models, such as computational fluid dynamics, finite element analysis, thermodynamics, kinematic, dynamic, and machine learning models. These models can be simulated or experimented with real-world data [14]. The digital twin is used to simulate and generate data under healthy environmental and harsh conditions and properties, shuffling these generated data with the real-world collected data to improve the digital twin accuracy. Using digital twin helps decision-makers better understand the system and improve and optimize the design, manufacture, health monitoring, and performance. Digital twins can also be used in predictive maintenance by generating sets of faulted data under different harsh conditions and integrating them with machine learning and real-time control algorithms to teach the physical system to detect and classify the faults in real-time and react accordingly to each type of failure. Augment digital twin model in the predictive maintenance area aims to predict and prevent future faults from occurs [1]. In our research paper, the machine learning model and saw-tooth model will be integrated together to detect cavitation and implement more unsupervised algorithms to the machine learning model to generates several faults data sets and classify the fault severity. For example, our use case in this paper is the cavitation fault the machine learning model will be able to classify what type of cavitation based on the location of bubbles implosion, the location of the cavity inception, and the difference in the frequency range. After integrating the HPP

digital model together and achieve HPP digital twin move forward to the following water desalination system components such as the RO membranes to the next element. When each component has its own digital twin, start to connect all these digital twin models to achieve a smart water desalination plant; after that, it combines more than one plant to be monitored from one dashboard. The following are the steps to build a digital twin:

- Understand the physics that governs the operation of the physical system (pump)
- Determine the input/output variables (that can be measured) and the design parameters that control the performance
- Build physics-based digital models to simulate the pump behavior under healthy environmental and harsh conditions and to detect and predict the future faults.

  Interconnect the physical system (pump) and its digital models.

3.2 AMESIM MODEL FOR CONVENTIONAL 3 PISTON PUMP

In order to model the three-piston high-pressure pump energy recovery device, we started by modeling a single-piston pump, including suction and discharge check valves without the energy recovery section. Validated the dynamic behavior of the model using pressure, flowrate, valve displacement waveforms, we extended the model to include three pistons by repeating the model of a single piston with 120 phase shifts and then validated the results with the real-world data. When the three-piston pump was ready and validated, we integrated it with the energy recovery device and validated it as well. The Flow chart illustrating the steps of modeling 3-piston reciprocating pump energy recovery device in Amesim is shown in Figure 3.2, and those steps are listed as follows:

1. Build an Amesim model for 1-piston pump including suction and discharge check valves.

2. Validate the dynamic behavior of the model using P, Q, valve displacement waveforms.
3. Extend the model to include 3-pistons.
4. Validate the dynamic behavior of the 3-pistons pump model.
5. Integrate the three-piston pump with energy recovery.
6. Validate the dynamic behavior of the 3-pistons pump energy recovery device model.
7. Validate the whole HPP digital model using dynamic simulation data with the real-world data and the HPP physics.

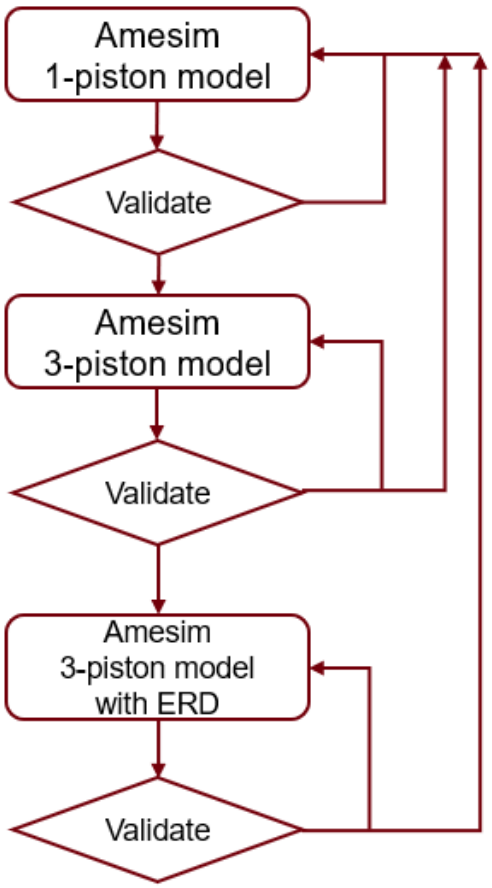

Figure 3.2: Steps to Model the 3-piston HPP of RO Desalination Plant in Amesim

3.2.1 Reverse Osmosis Membrane Digital Model:

In order to build a reverse osmosis membrane digital model, we started by modeling the membrane as a black box which is generating feed pressure (Load) on the high-pressure pump. Starting by deriving equations by two different methods, comparing these methods together and calculate the mean square difference between them, choose a final method to go with, validating this method sensitivity with different tests such as:

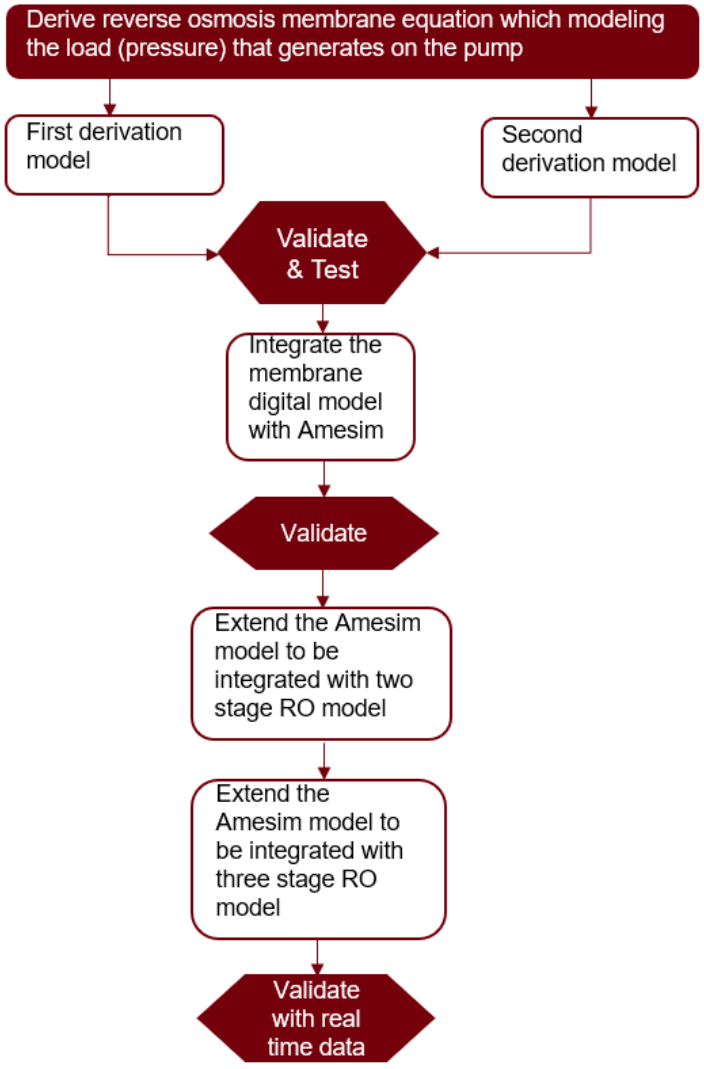

Figure 3.3: Membrane Digital Twin Modeling & Integration Plan

Recovery test: changing the membrane recovery variables and plot the high-pressure pump feed pressure versus time with different membrane recoveries and study the relation of increasing the recovery with the generated feed pressure as Recovery impact both the flow rate and the average solvent flux (J_v) which took place in our equation in permeate flow rate and hydrostatic pressure terms. which generate extra feed pressure or reduce it.

Salinity test: changing the feed water salinities and plot the high-pressure pump feed pressure versus time with different salinities to study the relation of increasing the feed water salinity with the generated feed pressure as Salinities impact $\Delta\Pi$ and the average solvent flux (J_v) which are important factors which generate extra feed pressure or reduce it.

Temperature test: changing the feed water temperatures and plot the high-pressure pump feed pressure versus time with different temperatures to study the relation of increasing the feed water temperature with generated the feed pressure as Temperature impact both $\Delta\Pi$ and the average solvent flux (J_V)which are important factors which generate extra feed pressure or reduce it.

Hydraulic losses sensitivity test: by removing the hydraulic losses term from the feed pressure equation to observe and study the membrane hydraulic losses impact on the feed pressure.

Order of magnitude analysis test (weighted analysis): that test had been done by analysis each term in the equation to study and observe which term impact most and the model is more sensitive to it.

After validating the reverse osmosis membrane digital model with these tests. compared and validated it with theoretical membranes models as well as real world data model, integrated it with the high pressure pump with energy recovery device digital model in Amesim with integrated damper and without the damper, validating the simulation results and comparing it with real-world data and theoretical models, extended the reverse osmosis to be two stage membrane model, integrated the two stage model with Amesim and validating it then we moved on to extend the membrane digital model to be a three stage membrane model, integrated it with the Amesim model, validated and calibrated the model with the physical system in Egypt.

CHAPTER 4

PHYSICAL SYSTEM

This chapter represents each team role in the project, the water desalination physical system designed, manufactured, and took place in Egypt. The adequate sensors and data acquisition system used to collect real-world data, the frequent faults that occur in both the piston pumps and centrifugal pumps.

4.1 SYSTEM COMPONENTS

- 250 Gallon Bottom Tank: the tank is made with FDA-approved resin - 100% potable and safe for drinking.
- Valving and cleaning assembly: The valving and cleaning assembly can be mounted above or below the waterline and is designed to be mounted vertically using the integral mounting bracket. The control valves mounted on the assembly will need to be accessed each time the water maker is in operation to perform the system freshwater flush and for pickling the water maker for longer-term storage. The valving and cleaning assembly has two three-way valves in the standard operating configuration.
- Boost pump: is the feed pump for the high-pressure pump it should be self-priming pump, in an accessible place below or above the waterline aiming easier future

maintenance. and the feed pump motor must always be run with the fan turning to keep the DC motor cool.

- Pre-Filter: The pre-filter should be in an accessible place for assemblies as it requires periodically changing.
- High-pressure pump and motor assembly: High-pressure pump is assembled with the motor by mounted them on a horizontal platform.

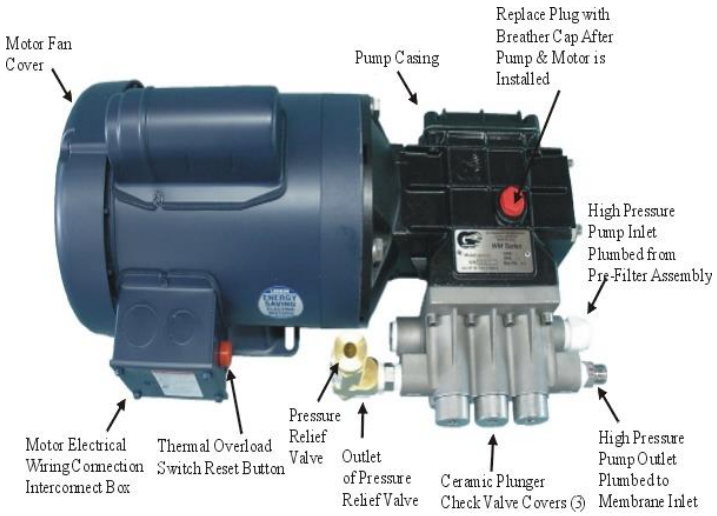

Figure 4.1: 2.3 gpm Pump and 1.5 HP Motor

- RO Pressure vessels: The reverse osmosis membrane can be assembled in any place within the system. It also can be assembled in any orientation either vertical or horizontal whatever gives better control access. Attaching to the pressure vessels is a flow meter which needs to be vertical.
- RO membranes: The demo includes DOW Filmtec® reverse osmosis membranes. with three 2.5" × 40" As per Dow's technical specifications, permeate water flowrate for each element may have the variance of +/- 20%. Based on DOW Filmtec® data sheet the membrane can work with 32,000 ppm NaCl.

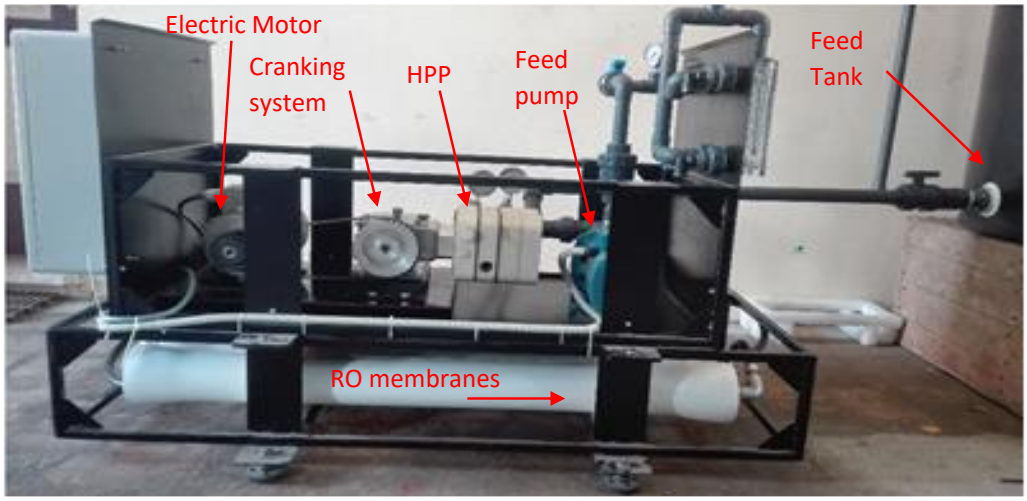

Figure 4.2: Small RO desalination plant designed by the Egyptian team at the BUE and EDRC

4.1.1 Sensors and data acquisition system:

In the last decade identifying fault occurrence in time was a challenge not only in mechanical components but in several industrial components. These industrial components are subjected to different uncertain environmental conditions and damage caused by acoustic emissions, misbalance, misalignment, occasional shocks, poor power quality, supply imbalance, and vibrations, and the way it is handled, which can lead to unscheduled maintenance interventions which is difficult to perform and expensive [5, 8]. Nowadays with the development of the diagnostic abilities in the health monitoring area because of the enhancement of the sensor's technologies, data driven techniques, big data analytics, data preprocessing, machine learning, signal processing algorithms, smart control, artificial intelligence, and the development of the computational power. Health monitoring advancing the evaluating and monitoring of the industrial systems by improving the systems reliability and life cycle management and avoiding machines shutdown for more periodic maintenance and breakdown time. To monitor the health Water desalination

system, we should start by monitoring the three main physical components: Motor, HPP, and RO membrane. Achieving a smart fault detection system for the water desalination system is our product goal.

To monitor the HPP: we should start by monitoring the pump flow rate and pressure behavior. We need to attach two pressure sensors at the pump outlet (static & dynamic). The static pressure sensor is used to study how much is the requiring pressure to beat or overhead the osmotic pressure generated. In contrast, the dynamic pressure sensor is used to monitor the behavior of each piston of the pump and detect pump fault root causes (such as if there is a broken seal or damper). A third pressure sensor is attached to the pump inlet to measure feed pressure and detect if feed suction pressure is insufficient. One flowrate sensor is attached at the feed tank outlet or at the HPP inlet. It compares the flowrate measurements from this sensor with the theoretically calculated flowrate to detect a flowrate leakage. Vibration sensors are used at the pump casing perpendicular to the pistons to monitor the three pistons and study from the vibration peaks if there is a broken piston, seal, bearing, etc., and the piston's behavior and if there are contaminations in the pump casing. Two other vibration sensors are attached to the crankcase beside the poly and perpendicular to the bearing and the other sensor perpendicular to the second bearing. There are two bearings in the pump to bearings and crank behaviors as crank rpm.

To monitor the RO membrane: Two flowmeters are attached; one at the brine water outlet and the second one at the permeate water segment outlet to monitor the membrane recovery and detect any faults such as fouling and scaling. A pressure sensor should be attached at the brine segment outlet to detect the pressure drop and to check the inlet recovery unit pressure to monitor the recovery unit efficiency to calculate the saving power.

Two salinity sensors should be attached to the brine segment and the other one at the permeate segment to measure the salinity and monitor the membrane efficiency.

To monitor the motor: we can start using a stroboscope to study the motor rpm behavior and detect the vibration. Two vibration sensors on the motor are at the drive end (bearing) and the other sensor at the non-drive end (fan) to monitor the health of the motor bearings and a coupling misalignment.

The water desalination system digitalization process is helping the system to recognize any changes happening in the operation and monitoring the system components performance. Digitalization the system will also protecting the system component from damages and monitoring the system components performance in response to variable factors such as changing in the flowrate, pressure fluctuation, and power which leads to vibration and other mechanical and hydraulic failures. For achieving system performance most efficiency, health monitoring, performance, and fault prediction it requires placing sensors in system essential locations which we determined above.

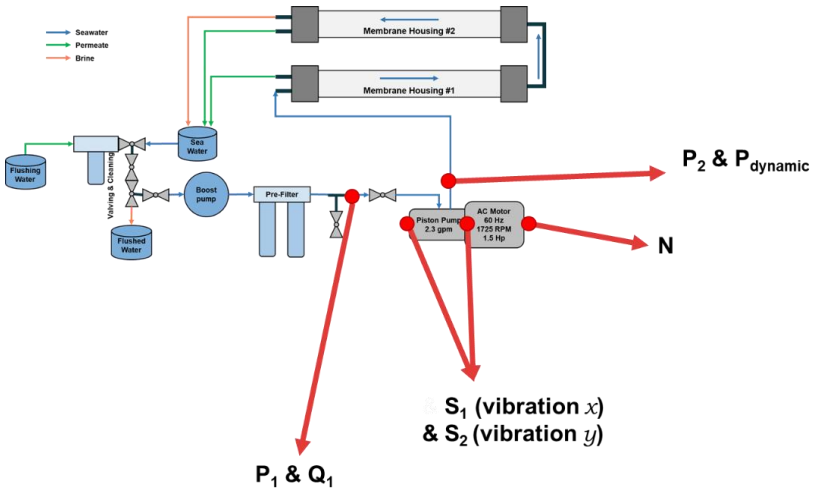

Figure 4.3: Diagram of sensor distribution

A. **Vibration Sensor:** The 603C01 is one model in a very diverse line of 603-Series accelerometers. The 603-Series includes alternative sensitivity models, hazardous area approved models, dual output models and models with an integral cable.

B. **Dynamic pressure sensor:** High frequency ICP pressure sensor, 5000 psi, 1 mV/psi, 3/8-24 mtg thd, accel. comp., ground isolated.

C. Static pressure sensor: Measuring range 0: 10 bars, Analog output: Analog, current 420 mA, Operating voltage: 8.32 VDC, Accuracy: ±0.5 % FSO BFSL, Connection: Connector, M12x1-Male, 4-pin, Process connection: G 1/4" (DIN 3852), Process connection material: Stainless steel (1.4301), Housing material: Stainless steel (1.4301), media temperature: -40 to 125 °C.

D. **Flow meter:** Precise detection of flow and medium temperature. Suitable for water, coolants, oil, and glycol solutions thanks to integrated measurement graphs. Reliable backflow prevention with very fast response time. With switching output, analog output or frequency output and IO-Link. Clearly visible LED display with red/green color change

E. **Photoelectric sensor:** Compact, High-Performance Sensors with 18 mm Threaded Lens or Side Mount, Maximum Operating Temperature: 70 C, Minimum Operating Temperature: -20 C, Switching Current: 150 Ma.

Figure 4.4: A. Vibration Sensor, B. Dynamic Pressure Sensor, C. Static Pressure Sensor, D. Flow Meter, E. Photoelectric Sensor

4.2 FAILURES & FAULT DETECTION:

According to all engineering principles, models and concepts are working forward to reduce money, time, and effort. Nowadays a lot of countries are suffering from shortage of water supply and hence using RO water desalination is one of the commonly used systems. One of the major parts in the water desalination system is the Pump as it is the most expensive part of the system. The system membranes are acceptable to change them every 6 months to one year, but you cannot change your pump every 6 months or even every year. Fault detection digital twin is essential in the water desalination industry. There are many water desalination systems in remote areas, which may be for civilians like cities or hotels or maybe for the army like army basis. Sometimes these systems are the only source of freshwater for these areas, and if it did break, it would be a nightmare for the people living/settled as water is an actual human need.

Either single-stage or multi-stage centrifugal pumps prevail the desalination plants for feeding and pressurizing the feed stream. Common problems experienced by

centrifugal pumps such as cavitation, water hammering, sludge, high-pressure pulsation, excessive power consumption, and other mechanical and hydraulic failures may be attributed to one or several probable causes. Low suction pressure and low flow rate problems can be attributed to either air leaks in inlet piping or a faulty mechanical seal [1]. Centrifugal pumps cavitation can also lead to the same problems. Excessive lateral or axial vibration and noise can also be attributed to either pump rotor misalignment, excessive axial thrust or cavitation and reduces the pump efficiency.

4.2.1 Fault Detection

Fault detection improves the system reliability, safety, energy, and cost-efficiency, extends the pump lifetime and performance, achieves the efficient maintenance strategy, and reduces occurring unpredicted events that can lead to system shutdown and breakdowns. Early fault detection and diagnosis are essential to ensure cost-effective and safer operation to avoid performance degradation, unpredicted maintenance events, product deterioration, minor and major damage to the physical system, damage to human health, or even loss of lives. This paper focuses on one type of fault which is the cavitation as a use case due to its frequent occurrence. Many papers have been done fault detection in the pumping system based on speed variation and vibration details using signal processing and statistical models or based on machine learning algorithms that identify the cavitation using speed and pressure historical data [6, 7]. This research presents three different digital models that is used for fault detection. The first model was built using Amesim software by simulating the water desalination digital model under harsh and uncertain environmental conditions, generate different faults to train the system on detecting them.

Hydraulic Failure:

Hydraulic failure arises from changes in pressure either in the volute or the pipes leading to the pump due to changes in factors such as temperature, velocity, and volumetric flowrate of the fluid. Common failure types:

- Cavitation,
- Pressure pulsation,
- Radial and axial thrust,
- Suction and discharge recirculation
- Valve Fault
- Membranes

Mechanical Failure:

Mechanical failure can be generated from several different parts of the pump including bearing, seals, lubrication in the pump and other miscellaneous parts. Types of failures:

- Bearing Failure
- Seal Failure
- Lubrication Failure
- Excessive vibration
- Piston leakage
- Damper fault
- Crank shaft fault
- Fatigue

This Model will focus on four types of faults which take place in:

- Crank shafts
- Valves
- Pistons
- Dampers
- Membranes
- Cavitation

The second and third models presents two different fault detection digital models one using the saw-tooth model that can express the excitation of the centrifugal pump under cavitation with Fourier expansion and describe the periodic function with combination of sine and cosine waves instead of transfers the real-world data from time domain to frequency domain which made this model more cost and time effective. As the pressure pulses within the diffuser tongue region can be modeled as a sawtooth wave, each pressure pulse acts on the blade's projected area, resulting in a periodic exciting force on the rotating impeller. Each blade projected area has a zero value at both the beginning and the endpoints of the blade-diffuser interaction region. Therefore, it can also be approximated in terms of another saw-tooth wave. The saw-tooth digital model was successfully integrated and tested with the physical system, and it showed its accuracy, as shown in the section below. The second cavitation detection model is a machine learning model that integrated three machine learning algorithms-- the support vector machine, k-nearest neighbors, and logistic regression. The data analysis is based on millions of real-world historical data points that are processed from mounted sensors on the physical system, the data were mainly collected from six different parameters vibration sensors, dynamic and static pressure sensors, and flow rate sensors. Based on this machine learning model, potential

cavitation faults are successfully classified and recognized, ensuring 99.5% prediction accuracy after preprocessing and training 80% of these data sets and testing the 20%. Faults Results and simulation will be discussed in the results and discussion chapter.

Cavitation can be considered as a major cause for centrifugal pump failures. In the first phase of cavitation, vapor bubbles are formed around the pump's impeller in areas of relatively low pressure below the associated vapor pressure of the working fluid. While in the second phase of the cavitation, the collapse of these bubbles allows the triggering of intense shockwaves leading to high-speed fluid particles impact causing significant pitting and erosion of the internal pump parts [9]. Cavitation is a main source of centrifugal pumps health and performance degradation. Several researchers employed CFD analysis [1] to detect cavitation and evaluate its effect on the rotor and the pump's casing, which allowed the minimization of the experimental investigations.

Cavitation analysis is performed at different operating conditions including different pump speeds and flowrates. The detection of bubbles formation by CFD analysis is performed by allocating the zones where pressure is lower than the associated vapor pressure of water. Figure 2 presents a flow field visualization at the suction side of a centrifugal feeding pump impeller-diffuser arrangement where symptoms of vapor bubbles formation at the leading edges of vanes are shown [1].

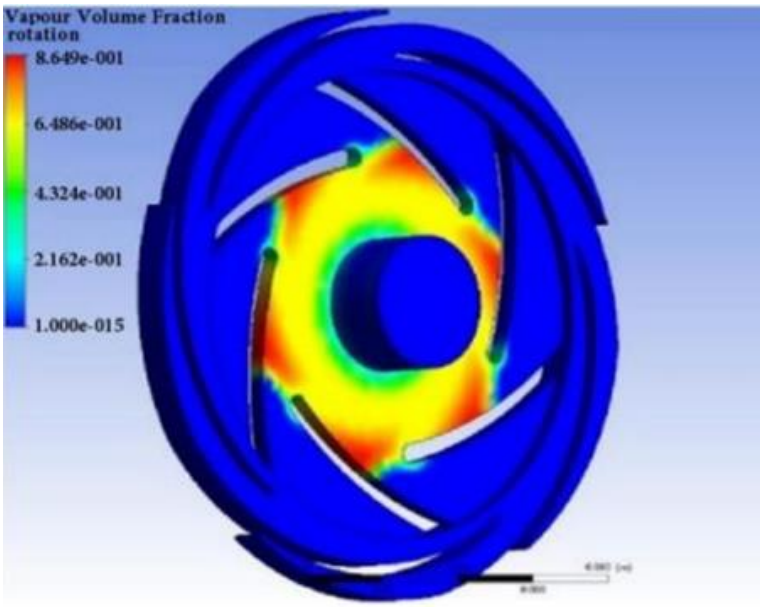

Figure 4.5: CFD Cavitation Zones Detection [22]

CHAPTER 5

DIGITAL MODELS

The purpose of this chapter is representing the three digital models that were used in this research from each one methodology and what was it's used for. A description of the Amesim software and how it was used and applied the physical water desalination system parameters and validating it is behavior. A brief description on the machine learning models that was used in this research for fault detection and the type of data that was implement with these models.

5.1 Amesim model

5.1.1 Amesim Methodology

Simcenter Amesim is a commercial simulation software for the modeling and analysis of multi-domain systems. It is part of the systems engineering domain and falls into the mechatronics engineering field. The software package is a suite of tools used to model, analyze, and predict the performance of mechatronic systems. Models are described using nonlinear time-dependent analytical equations representing the system's hydraulic, pneumatic, thermal, electric, or mechanical behavior. To create a simulation model for a system, a set of libraries is used. They contain pre-defined components for different physical domains. The icons in the system must be connected, and for this purpose, each icon has ports, which have several inputs and outputs. Causality is enforced by linking the inputs of one icon to the outputs of another icon (and vice versa).

5.1.2 Amesim model for water desalination system.

In order to model the main components of a water desalination system contains an electric source, feed pump, filter, three-piston high-pressure pump energy recovery device, three-stage reverse osmosis membranes. We started by modeling the HPP with a single-piston pump, including suction and discharge check valves without the energy recovery section. After validating the dynamic behavior of the model using pressure, flowrate, valve displacement waveforms, we extended the model to include three pistons by repeating the model of a single piston with 120 phase shifts and then validating the results with the real-world data. When the three-piston pump was ready and validated, we integrated it with the energy recovery device and validated it as well. In parallel modeling one-stage RO membrane as a black box in the WD system in order to calculate the required generated system feed pressure, brine pressure and the permeate flowrate under different conditions. After validating the dynamic behavior of the model, extended the membrane digital model to be a 3-stage RO membrane and integrated it with the three-piston high-pressure pump energy recovery device. Then connect this model with a small centrifugal feed pump, a filter, and a motor (electric source). The Flow chart illustrating the steps of modeling water desalination system in Amesim is shown in Figure 3.1 in chapter 3. Below will be attached a few Amesim simulations and modeling screen shots.

Figure (a) shows the mechanical, hydraulic, and thermal components used for modeling this pump and how they are connected after assigning the fluid properties and the motor parameters. The piston-cylinder is simulated of three parts: the piston, a suction valve, and a discharge valve.

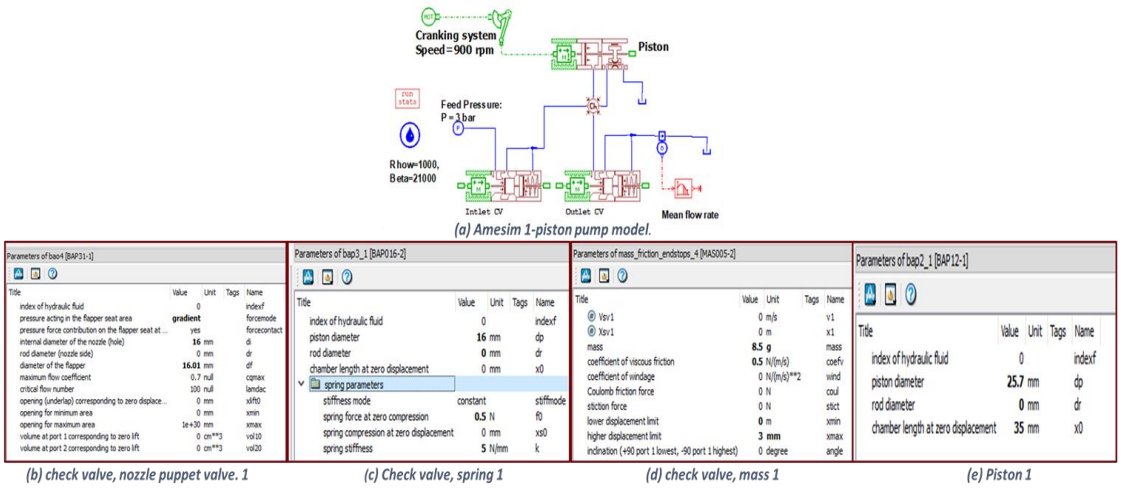

Figure 5.1: Amesim model for a one-piston pump

This cylinder is connected with a crankshaft that takes its rotational power from the attached motor. While figures (b, c, d, e) show each component's parameter setting from the check valve, the spring, piston, and the masses.

One of the advantages of using Amesim to model the piston pump (or any other mechanical system) is that it requires minimal effort to understand the physics governing the system. Amesim uses components from its library to build all governing mathematical equations of the system and solve them to describe the dynamic behavior. Mechanical components such as piston, mass, spring, and crankshaft are used to build a 1-piston pump as shown in Figure 5.1. All the physical parameters of the components are adjusted to replicate the actual HPP used in a small RO desalination plant in the EDRC in Egypt.

The way of assigning the parameters helps to achieve a more accurate model, giving the user a better chance to start working on different designs to improve the system's efficiency. Try different kinds of highly recommended candidate materials which can be cheaper, like composites and 3D- plastic, and simulate the system

behaviors with these new designs and materials and check if they will give more accurate results. Also, generating different kinds of faults to study and train the system to detect it. Figure 5.2 shows separate one-piston pump Amesim model simulations. The first one at the top shows the flowrates behavior of the piston as the red plot shows the piston's discharge flow rate, the yellow plot shows the piston's suction flow rate, and the blue plot shows the overall piston's flowrate. This figure shows the accuracy of the flowrate behavior model and the valves as observed here while the suction process takes place, no discharge takes place, and vice versa.

The middle simulation below shows the pressure behavior at the cylinder’s chamber, where the behavior shows how the suction phase, pressure build phase, and discharge occur at this plot. In contrast, the third simulation at the bottom shows the physical displacement behavior of both the suction and discharge valves. The yellow curve shows the suction valve displacement, and the red curve shows the discharge valve displacement. After building the 1-piston pump and validate its dynamics, we duplicate the same components to build a 3-piston pump. Crankshaft with 120^{o} angular phase shift is used to drive the three pistons, as shown in figure 5.3

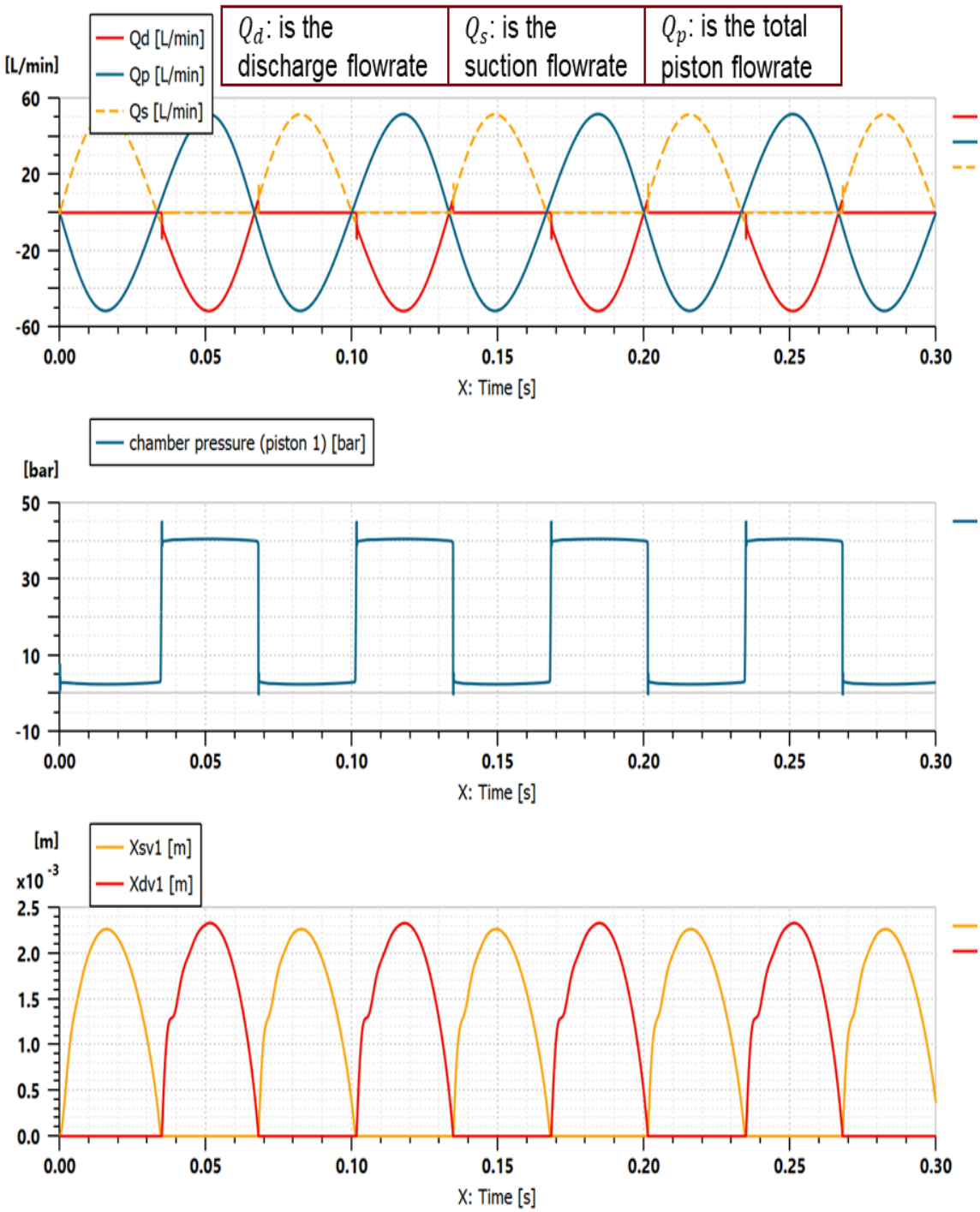

Figure 5.2: Amesim Simulation of the Dynamic Characteristics for the single piston model

.

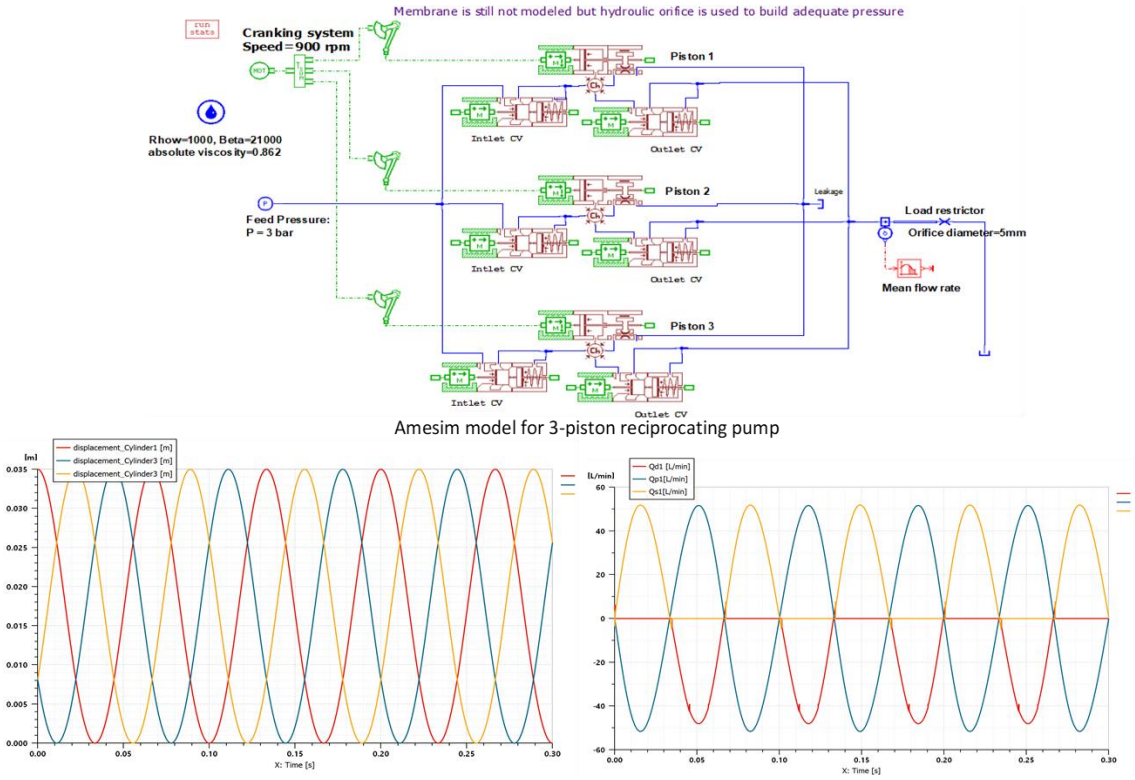

Figure 5.3: Sample signals showing dynamics of the 3-piston pump

Figure 5.3 shows the dynamic simulations of the three-piston modeled pump without integrating the energy recovery device and the damper yet. After validating the model's dynamical and physical behavior, we integrated the three-piston pump model with the energy recovery device and a damper, as shown in figure 5.6. The energy recovery device (EDR) has the same concept as the pressure exchangers used in the pumps. The pressurized brine water will be heading back to the energy recovery device side of the pump's pistons to reduce the amount of power required from the motor. In other words, using the hydraulic brine pressure as a hydraulic power instead of the required electrical power, as shown in figure 5.4. Reciprocating pumps proved themselves in the market as more efficient than the centrifugal pumps.

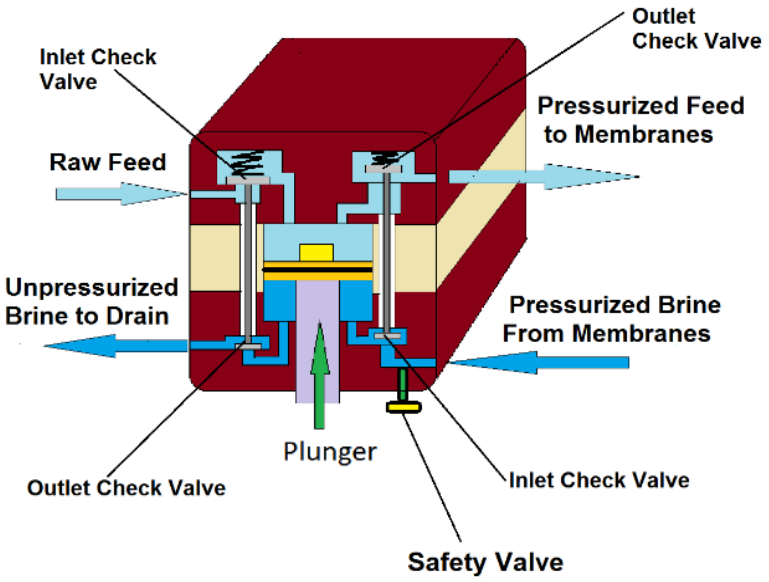

Figure 5.4: High-Pressure Reciprocating Pump with
Energy Recovery (Cross-section showing one piston)

5.1.3 Integrated high pressure pump with ERD with one-stage reverse osmosis

The model has been integrated by following these procedures and as shown in figure 5.5.

1. Build a mathematical **C** model for RO-membrane as a black box in the system which is generating load on the pump.

2. Integrating the **C model with Amesim**

3. Validate the **Amesim** model using the mathematical and physical behaviors of the system and using a MATLAB mathematical model the Egyptian team built it for the whole completed system.

4. Cross-validate the **simulation** results Amesim using **real-world data** from physical system.

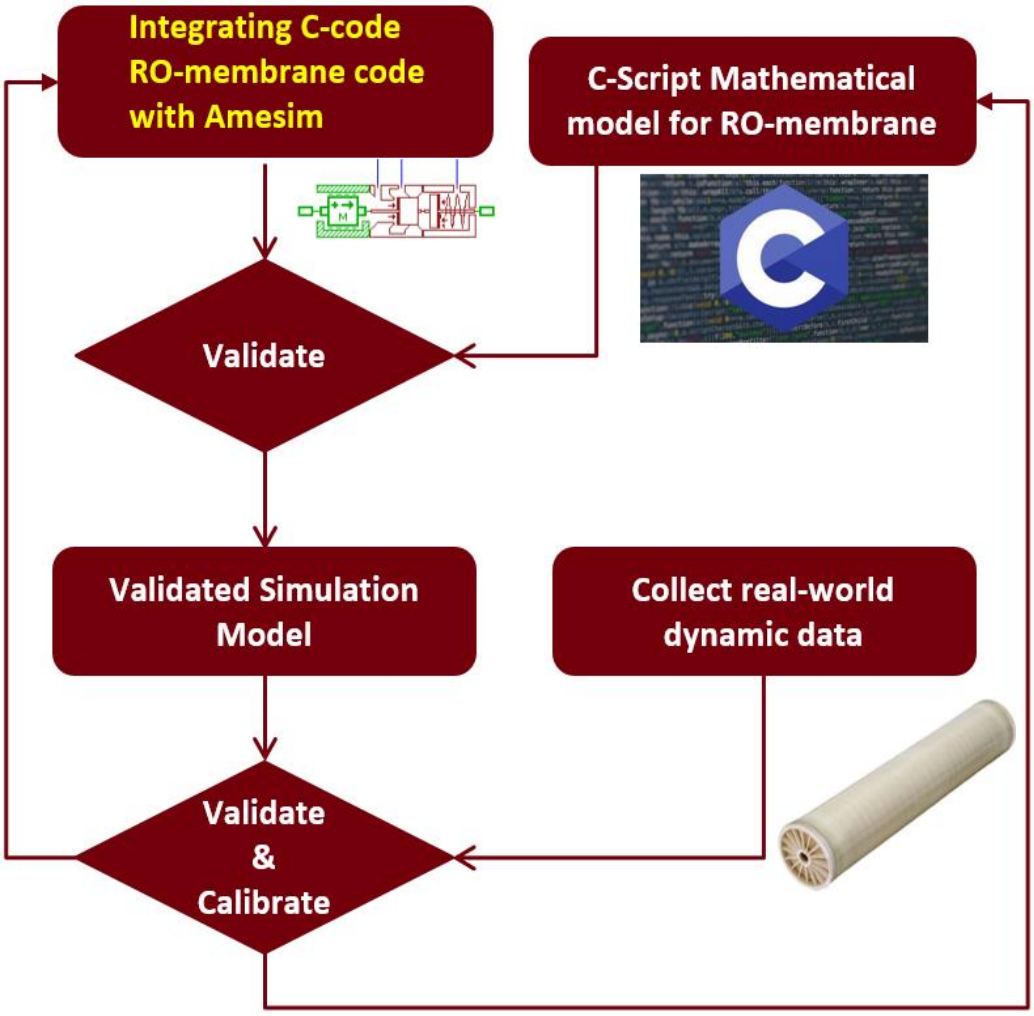

Figure 5.5: Integrating Amesim model with C-Script plan

The model below represents a three pistons pump with energy recovery device integrated with damper and one stage reverse osmosis membrane digital model. the three pistons are connected with a crankshaft with an of 120º between each piston and the other. The high-pressure pump is attached with a motor which rotates with 900 RPM also a feed pump is connected to the high-pressure pump aims to prime the pressure to the HPP to avoid cavitation. Each cylinder includes front side where the suction came from the feed tank and the discharge go to the RO membrane.

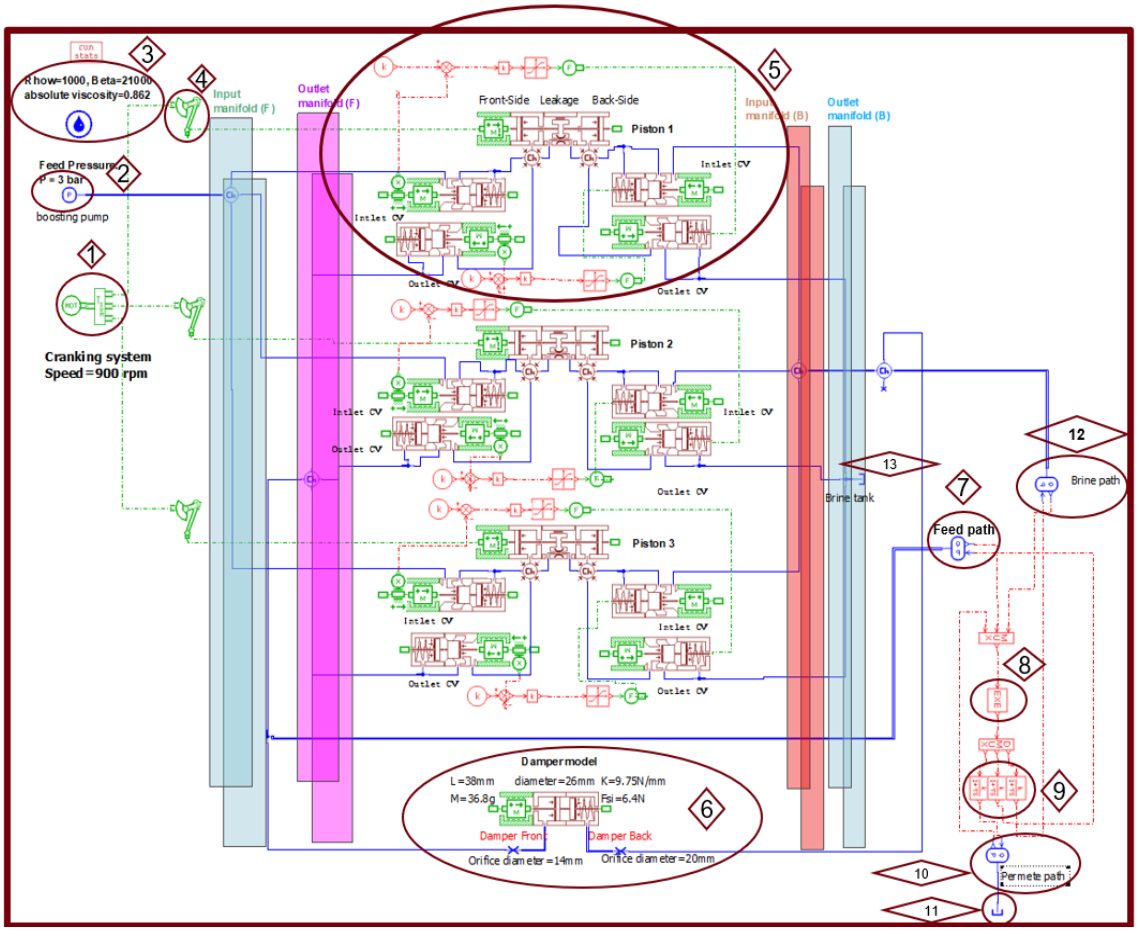

Figure 5.6: Amesim model for 3-piston reciprocating pump with energy recovery, damper, membrane, and displacement sensors.

While the back side which is the energy recovery side the suction come from the brine water discharged from the membrane aims to generate a hydraulic power to save energy by pushing the pistons instead of requiring electric energy from the motor and the discharge flows to the brine tank. Each side includes of two valves one responsible with suction and the other responsible for discharge. Where the main components of this damper are mass to simulate the weight, piston, orifices, and a spring. Also, the digital model is integrated with a one-stage spiral wound membrane which is modeled as a C-script code and attached in the model as an executable file which contains mathematical equation running together in parallel and exchange these variables with the Amesim model in each

part of a second. The membrane digital model simulates the feed path pressure and flowrate, the brine pressure and flow rate, and the permeate pressure and flowrate. Which helps to study the membrane behavior and faults that might occurs at any time such as the fouling, and scaling. The model includes a damper to reduce the vibration, pressure, and flowrate pulsations and fluctuations to extend the pump lifetime by reducing the vibration level, which can harm the pump and the membranes. Where the main components of this damper are mass to simulate the weight, piston, orifices, and a spring. In this model the system runs with 900 RPM to fits the collected data that was gathered in Egypt and be running under the same operating conditions. The system is also running under the same salinity, flowrate, and temperature operating conditions as the physical system in Egypt.

5.1.3.1 The Model Components:

1- The motor attached to cranking system with speed of 900 rpm where the speed is completely independent of the torque on the shaft.

   With N the number of ports on the right, the total torque is computed as

$$ttorq = \sum_{i=1}^{N} torque_i$$

2- Feed pump which builds the pressure up to 3 bars.

3- Hydraulic fluid properties (water) as the liquid have a constant bulk modulus and a constant absolute viscosity which are set with the corresponding parameters. These two parameters must be given at saturation pressure and current temperature. The “density” parameter is used to adjust the liquid density at atmospheric pressure (0 [bar]). The parameter is independent of the temperature. From simulating and including this component in the model A cavitation model can also be included depending on the type of fluid properties.

For example, the diesel fuel is not a single chemical compound but a mixture of chemical compounds with different boiling points and saturated vapor pressures. It follows that cavitation does not occur at a single pressure but rather over a range of pressures. Hence you can set a "high saturated vapor pressure" at which the liquid begins to vaporize and a "low saturated vapor pressure" at which it is complete. Obviously the "high saturated vapor pressure" must be higher than the "low saturated vapor pressure".

4- The first crank shaft with 0º degree angle and the other two crankshafts for the second and third pistons are shifted with a 120º. It is modeled as a perfectly efficient transformer between rotary and linear motion.

5- Is the first pump cylinder which is attached with the first crank shaft with 0º degree angle. Which consists of one piston and four control valves two inlets and two outlets. One inlet and one outlet are taking place either on the pump frond side and the others took place at the pump energy recovery device side (Back side). Main components for the first cylinders are mass components, pistons, chambers, springs, displacements sensors, etc.

6- Is the damper model which took place in the system to reduce the vibration, pressure, and flowrate pulsations and fluctuations to extend the pump lifetime by reducing the vibration level which can be harmful to the pump and the membranes. Where the main components of this damper are mass to simulate the weight, piston, orifices, and a spring.

7- Membrane Feed path where the feed pressure and feed flow rate are simulated.

8- The executable file contains the C-script file code, which is modeling the reverse osmosis membrane as a load (feed pressure) that the high-pressure pump is required to build. The permeate flow rate, brine pressure, Hydraulic pressure (Friction losses), and modeling all the parameters effects the membrane model such as temperature, salinity, recovery etc.

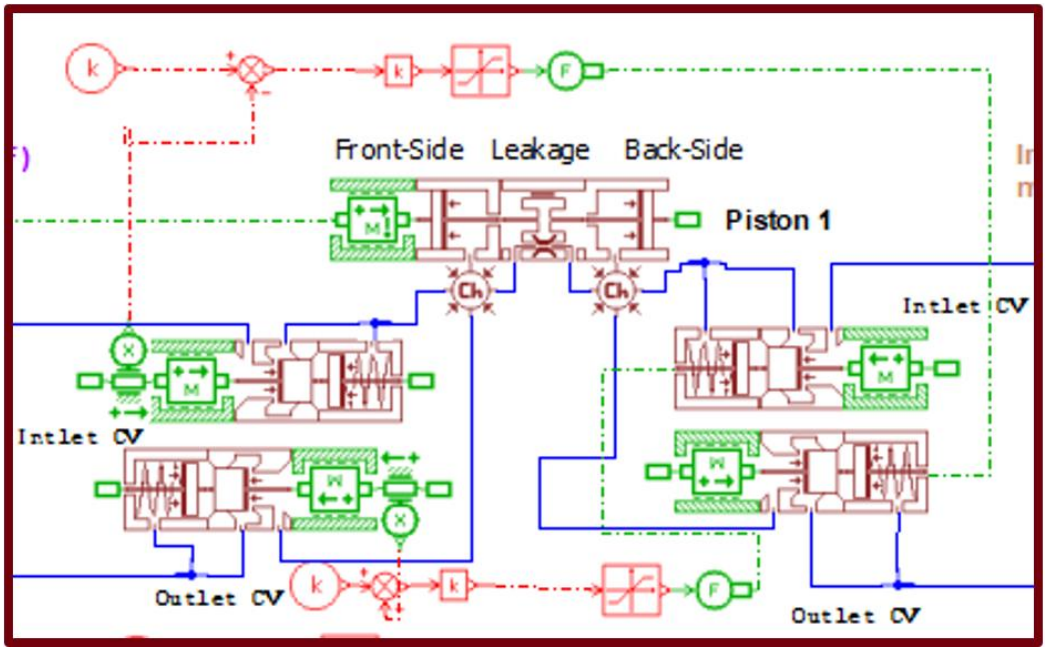

Figure 5.7: The First Cylinder in the Amesim Model

9- They are three components which is simulating the time lag between the executable file and the Amesim model as the simulation results changes with time (part of a second) (k/1+τs)

10- K being the value of gain and τ (tau) is the time constant and the τau unit is second.

11- Membrane permeate path where the permeate pressure and permeate flow rate are simulated.

12- Is the permeate tank.

13- Membrane brine path where the brine pressure and brine flow rate are simulated.

14- Brine tank.

- ❖ More details present about the membrane modeling mathematical derivation.

5.2 SAW-TOOTH MODEL FOR CAVITATION DETECTION IN CENTRIFUGAL PUMPS:

Pressure pulsations developed due to cavitation in centrifugal pumps were investigated experimentally by several researchers [2, 3]. It was reported that interaction between impeller blades and the diffuser results in pressure pulsations which is dominated by the Blade Pass Frequency (BPF)times the number of diffuser tongues [2, 4]. These pressure pulsations are converted into periodic force pulsations affecting the rotor as well as the casing of the pump through the impeller projected area. Ref. [1] presented an illustration that describes how blade-diffuser tongues interaction causes sudden changes in pressure over each blade. This sudden change in pressure is repeated five times which matches the number of diffuser tongues.

In this work the pressure pulses within the diffuser tongue region can be modeled as a sawtooth wave. Each pressure pulse acts on the blade projected area which results in a periodic exciting force on the rotating impeller. Each blade projected area has a zero value at both the beginning and the end points of the blade-diffuser interaction region. Therefore, it can also be approximated in terms of another sawtooth wave.

Equation (39) and Equation (40) presents the saw-tooth function that expresses the pressure pulses.

$$P(t) = 2.Pmax.t/(Tp) \qquad [0 \leq t \leq Tp/2] \qquad (39)$$

$$P(t) = Pmax - 2.Pmax\left(\frac{t - \frac{Tp}{2}}{Tp}\right) \qquad \left[\frac{Tp}{2} \leq t \leq Tp\right] \tag{40}$$

Where; $Pmax$ is the peak value of the pressure pulse and Tp is the period of the pressure pulse. Equation (41) and Equation (42) presents the saw-tooth function that expresses the blade projected area.

$$A(t) = (2.Ao.n.N).t \qquad [0 \leq t \leq 1/(2.n.N)] \tag{41}$$

$$A(t) = (2.Ao.n.N).\left(\frac{1}{n.N} - t\right) \qquad [1/(2.n.N) \leq t \leq 1/(n.N)] \tag{42}$$

Where; Ao is maximum projected area of the blade. n is the number of the diffuser tongues and N is the rotational speed of the pump c.p.s. Fig. 5.9 and Fig. 5.10 present the normalized saw-tooth pressure pulses as well as the blade projected area the during one revolution (1/ N = 0.02857 sec) respectively. Equations (39) and (40) are combined to determine the periodic force acting on each blade due to its interaction with the diffuser tongues during each revolution at the cavitation condition. Fig.4 presents the resulting normalized blade force during one revolution.

Figure 5.8 depicts the normalized force pulsations on the six blades of the impeller, assuming that the first blade of the impeller is at a zero-degree angle and the six blades are equally spaced at 2π/6 rad (60-degree angle).

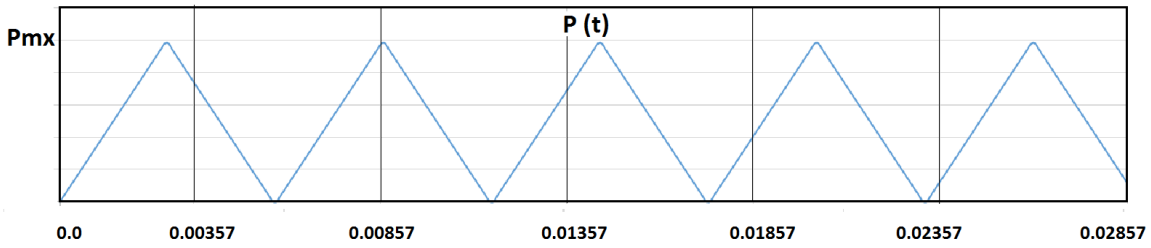

Figure 5.8: Normalized Saw-tooth Pressure Pulses During One Cycle.

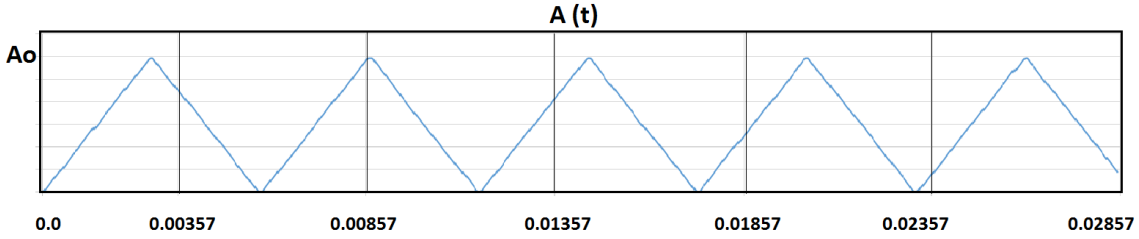

Figure 5.9: Normalized Sawtooth Projected Area of The Blade During One Revolution.

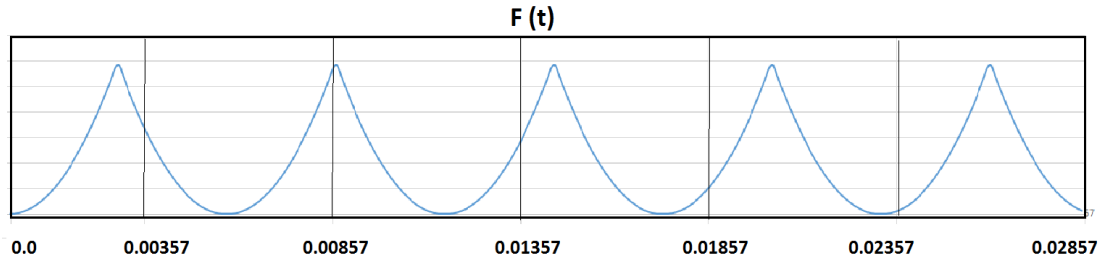

Figure 5.10: Normalized Force on a Single Blade During One Revolution.

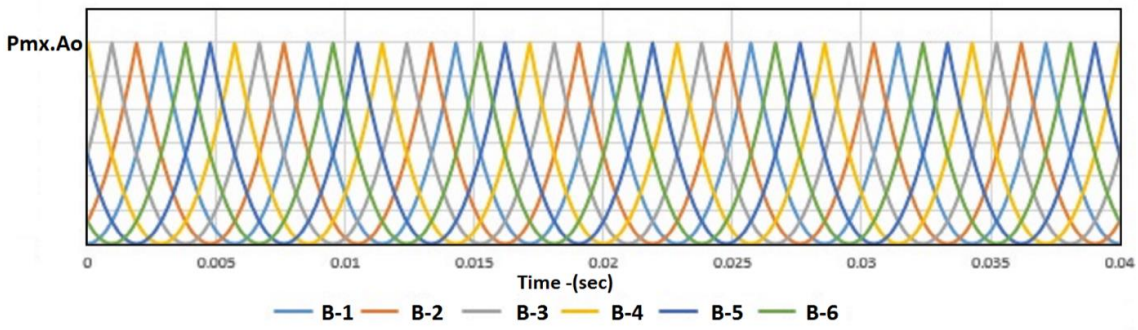

Figure 5.11: Normalized Forces on All Blades During One Revolution.

The summation of normalized forces on the six blades in time domain and frequency domain are shown in Figure 5.12 and Figure 5.13 respectively. The major frequency observed at 1050 Hz corresponds to the blade pass frequency (BPF) (6 x 35 Hz) times the number of diffuser tongues. It is worthwhile to note here that results of this pressure pulsation model agrees with experimental results obtained in [2, 4].

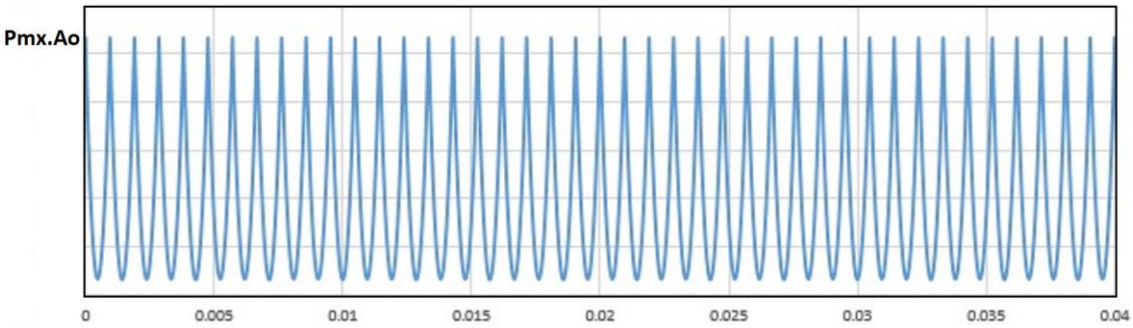

Figure 5.12: Time Domain of Net Pressure Forces on All Blades During One Revolution

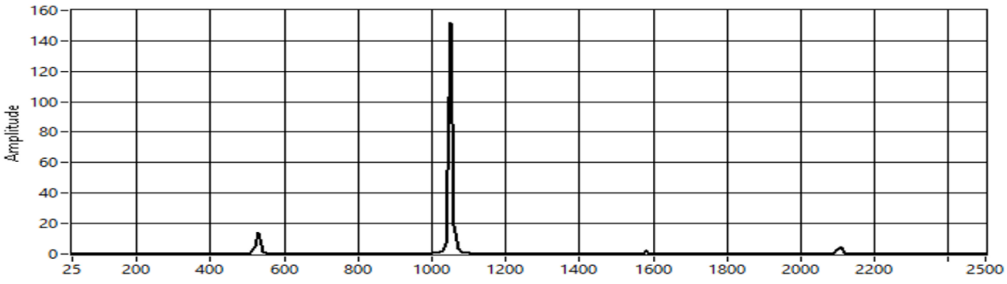

Figure 5.13: Frequency Domain of Net Pressure Forces on All Blades During One Revolution

5.3 USING MACHINE LEARNING MODELS IN FAULT DETECTION

Regarding the trendy automatisms and working in an uncertain, evolutionary environment the current industrial plants and systems become more and more mechatronics complex [90] [63] [91]. The classification and detection of the mechanical system faults is an essential task for a reliable operation. As mentioned above cavitation is one of the most disadvantage problems that occurs frequently in the centrifugal pumps Fault detection

using Machine learning algorithms attracted much attention this decade because it is a powerful, fast, computational method that can detect the centrifugal pumps faults efficiently [92] [93]. Fault detection using machine learning has been a promising technique of releasing the human labor contribution as it is recognizing the machines health state automatically [94]. The ML model is integrated three machine learning algorithms:

SVM: is a supervised classification and regression learning algorithm that has strong linear, nonlinear and kernel generalization ability functions. The goal of the algorithm is to create a hyperplane boundary between the possible outputs to separate them into the correct categories. Any new data point can be easily put in the correct category using the hyperplane. SVM algorithm trains different real-world historical data and can efficiently detect cavitation with high accuracy and excellent performance.

KNN: is a supervised classification learning algorithm and one of the simplest ML algorithms that help in fault detection. KNN algorithm assumes the similarity between the data and puts them into the most similar category to the available categories. KNN has been applied before for different fault detection mechanical use cases, and it showed high accuracy and good scalability.

Logistic Regression: is a supervised regression analysis method in which the outcome is binary or dichotomous using predictor variables. Logistic regression is also considered a supervised learning classification algorithm used efficiently in predicting the probability of a dependent variable. The model showed a high accuracy to detect the cavitation as it has been used to build predictive models as a function of predictors and because of the data linearity.

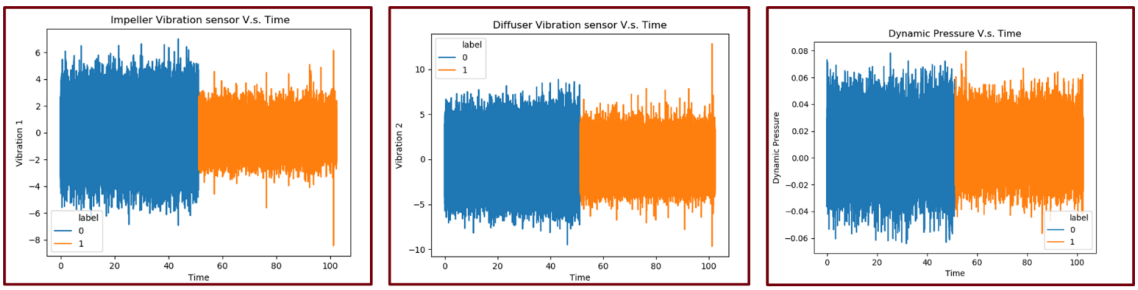

(a) (b) (c)

Figure 5.14: (a) and (b) Collected vibration data before and after cavitation, (c) Collected dynamic pressure data before and after cavitation.

Parts a and b of Figure 12 represents the vibration data that have been collected from two vibration sensors one is mounted to collect the pump's impeller vibration data and the second vibration sensor is mounted to collect the pump's diffuser vibration data. The blue plots represent the data before cavitation exist and takes 0 label, where the orange plots represent the data after cavitation and takes label of 1. The vibration amplitude before cavitation was greater than after cavitation and these real-world collected results can be explained by studying the pressure pulsation data that was collected by using dynamic pressure sensor and represented in part c of the above figure. Part c shows that the dynamic pressure amplitude before the cavitation was greater than after cavitation because of decreasing in the exciting force magnitude affecting the pump's rotor during the cavitation and this decreasing magnitude corresponds to the decrease in $\Delta P = (P_{2\_} P_1)$ [1]. Due to the bubble's explosion at this point during cavitation P_1 increase at this BPF frequency the spectral peak does not show any significant decrease from normal to cavitation condition [1].

CHAPTER 6

RESULTS AND DISCUSSIONS

This chapter presents the four digital models modeling, simulations, results, and discussion that are included in this thesis, from how the reverse osmosis membrane was modeled, to the three-piston pump, how they were integrated, and validating the digital model's results and accuracy with real-time data from the water desalination system located in Egypt. Furthermore, this chapter presents three different digital models techniques used in fault detection using Amesim digital model, physics-based model, and machine learning model.

6.1 REVERSE OSMOSIS MEMBRANE MODELING, SIMULATING, AND TESTING AS A BLACK BOX THAT GENERATES LOAD (FEED PRESSURE, BRINE PRESSURE, PRESSURE LOSS, AND THE PERMEATE FLOWRATE) ON THE HIGH-PRESSURE PUMP:

6.1.1 First method:

First Method: obtained this equation by deriving the feed pressure equation (derivations steps included in Appendix A) and plotted it with simulated feed rate and time. Then validating this digital model with different physical and hydraulic tests and with the real time collected data.

$$Pf = (Qp + 0.5 * A_{mem} * Lm * \frac{\lambda * \rho}{2\,Dh} * [\frac{(2 - rec) * Qf}{2\,nl * Wb * hb * \emptyset_b}] \text{ ^2} + A_{mem} * Lm * \Delta\Pi) / A_{mem} * Lm$$

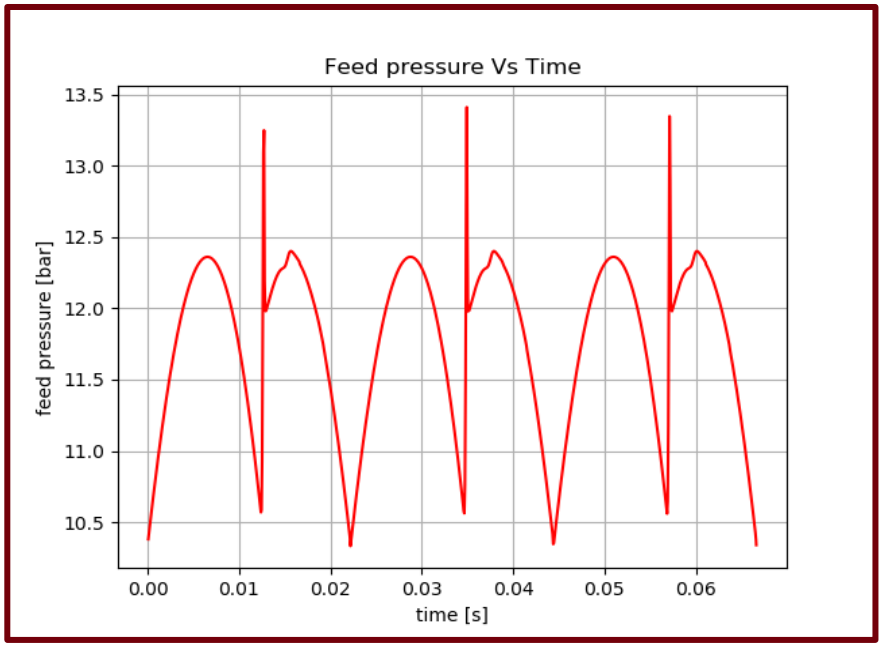

Figure 6.1: First method Feed pressure vs Time

The figure above shows the feed pressure in bars behavior with time in seconds by simulating the above equation using the parameters of a seawater spiral wound membrane 2.5" X 40" [SWRO]. Simulating these data with real-world permeate flow rate data that has been collected from the physical system. To get more permeate flowrate data points to make the model more accurate. A linear regression machine learning algorithm has been used to predict the missing permeate flowrate points with time data. The plot above presents the simulated feed pressure in one cycle as the motor runs with a speed of 900 RPM, which is 15 revolutions per second. Hence, a revolution takes 0.06667 seconds which is 1/15 second. The plot shows six peaks next to each other while there are just three pistons, and that is because there is one peak of each two peaks next to each other representing the fluid discharge, so three peaks represent the three pistons' discharge. Moreover, because the three pistons are connected to the crankshaft rod where this rod is

rotating by 360º around itself, this forces each piston discharge phase to take 180º out of these 360º and the suction phase to be in the other 180º out of these 360º. Each piston varies with an angle of 120º with the other piston, so two pistons will be doing a similar process of discharge or suction in 60º. This means that in the discharge or the suction process when one of the pistons is at the top dead center discharging, another piston is halfway discharging as well, and that is what the second peak represents. In other words, the second peak represents the discharge summation of the two piston's flow rates contribution in phase.

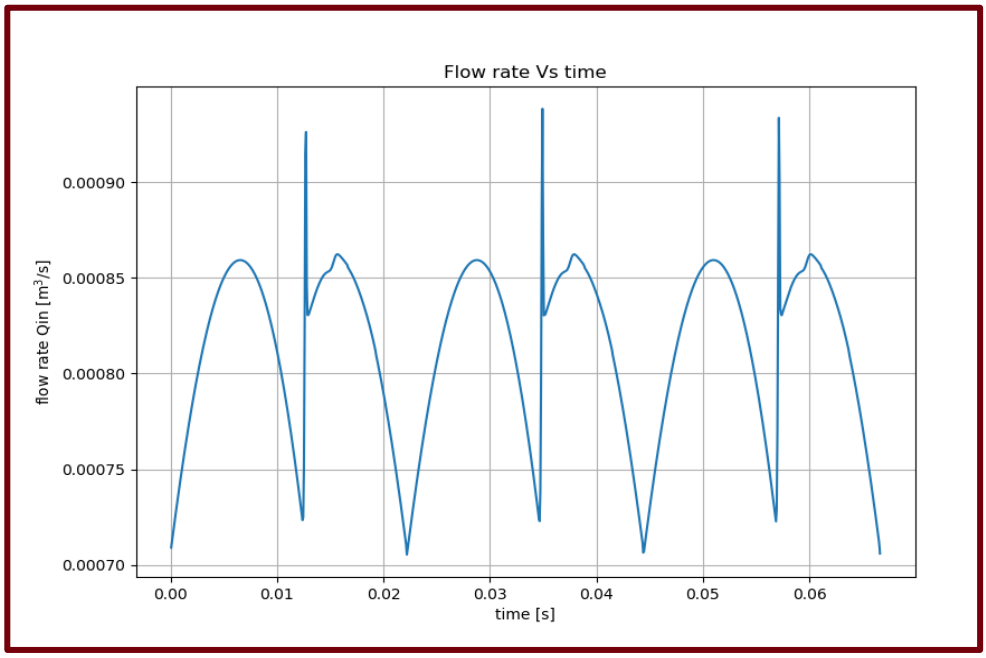

Figure 6.2: Feed flow rate vs Time

6.1.2 Second method:

Used the feed pressure equation listed below and plotted it with the same simulated feed flowrate and time and the same feed conditions and same RO-membrane parameters.

$$Pf = \frac{Ap * \rho}{Am * Km} * \left(Ap * (Vf - Vr) \right) + \Delta\Pi$$

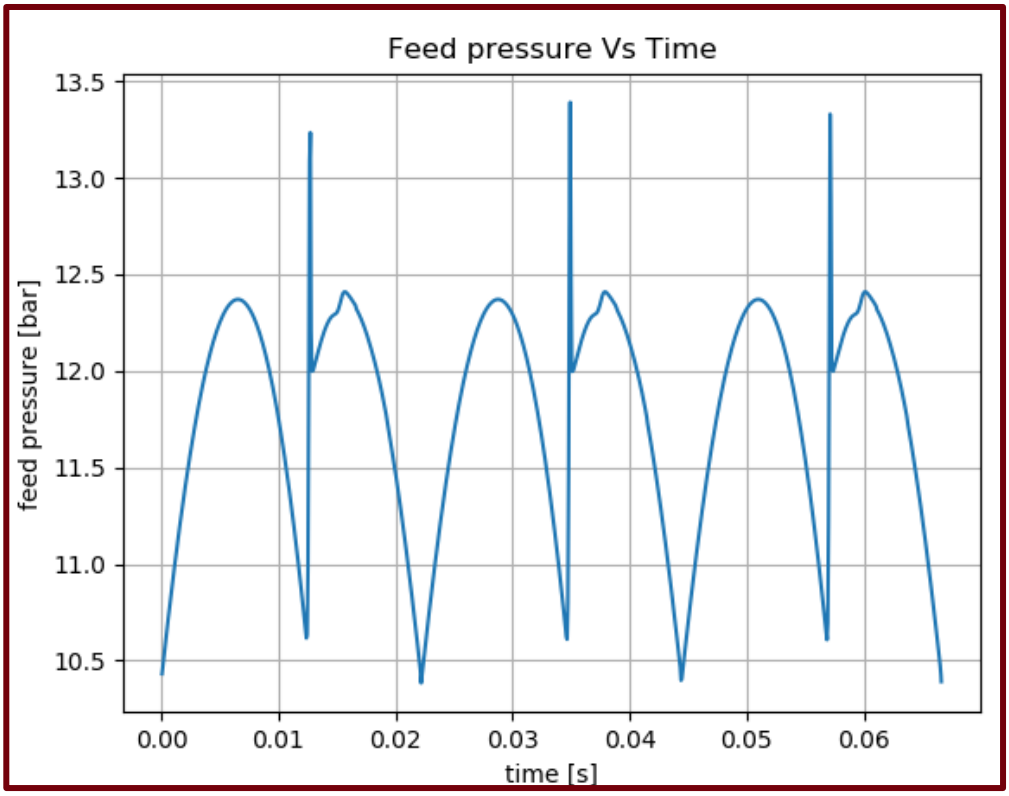

Figure 6.3: Second Method Feed Pressure vs Time.

The above equation was applied on the same real-world collected feed flowrate data vs. time from Egypt's physical water desalination system. These data were used to simulate the feed pressure vs. time and compare the simulated feed pressure data from the second method with the first method and calculate the mean square difference between them.

To validate the accuracy of the two methods and check the difference between both methods to decide which method we will go with for integrating it with the high-pressure pump digital model in Amesim and to expand this equation to start calculating more parameters. By Calculating the difference between the two feed pressure values using the

mean square difference method and plotting both feed pressures on the same graph and the mean square difference between feed pressure of the two methods equal **0.0006784290.**

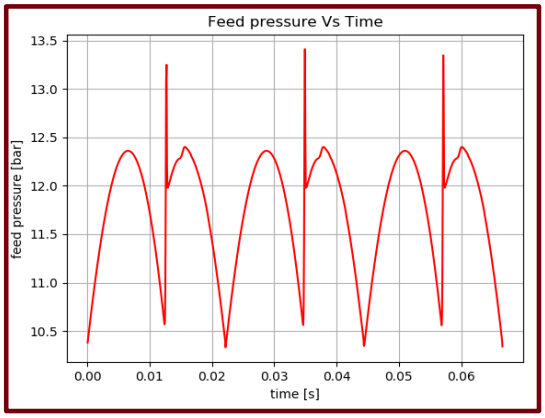

Figure 1: Feed pressure vs Time using 1st method

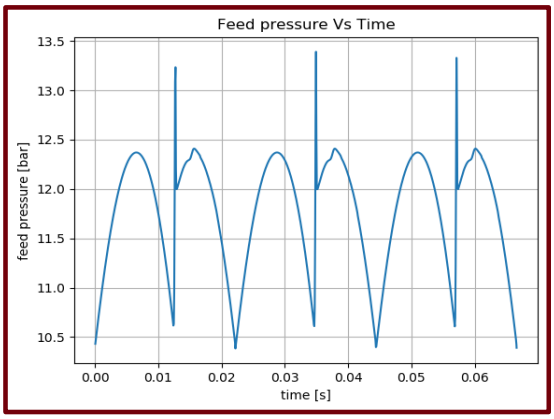

Figure 2: Feed flow rate vs Time using 2nd method

Figure 6.4: Feed Pressure V.S Time Using Both Methods.

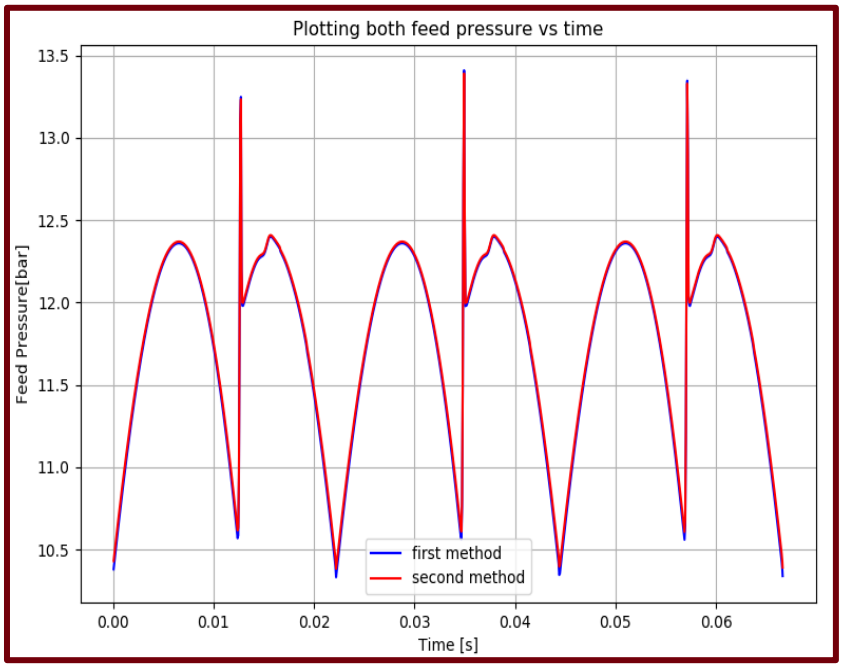

Figure 6.5: Using both methods to plot Feed pressure vs Time.

Due to the first reverse osmosis modeling method includes more membrane parameter which will gives us more accuracy while testing it and due to the low mean square difference between both methods. so, we decided to go with the first method.

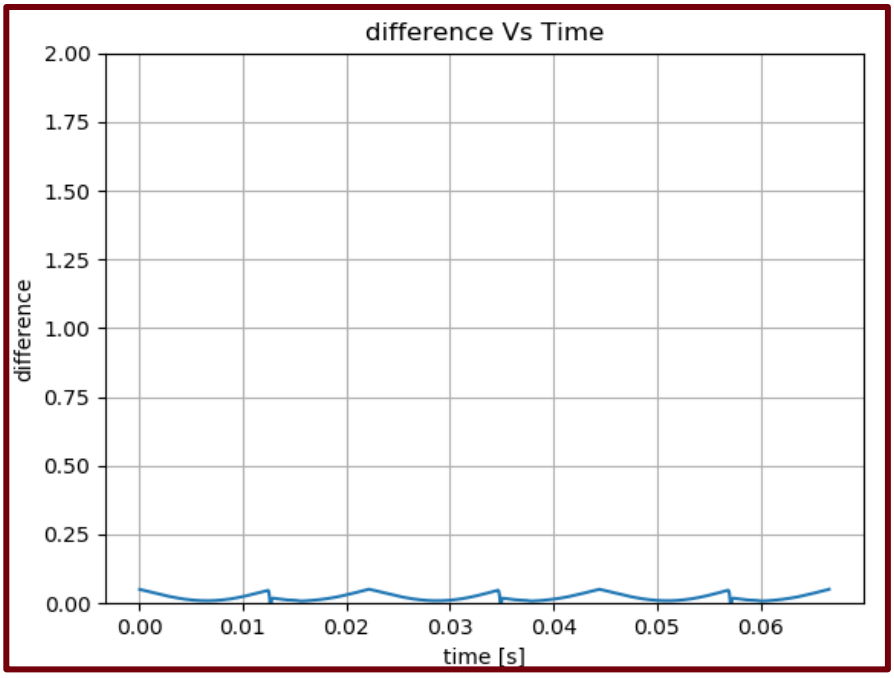

Figure 6.6: Mean square Difference vs Time

6.1.3 Testing and validating the reverse osmosis modeling equation using first method:

Using the first method to test the equation sensitivity and how the feed pressure will be impacted with different salinity, temperature, and recoveries. Then comparing these simulated results with the theoretical theories and equations.

6.1.3.1 Effect of the temperature on membrane performance.

The use of warmer water reduces saline water viscosity, which in turn increases membrane permeability. Some of this beneficial impact is reduced by increasing osmotic pressure with temperature (using Eq. below). However, the overall impact of temperature for most membranes is typically beneficial (Fig. 6.8). As a rule of thumb, the permeate flux increases by 3% for every 1°C of temperature increase. Because most RO membranes are made of plastic materials (polymers), warmer temperatures result in a loosening up of the membrane structure, increasing salt passage (i.e., deteriorates permeate water quality).

$$\Delta\pi = R \times (T + 273) \times \Sigma m_i$$

Where $\Delta\pi$ = the osmotic pressure of the saline water $\left(in\ bars — 1\ bar = 14.5 \frac{lb}{in^2}\right)$

$R = the\ universal\ gas\ constant\ [0.082\ (L \cdot atm)/(mol \cdot K) = 0.0809\ (L \cdot bar)/(mol \cdot K)]$

$T = the\ water\ temperature\ in\ degrees\ Celsius,$

$\sum mi$ is the sum of the molar concentrations of all constituents in the saline water

This formula is derived from Van't Hoff's thermodynamic law, which is applied to pressure caused by dissociation of ions in solution (Fritzmann et al., 2007).

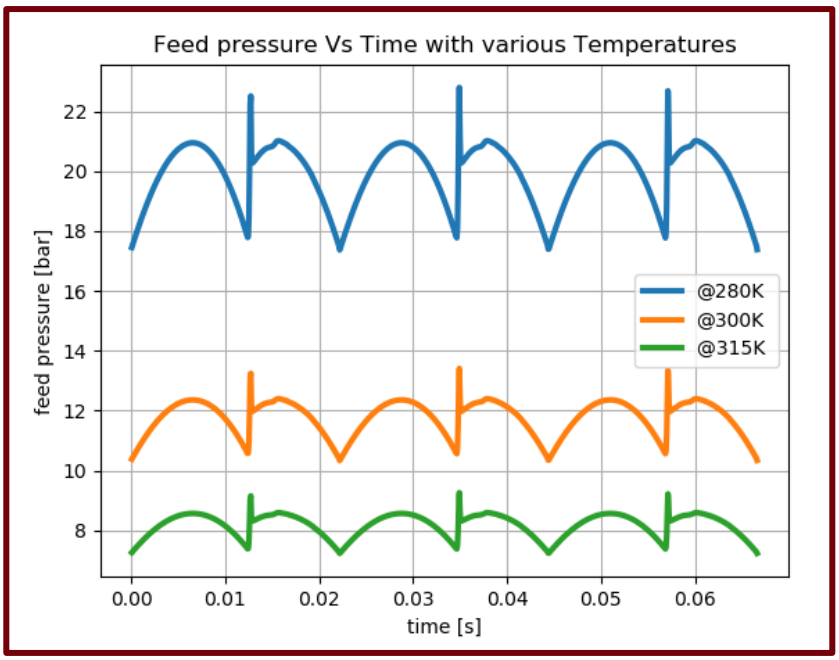

Figure 6.7: Feed pressure vs Time @different Temperatures.

Temperature impacts both ΔΠ and the average solvent flux (Jv), which are important factors which generate extra feed pressure or reduce it. As seen in Figures 6.7 and 6.8, the rate of permeate flux gain is typically much higher than the rate of deterioration of product water quality. For source water temperatures up to 30°C (86°F), warmer water reduces the feed pressure and energy used for desalination (Greenlee et al., 2009). Because of the negative impact of temperature on osmotic pressure, operation at higher temperatures

may or may not be beneficial. In addition, the use of warmer water accelerates biological fouling, which in turn also reduces membrane permeability. As discussed previously, operating conventional spiral-wound RO membranes at temperatures above 40°C (104°F) accelerates the compaction of the membrane support layer and is undesirable because it results in a premature and irreversible loss of membrane permeability. Most membrane suppliers recommend that the temperature of the source water processed by RO membranes should be maintained below 45°C (113°F) at all times to avoid permanent membrane damage.

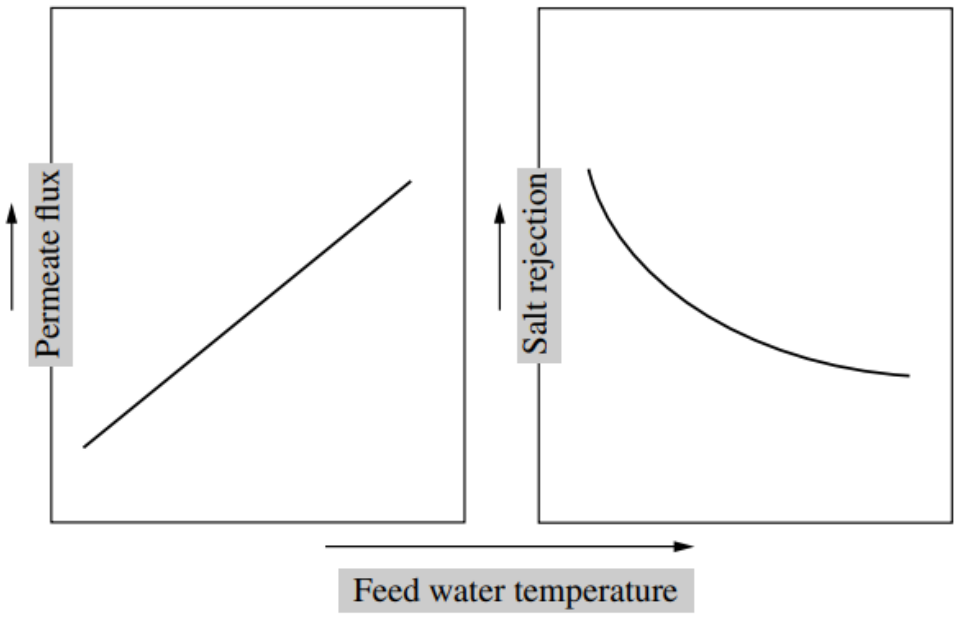

Figure 6.8: Effect of temperature on RO system performance [26].

Figure. 6.8 shows that when the feedwater temperature increases, it positively impacts the permeate flux as there is a direct proportion between the feedwater temperature and the permeate flux. However, there is an inversely proportional relationship between salt rejection and feedwater temperature. While in the figure.53 there is an inverse proportional between the feedwater temperature with the feed pressure as when the temperature increases the feed, pressure decreases and when the temperature decreases the

feed pressure increase which means regarding the feed pressure and system energy the hotter is, the better with respect to each membrane datasheet as by increasing the temperature more than the maximum limit that will damage the membrane structure sheets. While regarding the salt rejection with high temperature, it gives us a lower salt rejection rate.

6.1.3.2 Effect of salinity on membrane performance:

Figure 6.9 illustrates the effect of source water salinity (TDS concentration) fed to an RO system on the system's productivity of freshwater (permeate flux) and product water quality (salt rejection). Higher feed water salinity reduces the net driving pressure (assuming that the system is operating at the same feed pressure and recovery) because of the increased osmotic pressure of the feed water, which in turn decreases permeate flux (freshwater production). In terms of salt transport, an increase in feed water salinity increases the salt concentration gradient (ΔC in Eq. listed below), which results in accelerated salt transport through the membranes and, therefore, in lower salt rejection (deteriorating product water quality.

$$Q_s = B \times S \times \Delta C$$

Salt transport rate: The salt transport rate Qs is proportional to the salt transfer coefficient B—which, as the water transfer coefficient, is unique for each membrane type—the surface area S of the membrane, and the salt concentration gradient ΔC, which collectively for all salts is measured as the difference between the TDS levels of the concentrate and the permeate.

$$\Delta C = C_b - C_p$$

Here is the solute (salt) concentration at the boundary layer/bulk feed flow and the concentration of solute (salt) in the permeate. The boundary layer is a layer of laminar feedwater flow and elevated salinity that forms near the surface of the membranes because of the tangential source water feed flow in the spacers and permeates flow in a perpendicular direction through the membranes on the two sides of the spacer (Fig. 6.9). In Fig. 6.9, is the solute concentration (i.e., salt) in the feed water, Cs is the concentration at the inner membrane surface (which typically is higher than that in the feed flow). It is the concentration of the solvent (i.e., freshwater salinity) on the low-salinity (permeate) side of the membrane.

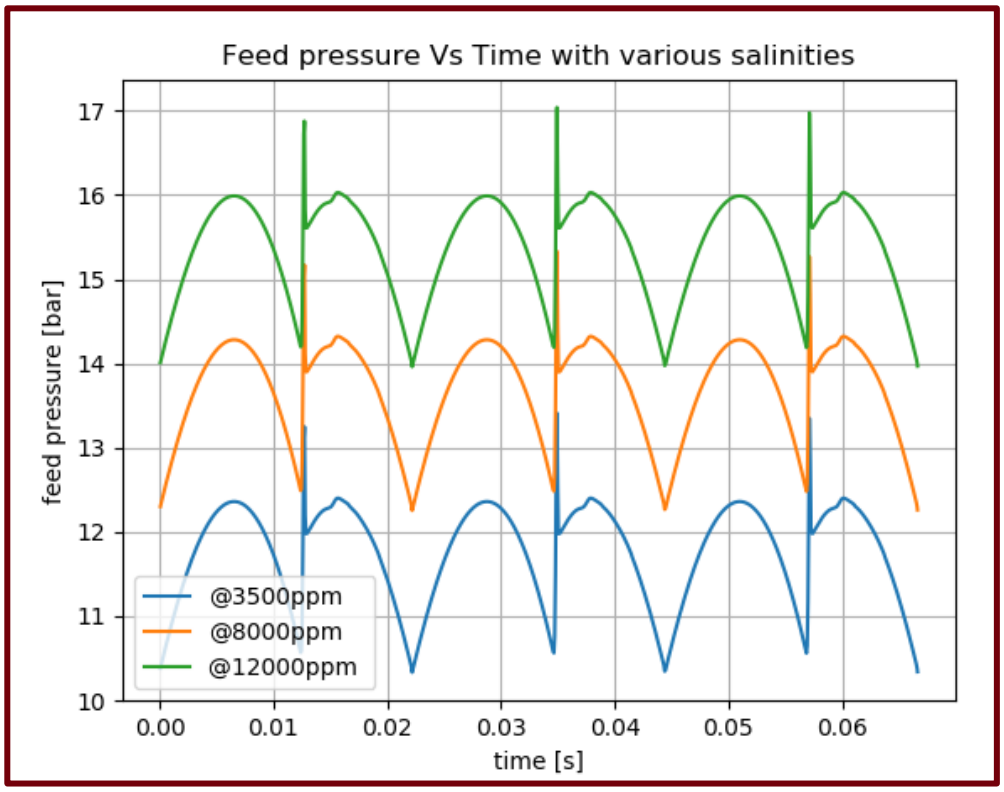

Figure 6.9: Feed Pressure vs Time @Different Salinities.

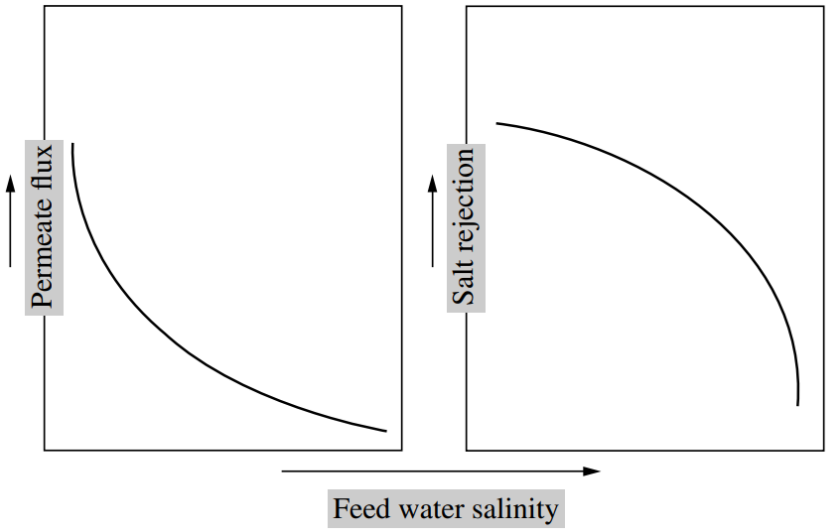

Figure 6.10: Effect of salinity on RO system performance [26].

Figure. 6.11 showed that when the feedwater salinity increases, it negatively impacts the permeate flux as there is an inversely proportional between the feedwater salinity and the permeate flux. Although, there is an inversely proportional relationship between salt rejection and feedwater salinity. While in the figure.6.10, there is a direct proportion between the feedwater salinity and the feed pressure. When the salinity increases, the feed pressure increases, and when the salinity decreases, the feed pressure required decreases. This means the lower salinity is, the better regarding the feed pressure and system energy concerning each membrane datasheet. When the feedwater salinity increases at some point, the salt rejection rate will be constant, and the salinity rate will not affect it. That means the higher the feed salinity water level is, the lower the permeate flux will be produced. The lower salt rejection will be achieved. The highest feed pressure and power consumption will be generated. Salinities impact and the average solvent flux which are essential factors that generate extra feed pressure or reduce it.

6.1.3.3 Effect of recovery on RO system performance:

As indicated in Fig.6.12, an increase in recovery results in a slow decrease in permeate flux until it reaches the point at which osmotic pressure exceeds the applied pressure and NDP is inadequate to drive flow through the membrane; at that point, freshwater flow production is discontinued. Recovery impact both the flow rate and the average solvent flux (Jv) which took place in our equation in permeate flow rate and hydrostatic pressure terms. which generate extra feed pressure or reduce it.

Figure.6.12 & 6.13 shows an increase in recovery results in a slight decrease in permeate flux until it reaches the point at which osmotic pressure exceeds the applied pressure and NDP is inadequate to drive flow through the membrane; at that point, freshwater flow production is discontinued. As it is inversely proportional between increasing in the recovery level and decreasing in both salt rejection rate and the permeate flux until it reaches a point and starts being constant. While in the figure.58, there is a direct proportion between the recovery level and the feed pressure. When the recovery increases, the feed pressure increases, and when the recovery decreases, the feed pressure required decreases. This means the lower the recovery level is, the better the feed pressure and system energy consumption with respect to each membrane datasheet. When the recovery level increases, the salt rejection rate and permeate flux will be constant, and the salinity rate will not affect it. That means the higher the feed salinity water level is, the lower the permeate flux will be produced, the lower salt rejection will be achieved, and the highest feed pressure and power consumption will be generated.

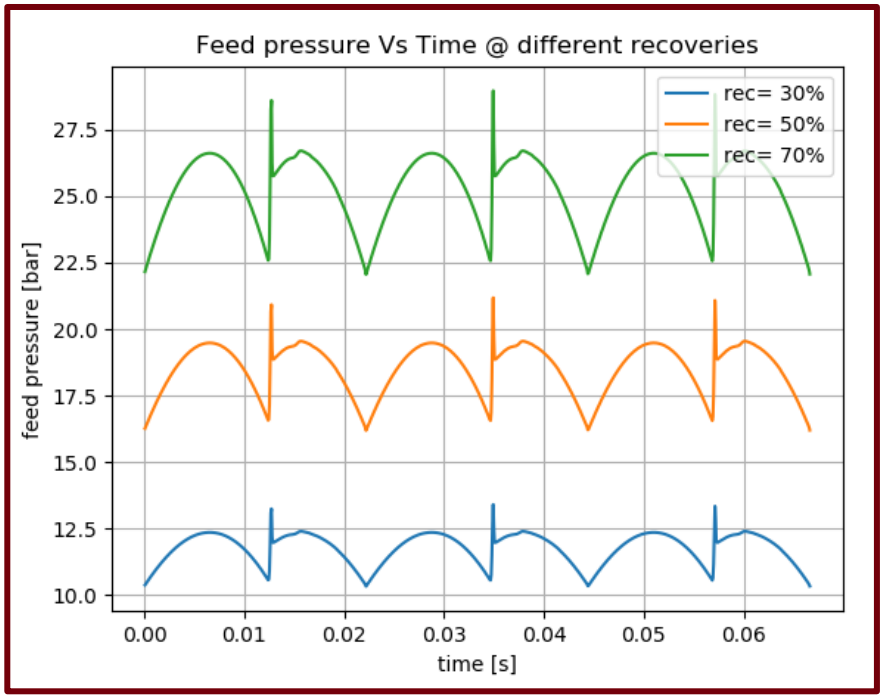

Figure 6.11: Feed Pressure vs Time @Different Recoveries

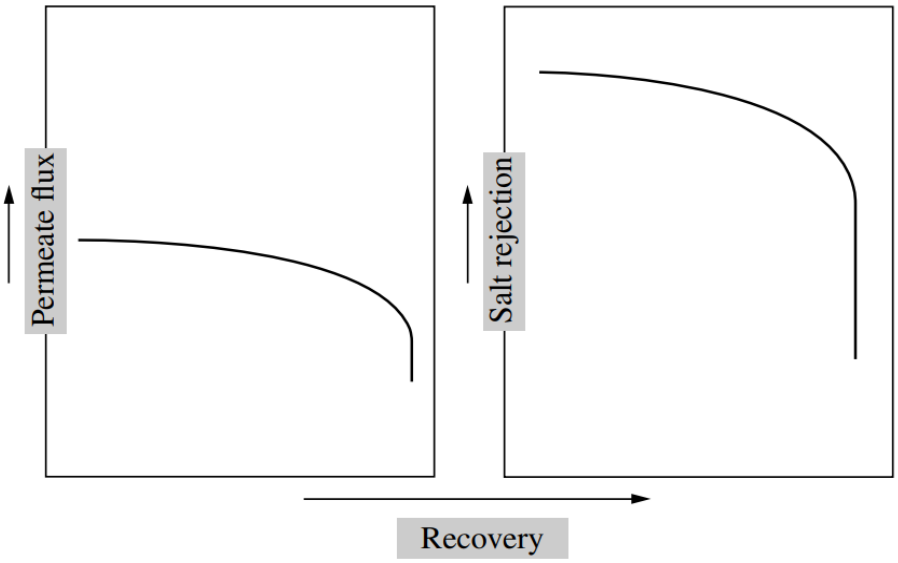

Figure 6.12: Effect of recovery on RO system performance [26].

6.1.3.1 Effect of feed pressure on the RO system performance:

As can be seen from analysis of Eq. below, membrane flux (productivity) increases along with operating feed pressure at the same source water salinity and temperature. This

occurs because the increase of feed pressure results in a proportional increase of the net driving pressure through the membrane.

$$J_w = A(\Delta P - \sigma\Delta\pi)$$

As per Eq. below, salt transport is unaffected by pressure. However, because more water is produced at a higher pressure and the same amount of salt is contained in this water, the permeate salinity concentration decreases (i.e., it appears that salt rejection increases) with pressure. For the salt transport equation above it can be modified as follows:

$$Q_s = B \times S \times (\beta \times C_b - C_p)$$

6.1.3.4 Effect of friction losses on the RO system performance:

The equation would be simulating the RO system feed pressure to study how the hydraulic friction losses affect the generated feed pressure if it was not calculated. Hydraulic pressure drops due to wall friction, solute concentration, fluid temperature, and velocity at the brine side vary linearly in the axial direction. Consequently, space-dependent effects on those operating variables are averaged by arithmetic mean.

$$Pf = (Qp + A_{mem} * Lm^{*}\Delta\Pi) / A_{mem} * Lm$$

After removing the friction losses term from the equation and run the equation with the same conditions and variables without this term it gives these results shows is the plot below which illustrate the relation between the feed pressure and the time.

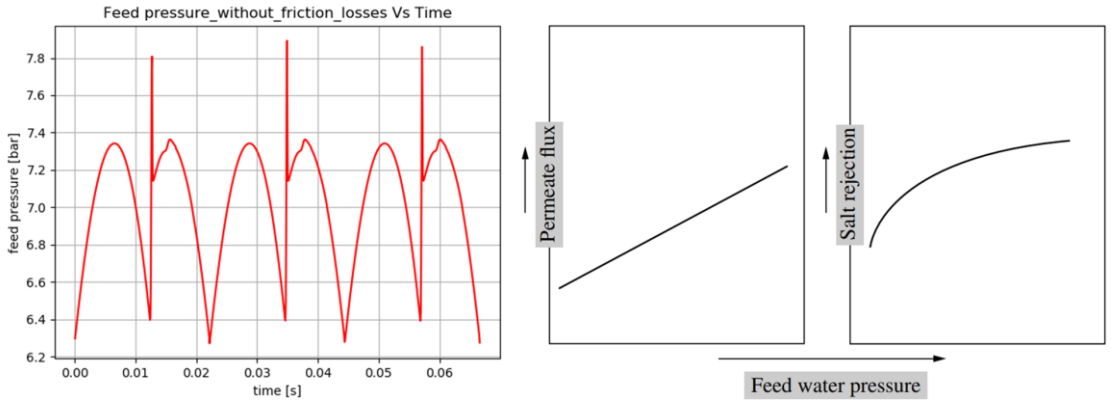

Figure 6.13: Feed pressure without Friction losses vs. Time, &
Effect of feed pressure on RO system performance.

6.1.3.5 Feed pressure Order of magnitude analysis (weighted analysis):

This section shows the order of the magnitude analysis for the feed pressure equation to determine which equation term is more effective in the equation and has more weight than the other term. Order of magnitude analysis is a powerful mathematical tool that determines which term in the equation is more sensitive and will change the behavior of the equation. Moreover, that is helpful in the predictive analytics area. If the feed pressure was not accurate or pressure pulsation found in the collected data from the system, it will be easier to figure out the problem by expecting the failure took place term.

$$Pf = (Qp + 0.5 * A_{mem} * Lm * \frac{\lambda * \rho}{2\,Dh} * [\frac{(2 - rec) * Qf}{2\,nl * Wb * hb * \emptyset b}]\,\hat{}2 + A_{mem} * Lm * \Delta\Pi) / A_{mem} * Lm$$

Where This equation consists of three terms:

First term = $\frac{Q_P}{A_{mem} * Lm}$

Second term = $0.5 * \frac{\lambda * \rho}{2\,Dh} * [\frac{(2 - rec) * Qf}{2\,nl * Wb * hb * \emptyset b}]\,\hat{}2$

Third term = $\Delta\Pi$

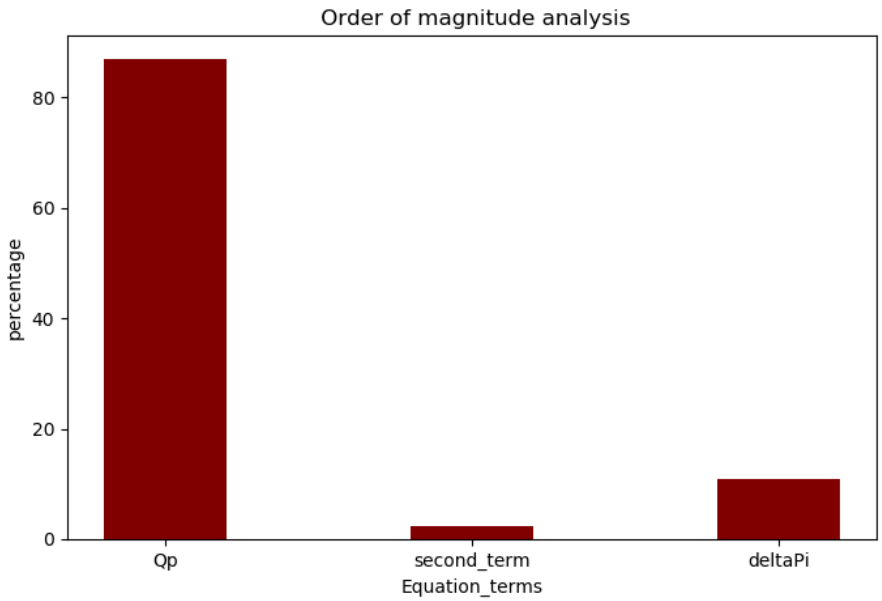

Figure 6.14: The percentage of each term in the equation.

It is evident here that the first term is the most effective in the equation, which is the flow rate, then it comes next to the osmotic pressure term, which is the third term of the equation, then third the second term of the equation. That makes sense, and the conclusion is that the feed pressure behavior follows the flow rate behavior. If the permeate flow rate increases, it requires an increase in the feed pressure to flow the more enormous amount of the feed flow rate to get a larger permeate flow rate portion. The second term that comes next also makes sense. If the osmotic pressure increases, the pressure needs to increase to head the osmotic pressure and allow the feed water to pass from the reverse osmosis membrane and produce permeate water. The second term is not that effective in the equation as it represents the membrane parameters such as the diameter, number of leaves, etc., which means here when the feed flow rate increase for the same membranes and the same water desalination system with the same operating conditions more permeate will be produced which will require more feed pressure.

6.1.3.6 Membrane life-time effect

$$J_v = Lm\ (\Delta P - \boldsymbol{\sigma}\ \Delta \Pi)$$

Where:

- $\boldsymbol{\sigma}$ is the Staverman or reflection coefficient which take value in the interval $0 \leq \boldsymbol{\sigma} \geq 1$.
- The closer the σ to 1 the greater membrane separation.

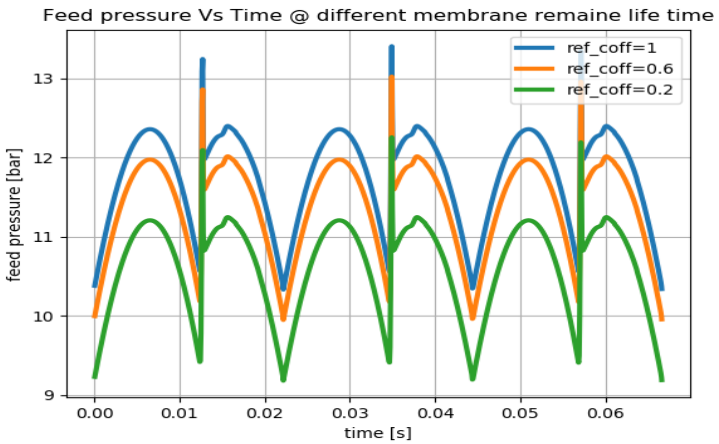

Figure 6.15: Feed pressure vs Time @different reflection showing the membrane lifetime.

The figure above shows the reflection coefficient effect on the feed pressure with time. In contrast, the reflection coefficient takes a value from 0 to 1 ($0 \leq \sigma \geq 1$). The more σ, the more the membrane separation is, and the more membrane lifetime it has. The plot above it simulates that when the membrane was new and its reflection coefficient equals 1, the generated feed pressure from the high-pressure pump will be accurate. When it decreases to zero, the pressure will decrease, which will affect both the membrane recovery and the salt rejection

6.2 3-PISTON PUMP WITH ERD INTEGRATED WITH DAMPER AND 3-STAGE RO MEMBRANES:

Three piston high-pressure pump integrated with three stage reverse osmosis membranes is the digital twin of the physical system and in these two chapters both models the one integrated with the damper and the one without the damper will be simulated to compare and discuss between the digital twins and the real world collected data from the water desalination system located in Egypt.

The model above represents a three pistons pump with energy recovery device integrated with damper and three stage reverse osmosis membrane digital model. the three pistons are connected with a crankshaft with an of 120º between each piston and the other. The high-pressure pump is attached with a motor which rotates with 690 RPM also a feed pump is connected to the high-pressure pump aims to prime the pressure to the HPP to avoid cavitation. Each cylinder includes front side where the suction came from the feed tank and the discharge go to the RO membrane. While the back side which is the energy recovery side the suction come from the brine water discharged from the membrane aims to generate a hydraulic power to save energy by pushing the pistons instead of requiring electric energy from the motor and the discharge flows to the brine tank. Each side includes of two valves one responsible with suction and the other responsible for discharge. Where the main components of this damper are mass to simulate the weight, piston, orifices, and a spring.

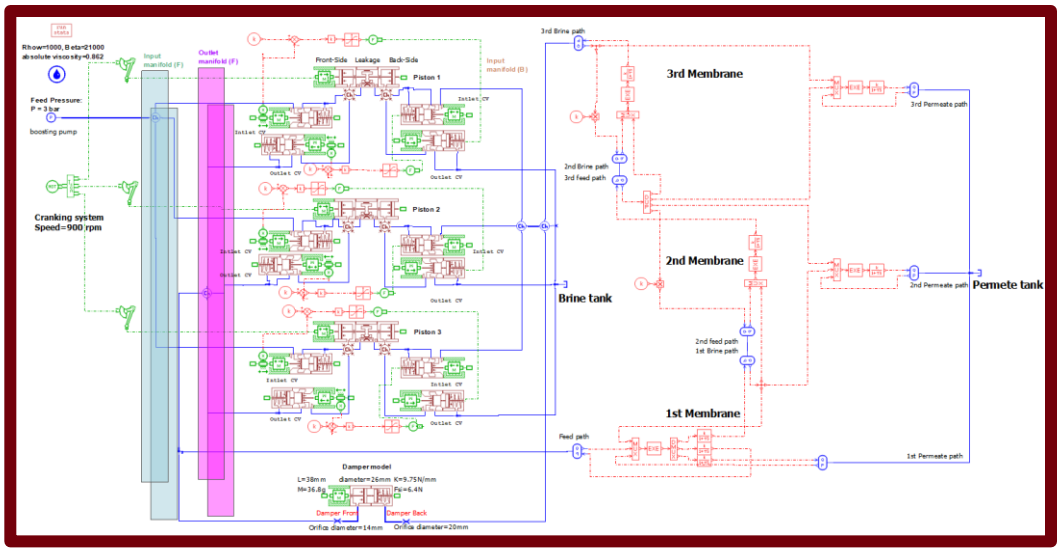

Figure 6.16: The WD Digital Twin Integrated with Damper.

Also, the digital model is integrated with a three-stage spiral wound membrane which is modeled as a C-script code and attached in the model as an executable file which contains mathematical equation running together in parallel and exchange these variables with the Amesim model in each part of a second. The membrane digital model simulates the feed path pressure and flowrate, the brine pressure and flow rate, and the permeate pressure and flowrate. Which helps to study the membrane behavior and faults that might occurs at any time. The model includes a damper to reduce the vibration, pressure, and flowrate pulsations and fluctuations to extend the pump lifetime by reducing the vibration level, which can harm the pump and the membranes. Where the main components of this damper are mass to simulate the weight, piston, orifices, and a spring. In this model the system runs with 690 RPM instead of 900 RPM like the other digital models to fits the collected data that was gathered in Egypt and be running under the same operating conditions. The system is also running under the same salinity, flowrate, and temperature operating conditions as the physical system in Egypt.

The amount of the permeate production in a pressure vessel of seven membranes are equally distributed as each membrane element should produce one-seventh of the total permeate flow of the vessel which are 14.3%. However, in actual reverse osmosis systems the flow distribution in a pressure vessel is uneven which makes sense as the first membrane getting the highest feed flowrate with the lowest water salinity, so it usually produces about 25% of the total permeate flow in the pressure vessel. While the last element produces around 6 to 8% of the total permeate flow in the pressure vessel. The decline in the permeate production is because of the increasing of the water salinity and the osmotic pressure. then the second membrane element will produce lower and in sequence to the rest of the membranes. [Book]

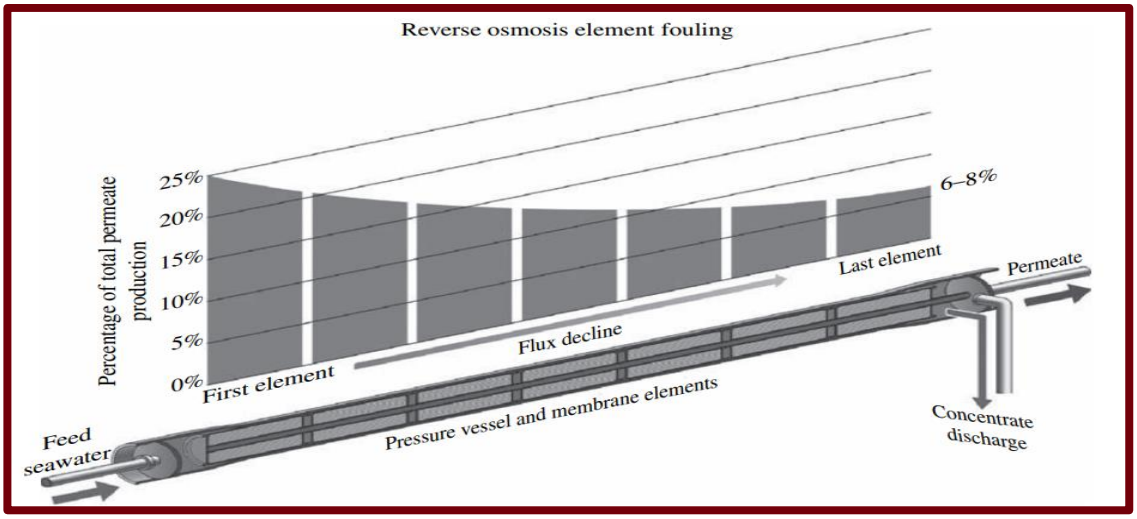

Figure 6.17: Membrane fouling and flux distribution in a membrane vessel [26].

As the physical system in Egypt includes three membranes in series to each other so the feed water flows to the first membrane and then the brine goes to the second membrane and the permeate flows to the permeate path, then to the permeate tank. Then the brine production from the second membranes goes to the thirds membrane element and the permeate water production go to the permeate path then to the permeate tank. However,

the brine production from the third membrane enters the energy recovery device which is the high-pressure pump back side and considered as a hydraulic power which aids in moving the pistons forward and backward to reduce the electricity consumption and without generating more load on the motor. And the way of calculating on it depends on the figure and the equations below.

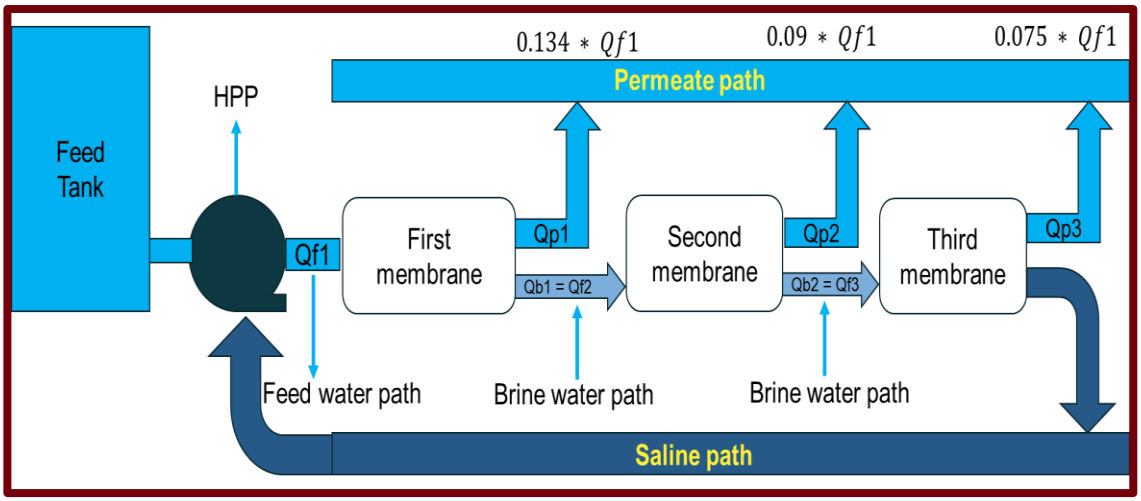

Figure 6.18: Flux Distribution in the Digital Model.

$$Q_{b3} = Q_{f1} \times 0.7$$

$$Q_{p1} + Q_{p2} + Q_{p3} = Q_{ptotal} = 0.3 \times Q_{F1}$$

$$Q_{p1} = 0.45 \times Q_{ptotal} = 0.45 \times 0.3 \times Q_{F1} = 0.135 Q_{F1}$$

$$Q_{p2} = 0.3 \times Q_{ptotal} = 0.3 \times 0.3 \times Q_{F1} = 0.09 Q_{F1}$$

$$Q_{p3} = 0.25 \times Q_{ptotal} = 0.25 \times 0.3 \times Q_{F1} = 0.075 Q_{F1}$$

6.2.1 The HPP simulations and discussion

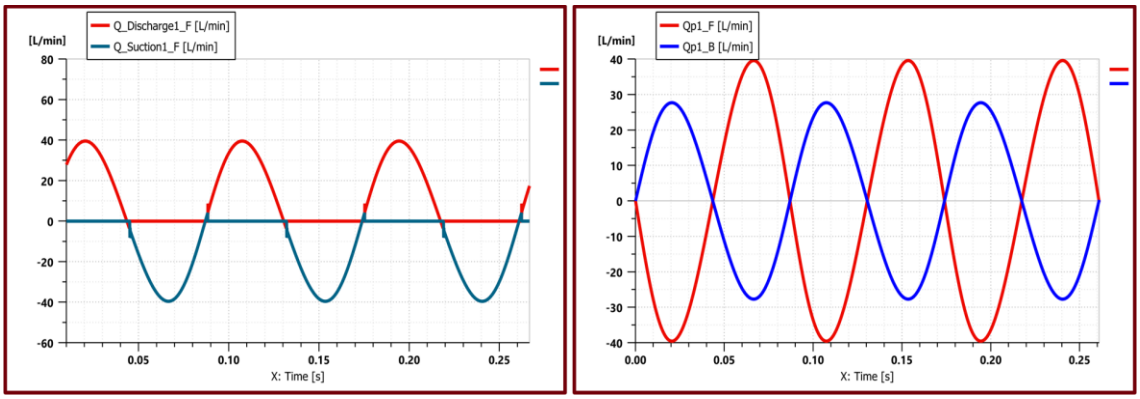

Figure 6.19: First chamber flowrates & The flow rates in both the front and energy recovery chambers.

The figure at the left represents the behavior of the discharge and suction flow rates in the first piston. The red plot is the discharge with a positive sign, and the blue plot is the suction with a negative sign to make the behavior more manageable. The discharge phase occurs while the suction phase is at a steady state of zero work and vice versa. When the suction phase occurs in the same piston, the discharge phase is zero until the discharge phase ends. The discharge and suction phase sharing the same behavior as the plot starts from 0º to 180º while the 0º is the angle when the flowrate phase starts to build, 90º is where the flowrate has the highest speed, and the 180º is where the process ends. The figure at the right shows the flow rates of the first front and energy recovery sides chambers. The red plot shows the flow rate of the front side, and the blue plot shows the flow rate of the energy recovery side. Obviously, the flow rate of the energy recovery (back) side is less than the flow rate of the front side, and that is because the energy recovery side is taking its flow rate from the brine membrane path. Which is around 70% of the feed flowrate, representing and taking place in the piston's front side. Also, the plot shows that while the suction process takes place on the front side, the discharge phase takes place on the energy

recovery side, and when the suction ends, the discharge starts on the front side while the suctions start on the backside.

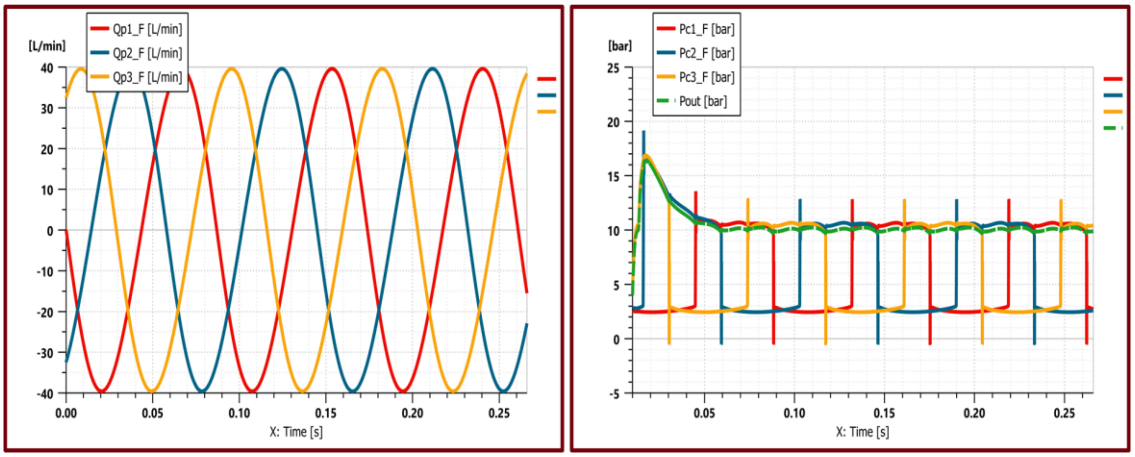

Figure 6.20: Three Pistons Flowrates, The Front Chambers Pressures & The Overall System Pressure.

The figure at the left shows the flowrate contribution of the three pistons together with time in three cycles. Where there is difference of 120º degree angle between each piston and the other and each two pistons are in phase are connected in 60º.so if the first piston started from 0º and ends its cycles at 180º the second piston starts from 120º and ends at 300º. The thirst piston starts from 240º and ends at 60º, making each piston connected with the other in 60º. Where the positive variables on the plot represent the discharge phase, and the negative variables represent the suction phase. The figure at the right represents the pressures of the first, second, third chambers, and the overall system pressure, the feed pressure for the reverse osmosis membrane. The red plot represents the pressure of the first front chamber, the blue plot represents the pressure of the second front chamber, and the yellow plot represents the pressure of the third front chamber. The green plot represents the overall system pressure. However, it shows that each piston forms three peaks, the first formed in phase with another piston flowrate as they are sharing 60º angle,

which makes them share the similar phase in this 60º, and the generated flow rate represents this peak. Similar like the third peak is in phase with another piston. The peak in between represents the pressure of each piston, and it is not shared with the other pistons' peaks. The overall system pressure, the membrane feed pressure, is taking the shape of the feed flowrates and is a behavior where it consists of two peaks. One peak represents one of the piston's discharge pressures. The second peak represents the summation of the flow rates of two in-phase pistons. So, in one cycle, we can observe six peaks as there are two for each piston. However, in each cycle, the piston pressure behavior includes three peaks.

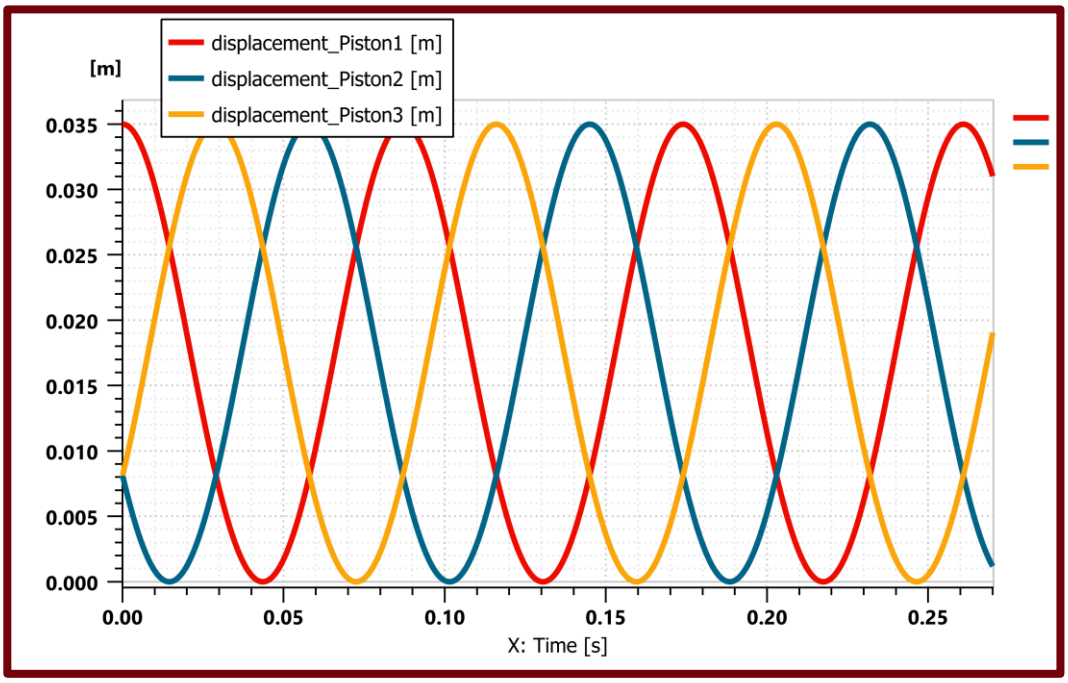

Figure 6.21: The Three Pistons' Displacements.

The plot above shows the piston displacement contribution of the three pistons together with time in three cycles. There is a difference of 120º degree angle between each piston, and the other and each two pistons are in phase are connected in 60º.so if the first piston started from 0º and ends its cycles at 180º the second piston starts from 120º and ends at 300º. The thirst piston starts at 240º and ends at 60º, making each piston connected

with the other in 60º. The positive variables on the plot represent the discharge phase, and the negative variables represent the suction phase. The zero meters represents the bottom dead center (BDC) while the 0.035m represents the top dead center (TDC), and this plot represents the displacement in 3 cycles.

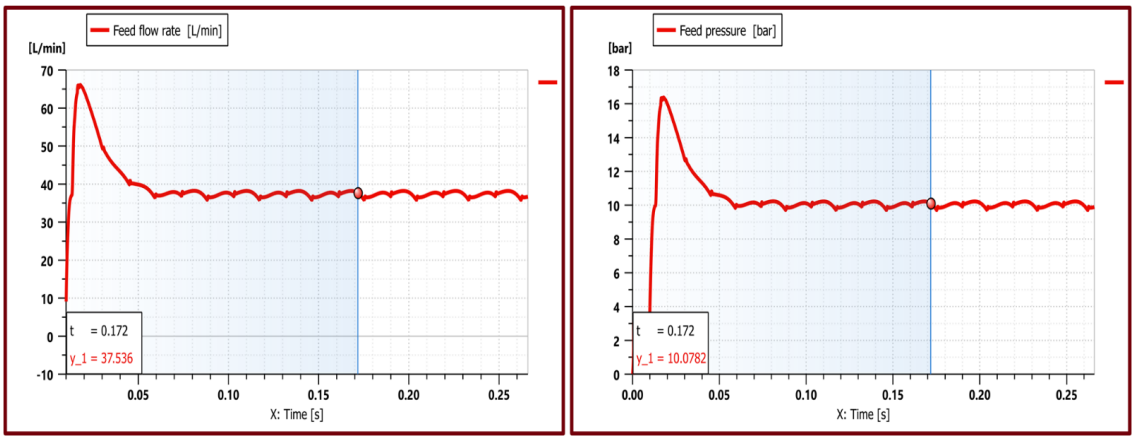

Figure 6.22: Feed Flowrate & Pressure.

The figure at the left shows the feed flowrate behavior of the system. The plot shows the feed flowrate of the system in three cycles and the average of the flow rate was equal to $37.523\ [L/M]$. The behavior shows that for one cycle there are six peaks as each two peaks of these six peaks represents one of the pistons flowrate behaviors. As one of these two peaks represents the flowrate built by one of the pistons and the other represents the flowrate that built by two of the pistons that are in phase in 60º. The figure at the right shows the feed pressure behavior of the system. The plot shows the feed pressure of the system in three cycles and the average of the pressure was equal to $10.078\ [bars]$. The pressure behavior takes the flow rate behavior as the flowrate forms the pressure. where each cycle consists of six peaks two for each piston the physical system takes the same pressure behavior as the pressure sensors in the physical system attached on the pump outlet manifold where it will be reading the discharge pressure of the three pistons at the

same time. When the feed pressure increases the pressure increase as well as the portion of permeate water will increase which effects the pressure.

6.2.2 Damper simulations and discussion

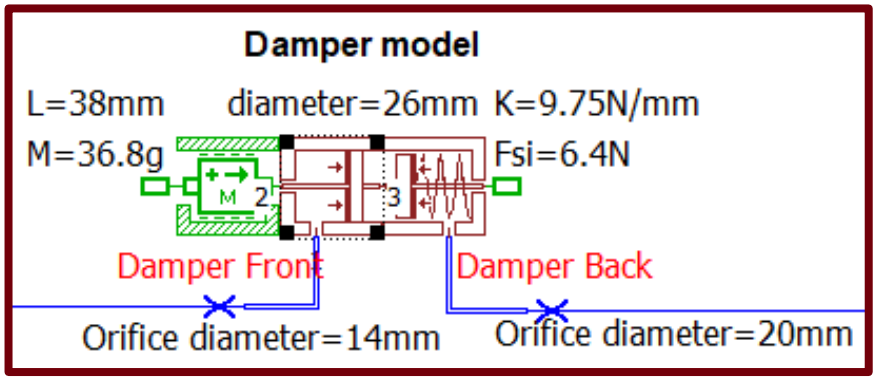

Figure 6.23: Amesim Model for the Damper Located Between the Front & the Back Sides of the Pump.

The figure below shows two plots the one at the left represents the damper front and back sides flowrates while the figure on the right represents the damper displacement. The figure at the left shows the flow rates in front of the damper and at the damper's back, where both plots have identical flow rates with just different signs, positive and negative. As the damper's back is the blue line and the damper's back is the red line. The suction phase of the damper takes place at the damper's back, and the discharge takes place at the damper's front side. Because if the damper did a suction as an example, the discharge would be the same. The damper consists of two springs, one in the front and the other on the back, absorbing the pressure, reducing the pressure pulsation, and smooths the signal.

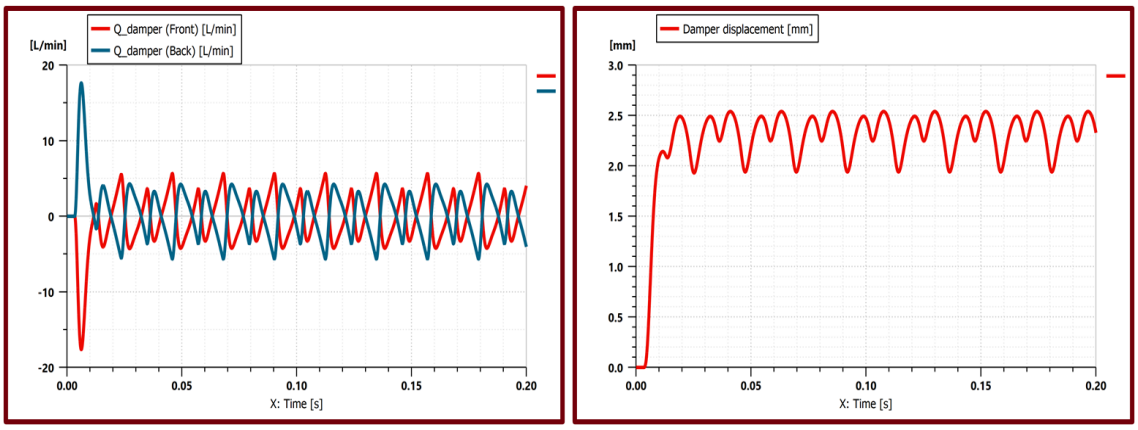

Figure 6.24: Damper Front, Back-Sides Flowrates & Displacement.

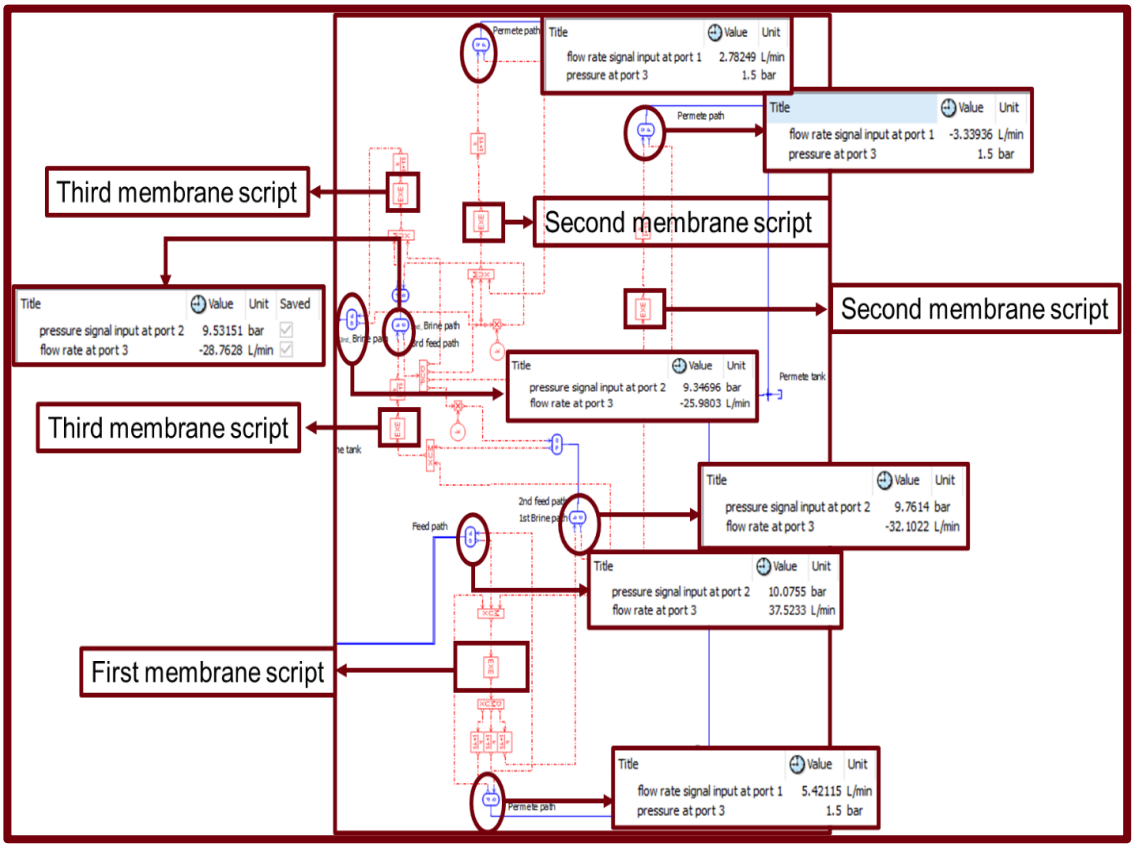

Figure 6.25: Three-stage Membrane Modeling & Results with Damper Effect.

The figure above shows the three-stage modeled membrane which is integrated with the 3-piston pump modeled in Amesim. Each membrane runs in parallel in a separate C-script file and the simulated results of each membrane are in the figure.

6.3 THREE-PISTON PUMP WITH ERD INTEGRATED WITH DAMPER AND 3-STAGE RO MEMBRANES WITHOUT DAMPER.

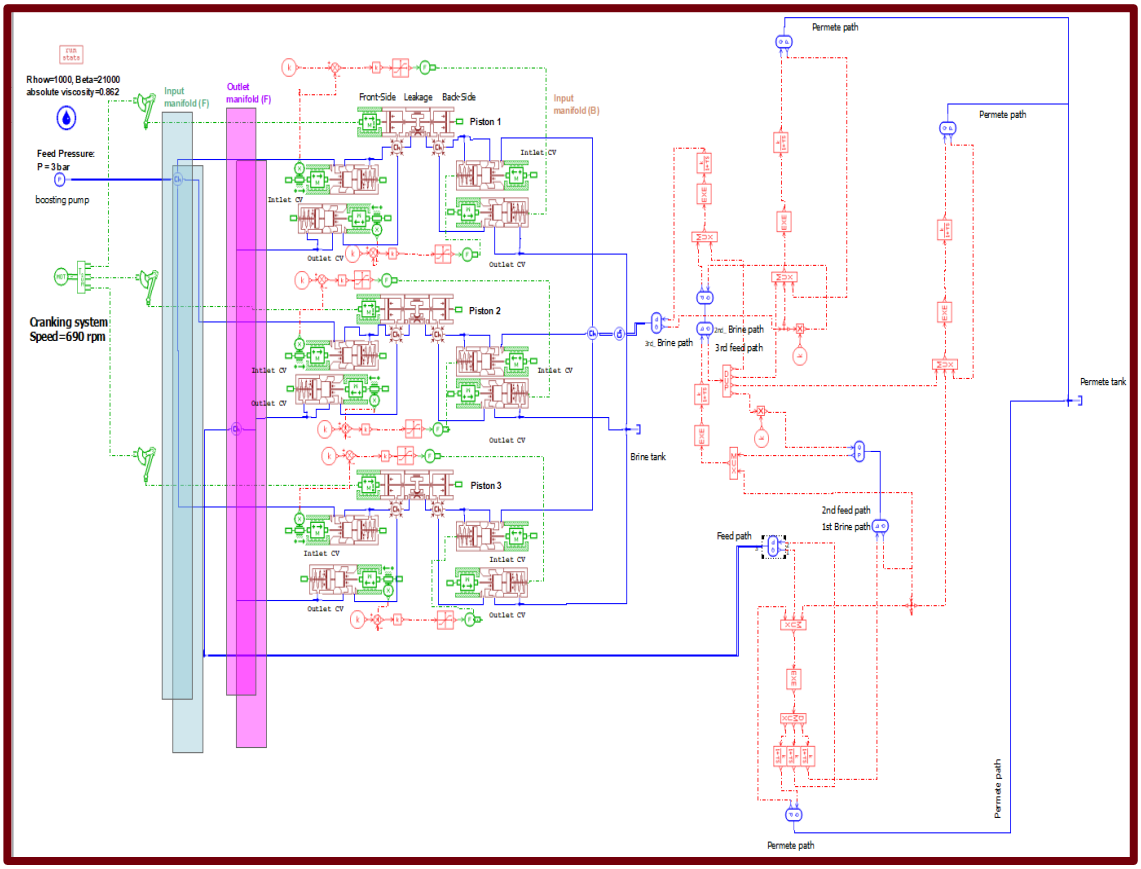

Figure 6.26: The WD Digital Twin Integrated Without Damper.

The model above represents a three pistons pump with energy recovery device integrated with damper and three stage reverse osmosis membrane digital model. the three pistons are connected with a crankshaft with an of 120º between each piston and the other. The high-pressure pump is attached with a motor which rotates with 690 RPM also a feed pump is connected to the high-pressure pump aims to prime the pressure to the HPP to avoid cavitation. Each cylinder includes front side where the suction came from the feed tank and the discharge go to the RO membrane. While the back side which is the energy recovery side the suction come from the brine water discharged from the membrane aims

to generate a hydraulic power to save energy by pushing the pistons instead of requiring electric energy from the motor and the discharge flows to the brine tank. Each side includes of two valves one responsible with suction and the other responsible for discharge. Where the main components of this damper are mass to simulate the weight, piston, orifices, and a spring. Also, the digital model is integrated with a one stage spiral wound membrane which is modeled as a C-script code and attached in the model as an executable file which contains mathematical equation running together in parallel and exchange these variables with the Amesim model in each part of a second. The membrane digital model simulates the feed path pressure and flowrate, the brine pressure and flow rate, and the permeate pressure and flowrate. Which helps to study the membrane behavior and faults that might occurs at any time. The difference between this model and the previous model is just this model does not include a damper to represents the pressure and flow rate behaviors in an obvious way without the damper effects. In this model the system runs with 690 RPM instead of 900 RPM like the other digital models to fits the collected data that was gathered in Egypt and be running under the same operating conditions. The system is also running under the same salinity, flowrate, and temperature operating conditions as the physical system in Egypt.

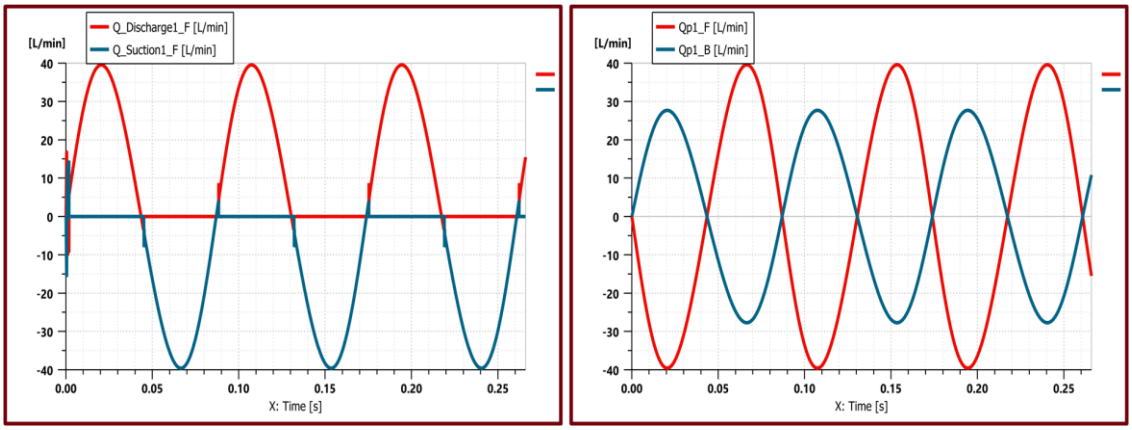

Figure 6.27: The Flowrates of the 1st Front Chamber & Flowrates of the 1st Front & Back Chambers.

In Figure 6.28 at the left is the behavior of the discharge, suction, and the overall system flow rates in the first piston. The red plot is the discharge with a positive sign, and the blue plot is the suction with a negative sign to better understand the behavior. The discharge phase occurs while the suction phase is at a steady state of zero work and vice versa. When the suction phase occurs in the same piston, the discharge phase is at zero until the discharge phase ends. The discharge and suction phase sharing the same behavior as the plot starts from 0º to 180º while the 0º is the angle when the flowrate phase starts to build, 90º is where the flowrate has the highest speed, and the 180º is where the process ends. The figure at the right shows the flow rates of the first front and energy recovery sides chambers. The red plot shows the flow rate of the front side, and the blue plot shows the flow rate of the energy recovery side. Obviously, the flow rate of the energy recovery (back) side is less than the flow rate of the front side, and that is because the energy recovery side is taking its flow rate from the brine membrane path. Which is around 70% of the feed flowrate, representing and taking place in the piston's front side. Also, the plot shows that while the suction process takes place on the front side, the discharge phase takes

place on the energy recovery side, and when the suction ends, the discharge starts on the front side while the suctions start on the backside.

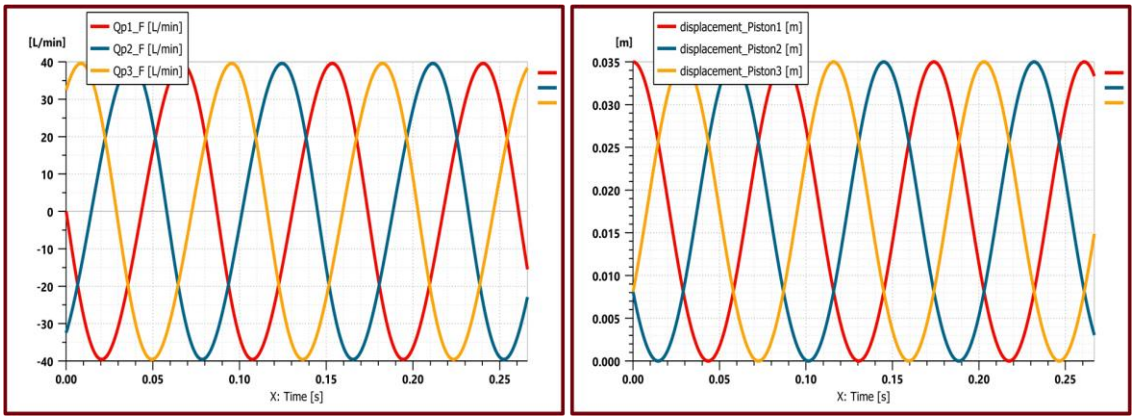

Figure 6.28: Flowrates of the Three Front Chambers & The Three Pistons' Displacements.

The plot above shows the flowrate contribution of the three pistons together with time in three cycles. Where there is a difference of 120º degree angle between each piston and the other and each two pistons are in phase are connected in 60º.so if the first piston started from 0º and ends its cycles at 180º the second piston starts from 120º and ends at 300º. The thirst piston starts from 240º and ends at 60º, making each piston connected with the other in 60º. The positive variables on the plot represent the discharge phase, and the negative variables represent the suction phase. The flow rates behavior in the pistons is not going to change by including the damper or not. That is why we will not include more flowrates plots, as it will be like the same model. The plot above shows the piston displacement contribution of the three pistons together with time in three cycles. There is a difference of 120º degree angle between each piston, and the other and each two pistons are in phase are connected in 60º.so if the first piston started from 0º and ends its cycles at 180º the second piston starts from 120º and ends at 300º. The thirst piston starts at 240º and ends at 60º, connecting each piston with the other in 60º. The positive variables on the plot

represent the discharge phase, and the negative variables represent the suction phase. The zero meters represent the bottom dead center (BDC) while the 0.035m represents the top dead center (TDC), and this plot represents the displacement in 3 cycles.

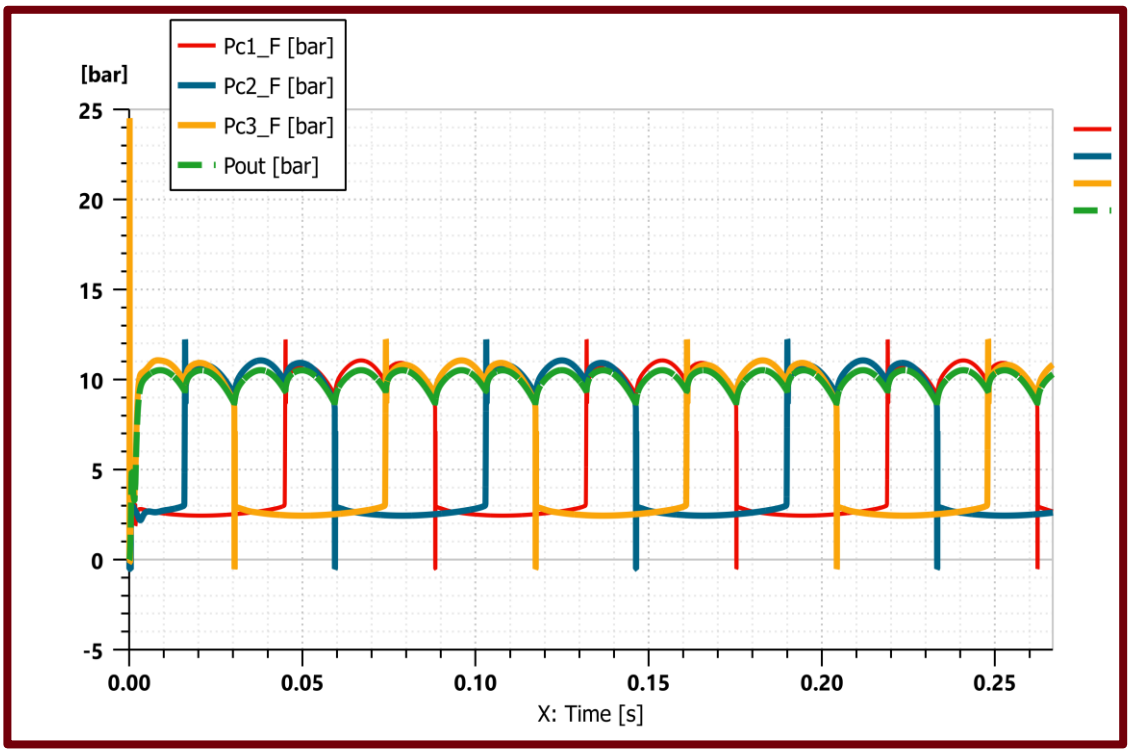

Figure 6.29: The Front Chambers Pressures & The Overall System Pressure.

The figure above represents the pressures of the first, second, third chambers, and the overall system pressure, the feed pressure for the reverse osmosis membrane. The red plot represents the pressure of the first front chamber, the blue plot represents the pressure of the second front chamber, and the yellow plot represents the pressure of the third front chamber. The green plot represents the overall system pressure. However, it shows that each piston forms three peaks, the first formed in phase with another piston flowrate as they are sharing 60º angle, which makes them share the similar phase in this 60º, and the generated flow rate represents this peak. Similar like the third peak is in phase with another piston. The peak in between represents the pressure of each piston, and it is not shared with

the other pistons' peaks. The overall system pressure, the membrane feed pressure, is taking the shape of the feed flowrates and is a behavior where it consists of two peaks. One peak represents one of the piston's discharge pressures. The second peak represents the summation of the flow rates of two in-phase pistons. So, in one cycle, we can observe six peaks as there are two for each piston. However, in each cycle, the piston pressure behavior includes three peaks.

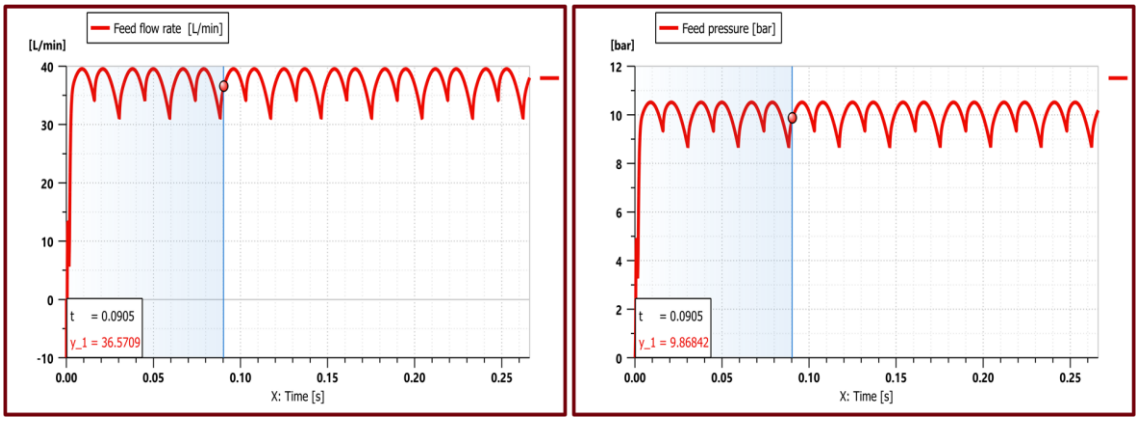

Figure 6.30: Feed Flowrate & Feed Pressure.

The figure at the right represents the feed flowrate behavior of the system. The plot shows the feed flowrate of the system in three cycles and the average flow rate was equal to 36.57 $[L/M]$. The behavior shows six peaks for one cycle as every two peaks of these six peaks represent one of the piston's flowrate behaviors. One of these two peaks represents the flowrate built by one of the pistons, and the other represents the flowrate built by two of the pistons that are in phase in 60º. The figure at the left shows the feed pressure behavior of the system. The plot shows the feed pressure of the system in three cycles and the average of the pressure was equal to 10.5 $[bars]$. The pressure behavior takes the flow rate behavior as the flow rate forms the pressure. Each cycle consists of six peaks, two for each piston; the physical system takes the same pressure behavior as the

pressure sensors in the physical system attached to the pump outlet manifold. It will read the discharge pressure of the three pistons at the same time. When the feed pressure increases, the pressure increases and the portion of permeate water will increase, which affects the pressure. One of these two peaks represents the flowrate built by one of the pistons, and the other represents the flowrate built by two of the pistons that are in phase in 60º.

6.4 COMPARISON BETWEEN COLLECTED REAL WORLD DATA AND THE MODEL WITHOUT THE DAMPER:

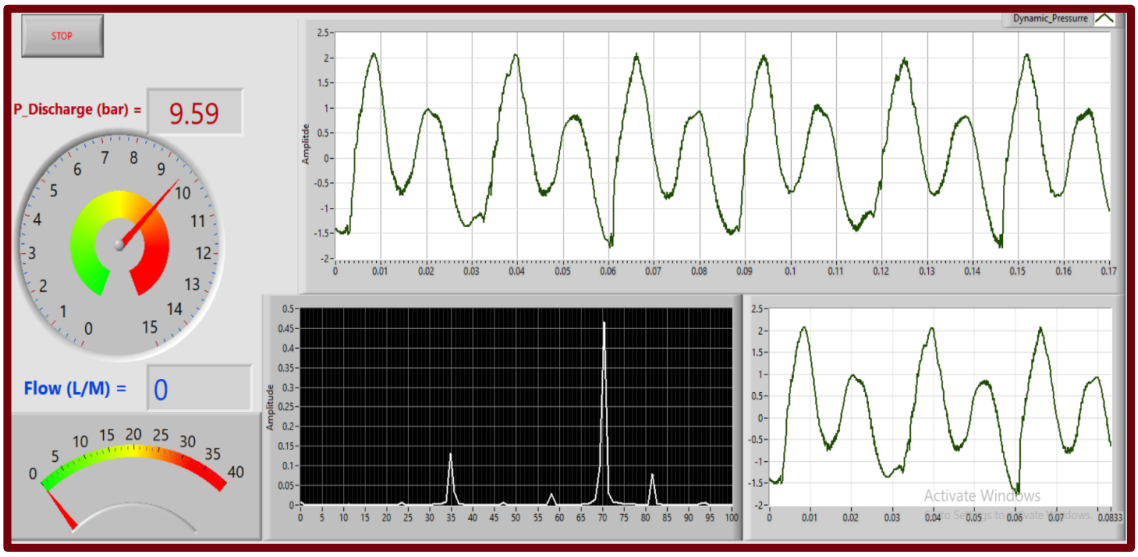

Figure 6.31: Real World Data.

The figure above is a screenshot from LabVIEW software representing the collected real-world data from the physical system in Egypt. The screenshot represented the collected data from a pressure sensor at the pump's outlet manifold that represents the generated pressure from the system that must head the hydraulic losses of the system and osmotic pressure. The figure is divided into four different portions:

- The first one on the left represents an analog measurement that shows the pump discharge static pressure, and its reading was 9.59 bars. While the below

measurement was supposed to read the flow rate, but the data was mistaken not saved.

- The figure at the top represents the dynamic discharge pressure of the pump for two cycles. The two cycles' time was 0.17 seconds as the system running at 690 RPM, which is 11.5 RPS, making each cycle run in 0.0869 seconds. The pressure amplitude represents this graph with time. The two cycles have 12 peaks which makes sense as each cycle represents six peaks as one of these two peaks represents the pressure flowrate built by one of the pistons and the other represents the flowrate built by two of the pistons that are in phase in 60º.
- The figure at the bottom left represents the amplitude with frequency as reading the pressure amplitude regarding to the vibration curve to study if the motor works in the right frequency and amplitude, which was correct as the peaks was respectively between the 34 to 36 and between the 68 and 70. Which is correct. Since the each the system runs at 11.5 RPS and the sensor was attached at the pump outlet manifold. That led the sensor to read the three pistons behavior the (3x) and 3 x 11.5 = 34.5. then it yielded to find the biggest two peaks one at the 34.5 Hz and then the second at 69 Hz. Also, there are minor peaks at 11.5, 23, 35, 46.5 and so on, as each piston reads individually.
- The figure at the bottom right represents the dynamic pressure in one cycle. The plot includes six peaks as one peak of each two peaks represents the pressure of discharging the flowrate of each piston. The other peak represents the flow rate built by two of the pistons that are in phase in 60º. Observing the first peak in every

two peaks representing the pressure built by the pistons, their amplitude is equal, which means that the pump's pistons are healthy.

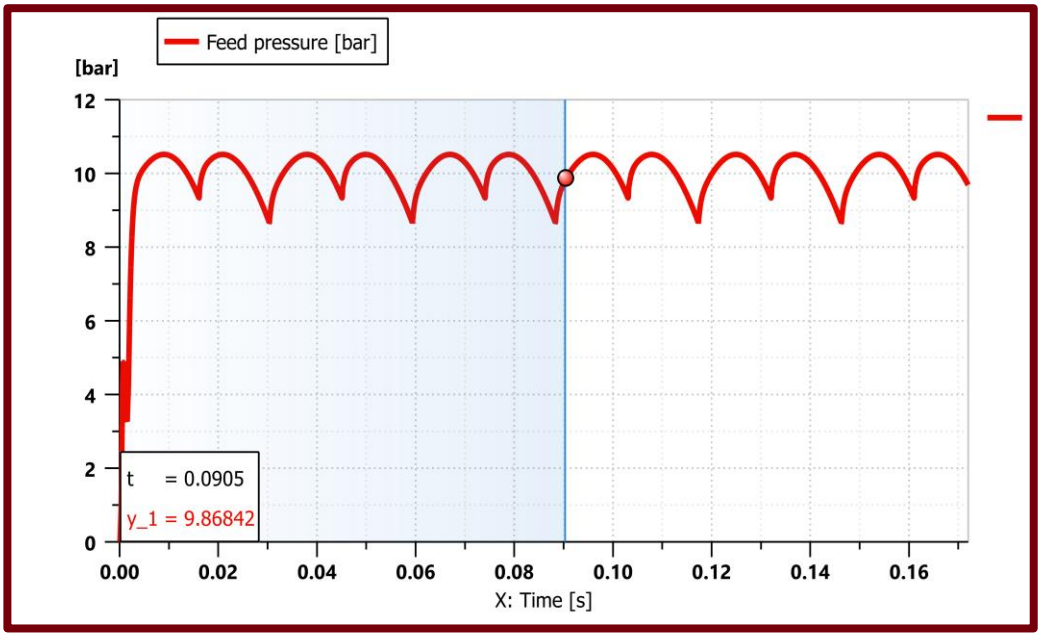

Figure 6.32: Feed Pressure for Two Cycles.

The figure above shows the feed pressure simulation after substituting with all the operating parameters and variables. We observe here that the static pressure average was equal to 9.9 bars which is greater than the average static pressure in the actual physical system with 0.3 bars. The conclusion for this was because when we modeled the feed pressure for the membrane, we used this equation and substituted. This is the reflection coefficient by the value of 1 as the membrane is new and healthy. It was expected to have the greatest value of membrane separation and the more membrane lifetime it has. The reflection coefficient simulations and their effect on the feed pressure is described and illustrated in figure 63. As far as the membrane separation and lifetime is shorter this value is closer to zero and the generated feed pressure is smaller which make sense as when the permeate flowrate is the major variable that effects the feed pressure so when the salinity is lower the generated feed pressure will be lower as well.

$$J_w = A(\Delta P - \sigma\Delta\pi)$$

While the membrane elements in the physical systems are not new as they have been used for experiments and data collection, which will affect this value, when we substituted that value with 0.71, it gives the same exact static pressure average.

Dynamic pressure

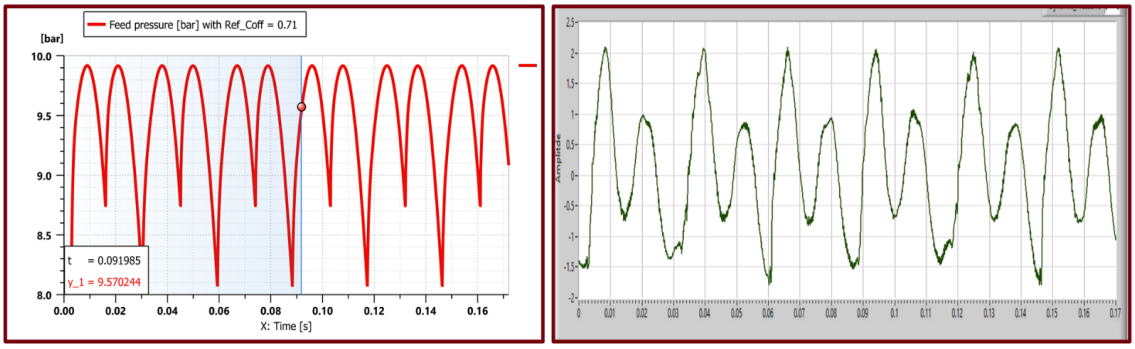

Figure 6.33: Comparison between the Digital & Physical System Feed Pressure.

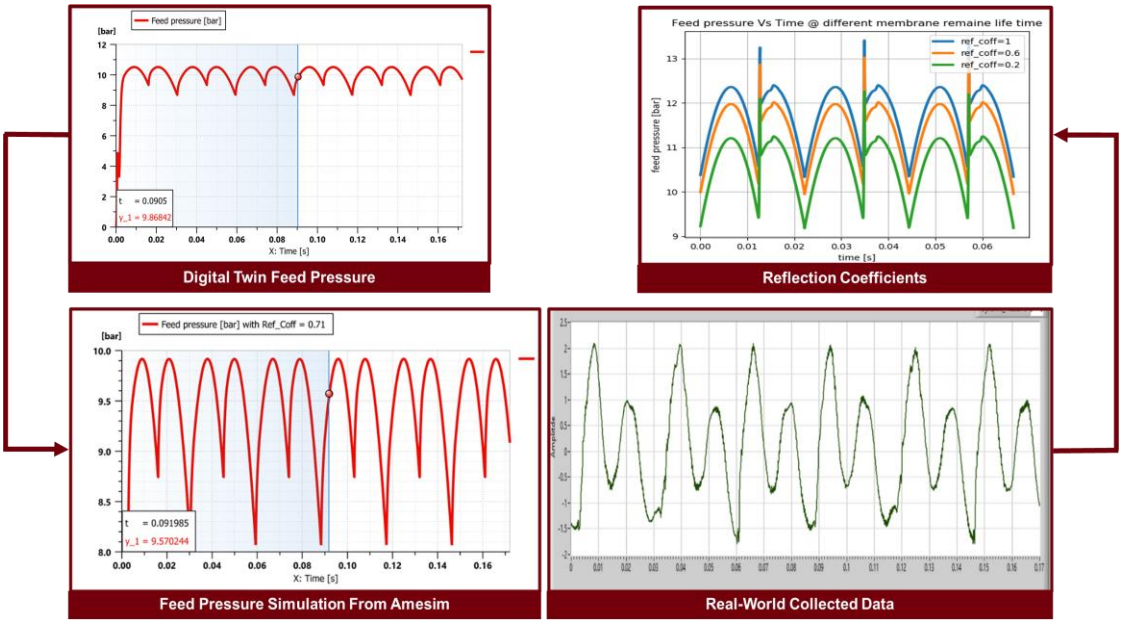

Figure 6.34: Dynamic Pressure Calibration & Cross-Validation.

The figure above shows that the static feed membrane pressure is the same in the digital twin and the physical system. While the dynamic feed pressure has the same behavior for each two peaks in the system as the first one is identical for all the first peak and the second one is identical as one and that's because the digital system is simulated and filtering the data and the waves before representing them and in a healthy condition.

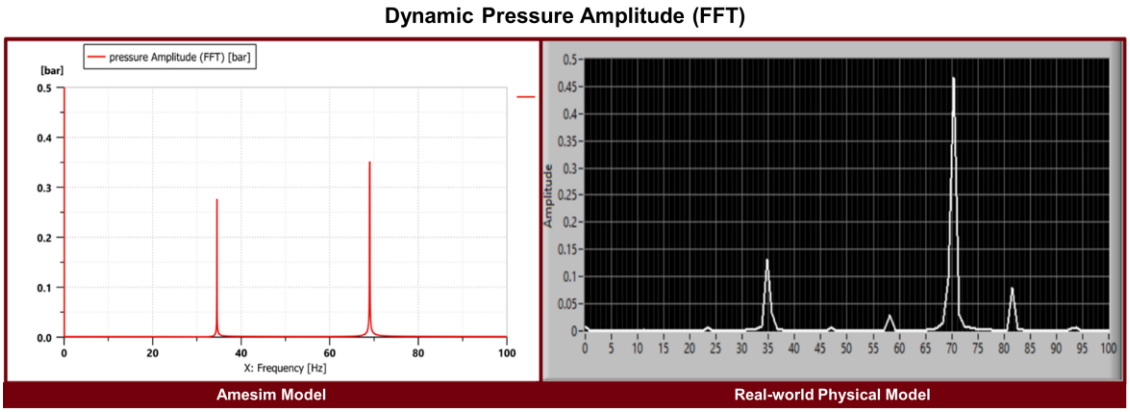

Figure 6.35: Comparison Between Digital and Physical Single Sided Power Spectrum of the signal of the Dynamic Pressure.

The figure above shows the single-sided power spectrum of the signal of the dynamic pressure. The plot on the right is the Amesim simulated plot, and the left figure is the collected signal from the physical system, where the simulated figure shows the peaks on both the 34.5 Hz and the 69 Hz. As the pressure sensor was attached to the pump's outlet manifold, it reads the pressure of the three pistons, and each was on 11.5 Hz, so the vibration curve of the 3x is 34.5. As the system runs with 690 RPM which is 11.5 RPS and the pump is a 3-piston pump and as mentioned above the vibration sensor is plugged at the outlet manifold that's why it reads 3 cumulative hits at each cycle at the 34.5 HZ. The same peaks were represented on the real physical data graph, and there are minor peaks at 11.5, 23, 35, 46.5 and so on, as the sensor reads each piston individually where these readings considered as noise.

6.5 FAULT GENERATION AND DETECTION

This section represents the water desalination system faults and failures from both hydraulic and mechanical faults. Since the water shortage in several countries nowadays, water desalination has been an alternative source for fresh drinkable water in many areas and countries. Keeps the water desalination system properly is vital to maintain human lives. The mechanical and hydraulic failures may cause severe damage to the system components, such as the high-pressure pump and the reverse osmosis membrane elements. The mechanical failures that will be represented in this chapter are:

- Crankshaft fault.
- Valve faults.
- Piston leakage.
- Damper fault.

While the hydraulic faults will be represented about the membrane operating conditions from temperature, salinity separation (salt rejection), membrane recovery and the membrane reflection coefficient.

6.5.1 Crankshaft fault:

This fault can occur while designing, manufacturing, or assembling the pump. The pump includes three pistons, and the pump was designed to vary each piston with 120º and be the angle between the three pistons (0º,120º,240º) respectively. The fault will be generated twice as a fault, and it also can be a smart system design simulation by making the angles vary and see if it will give better pulsations and results or worst. According to these data models, the system will be taught according to these models how to detect faults if that will happen in the future. The first model angles will be (0º,140º,240º), which will

occur as a fault detection case scenario as the second angle got assembled with 20º angle shift in the second crankshaft. In contrast, the second model will be (0º,130º,260º) as a smart system designing case scenario to study the system's pressure, flow rate, and energy consumption.

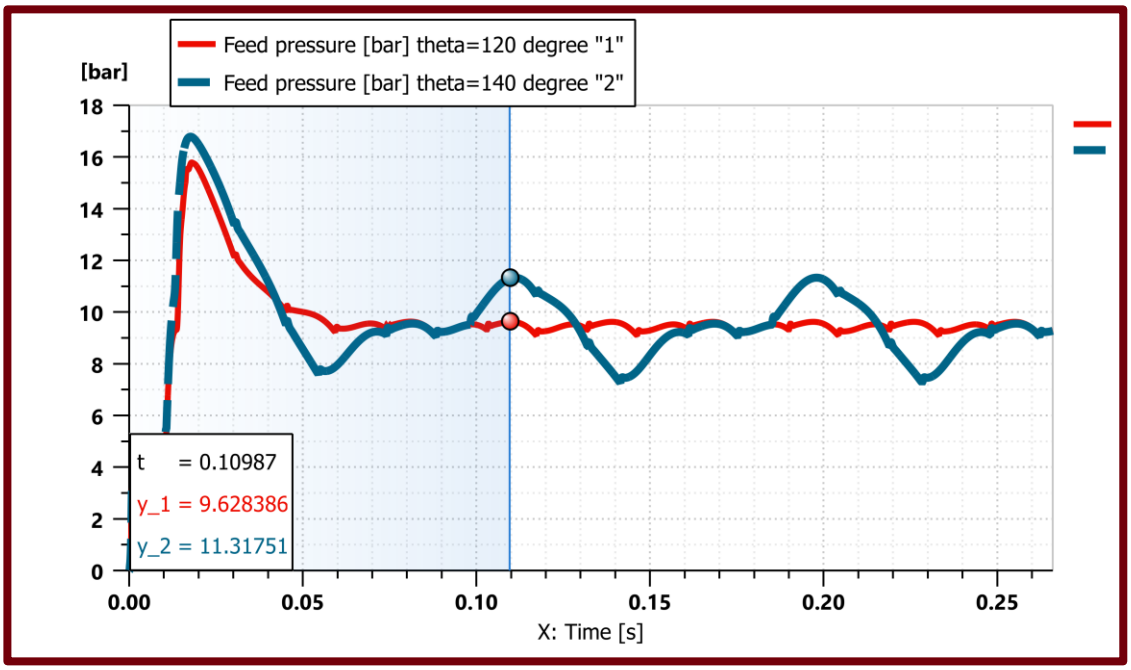

Figure 6.36: Feed Pressure Comparison with the second Crankshaft Different Angles.

The figure above it shows the simulation of the membrane system feed pressure. The red plot represents the Feed pressure with crankshaft angles of (0º,120º,240º) respectively, and the blue plot represents the Feed pressure with the second angle shifted to be (0º,140º,240º). The feed pressure plot with the shifted angle or the faulty one shows the more fluctuations and pressure pulsations that occur after the fault. The pressure was not stable, which causes real problems to the pump and the membranes. The pressure amplitude took place in 4 bars instead of being around 0.5 bars in the healthy scenario. This scenario can be existing because of misalignment, design, or manufacturing failures.

Pressure pulsation leads to vibration of suction and discharges piping, high levels of pump noise, and pressure pulsation appear in both suction and discharge. Which causes the frequency of pressure pulsation could come from known sources such as the running frequency or the vane frequency or coming from unknown sources such as resonance. Eddies from valves or poor upstream piping. Water hammer is essentially caused by the rapid closing of a valve or by a pump failure with the subsequent abrupt closure of the check valve or by a sudden switch over, and the pump starts the procedure. If the fatigue failure shows microscopic striations due to cyclic stress, then pressure pulsations may be the root cause of the problem.

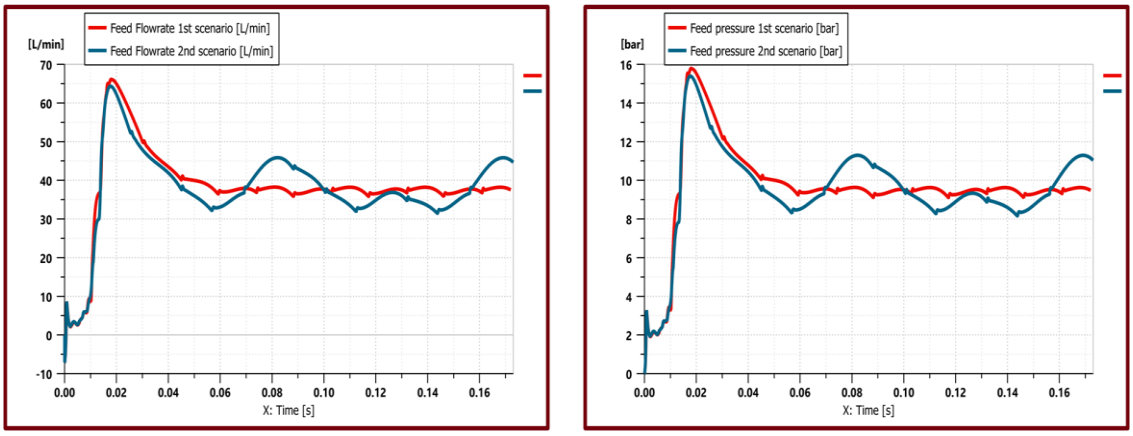

Figure 6.37: Comparison Between the Feed Flowrate and Pressure.

The figure above represents the second case scenario is a trial to enhance the pressure and flow rate pump behavior that improves the high-pressure pump. Instead of shifting the crankshaft angles physically in the pump, the digital twin is shifting and testing the pump after that angle shifting. The angles were shifted from (0º,120º,240º) the default angles to (0º,130º,260º); however, this design required more feed flowrate leads to more permeate flowrate which yields to requiring more feed pressure. The pressure pulsations

were not stable, which affects the pump and the membrane elements. Pressure pulsation leads to vibration of suction and discharges piping, high levels of pump noise, and pressure pulsation appear in both suction and discharge. Which causes the frequency of pressure pulsation could come from known sources such as the running frequency or the vane frequency or coming from unknown sources such as resonance. Eddies from valves or poor upstream piping. Water hammer is essentially caused by the rapid closing of a valve or by a pump failure with the subsequent abrupt closure of the check valve or by a sudden switch over, and the pump starts the procedure. If the fatigue failure shows microscopic striations due to cyclic stress, then pressure pulsations may be the root cause of the problem.

6.5.2 Valve faults:

This section represents the faults that can occur regarding the control valves in the high-pressure pump, not the valves in the water desalination system. The faults that can exist in these control valves are either the valve is not close/shut entirely because of salt concentration which can block the valve gate from being completely closed. The other valve fault can occur if the valve's damper was broken by either the suction or the discharge front pump side valves.

The figure below shows the behavior of the feed pressure before and after the valve break. The red plot shows the feed pressure behavior of the system under healthy conditions. In contrast, the blue plot shows the behavior of the feed pressure after the front suction control valve gets broken it affects the whole feed pressure behavior. Pressure pulsation leads to vibration of suction and discharges piping; high levels of pump noise and pressure pulsation appear in both suction and discharge. Which causes the frequency of pressure pulsation could come from known sources such as the running frequency or the

vane frequency or coming from unknown sources such as resonance. Eddies from valves or poor upstream piping. Water hammer is essentially caused by the rapid closing of a valve or by a pump failure with the subsequent abrupt closure of the check valve or by a sudden switch over, and the pump starts the procedure. If the fatigue failure shows microscopic striations due to cyclic stress, then pressure pulsations may be the root cause of the problem.

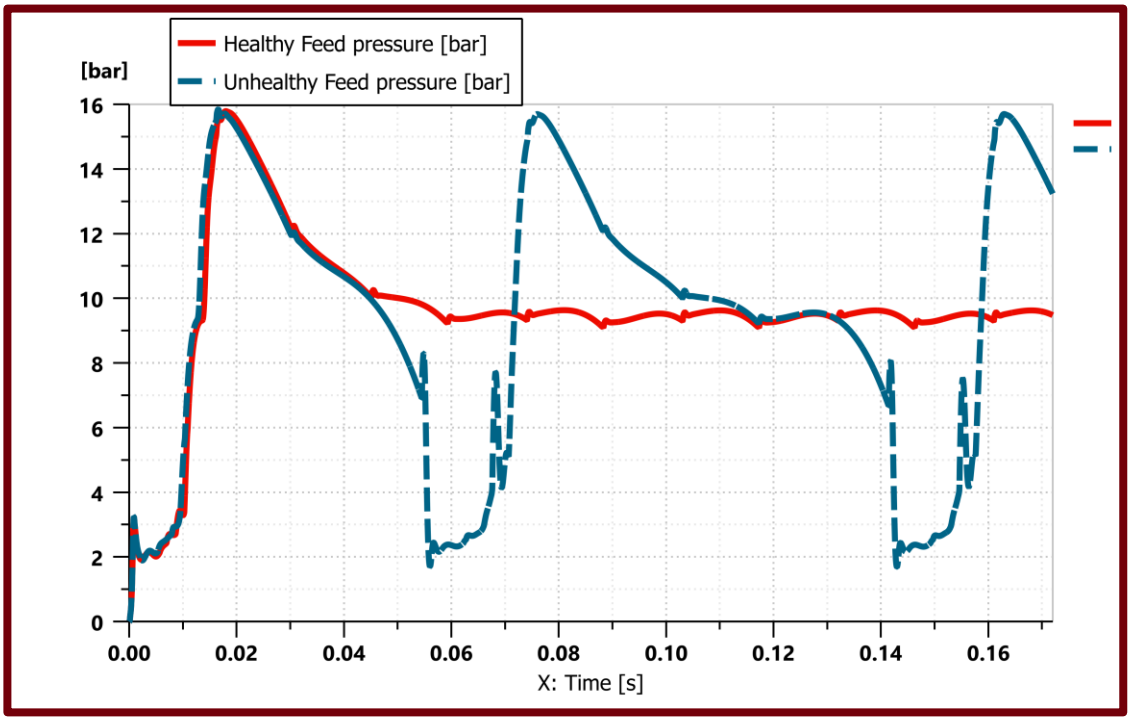

Figure 6.38: Feed Pressure Comparison Before & after the Suction Valve of the 1st Piston was Broken.

6.5.3 Damper fault:

This section represents the faults that can occur in the pump's damper. This section will represent the fault detection more profound as the feed pressure will be simulated before and after break the damper. During one of the experiments running on the physical system in Egypt, the damper got broke accidentally. The data was collected before and

after the damper was broken. Getting the real-world data from this accident and comparing it with the simulated data to observe and test the digital twin sensitivity.

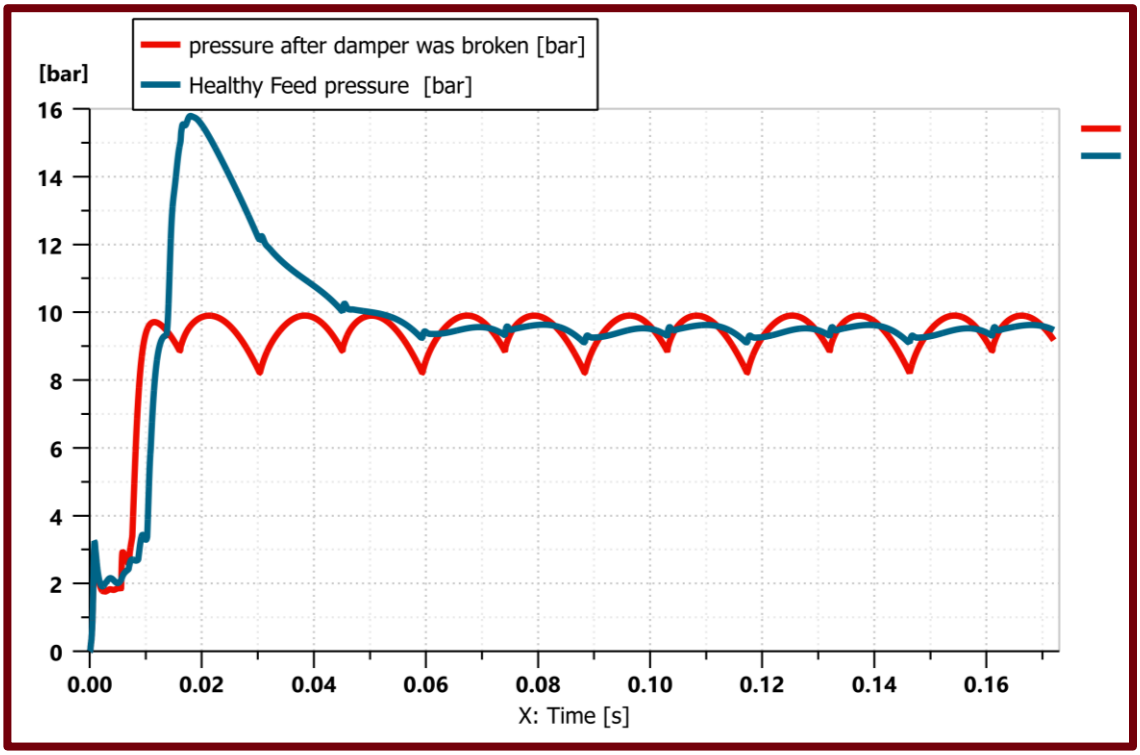

Figure 6.39: Feed Pressure Before & After the Damper Break.

The figure above shows the feed pressure behavior before the damper break, where the blue plot shows the feed pressure behavior when the system is healthy before the damper got to break. The red plot shows the behavior of the feed pressure after the damper did break; the difference between both behaviors is the damper effect where it reduces the pressure amplitude and pressure pulsation. This leads to vibration of suction and discharges piping, high levels of pump noise, and pressure pulsation appears in both suction and discharge. Which causes the frequency of pressure pulsation could come from known sources such as the running frequency or the vane frequency or coming from unknown sources such as resonance. Eddies from valves or poor upstream piping. Water hammer is essentially caused by the rapid closing of a valve or by a pump failure with the subsequent

abrupt closure of the check valve or by a sudden switch over, and the pump start the procedure. If the fatigue failure shows microscopic striations due to cyclic stress, then pressure pulsations may be the root cause of the problem.

6.5.4 Piston fault:

This section simulates the faults that can occurs in the high-pressure pump piston. These faults can exist if there was leakage in one of the pistons or more, also if the piston got broken at any time.

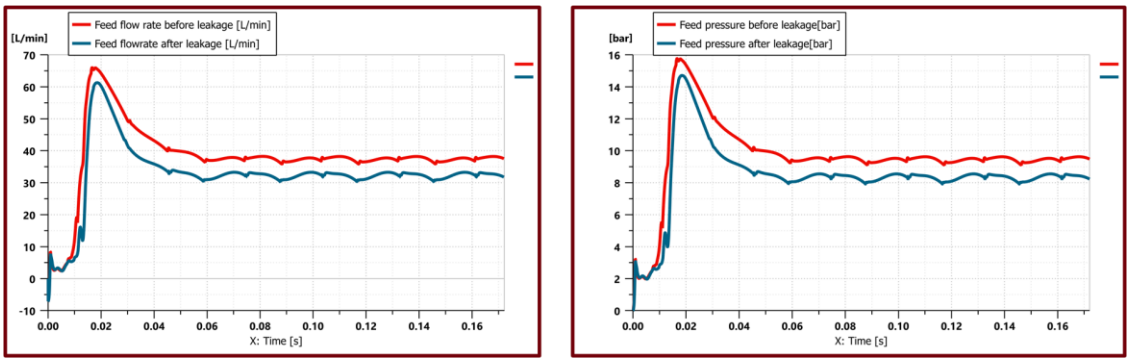

Figure 6.40: Feed flowrate & Pressure Before and After Leakage

The figures above show the feed flow rate and pressure before and after the piston's leakage exists. The leakage occurs in the three pistons that decreases the feed flowrate expected as the flowrate leaks outside the feed path, which also leads to a decline in the generated pressure as the permeate flowrate production will decrease. The leakage can also be detected if the leakage was just in one or two pistons, so the overlapping of the two plots will be at two peaks out of the six peaks in each cycle. The red plot represents the feed pressure and flow rate behavior, while the blue plot represents the feed pressure and flow rate behavior after the leakage occurs.

6.5.5 Reverse osmosis membrane faults:

This section represents the root causes that occur faults the reverse osmosis membrane from higher salinity, temperature, membrane lifetime, and membrane recovery. All these operating parameters affect the membrane elements' recovery and salt rejection. Regular maintenance of the reverse osmosis membrane elements improves membrane productivity. It reduces the fouling and scaling chances, decreasing the membrane and the whole plant lifetime. The first method tests the equation sensitivity and how the feed pressure will be impacted with different salinity, temperature, and recoveries. Then comparing these simulated results with the theoretical theories and mathematical equations.

6.5.5.1 Salinity test:

This section observes the sensitivity of the model by applying different salinities to study the feed pressure behavior. The figure below at the left shows the Feed pressure behavior with different salinities as one of the simulations was with feedwater salinity of 5000 ppm and the other was with 20,000 ppm. The red plot represents the feed pressure with feedwater salinity of 5000 ppm, while the blue plot represents the feed pressure with feedwater salinity of 20,000 ppm. This simulation shows that when the water salinity increases, the generated feed pressure increases as the water salinity is an essential factor in the osmotic pressure equation. When the salinity increases, the osmotic pressure increases, and the required feed pressure to head the osmotic pressure and the hydraulic losses increase.

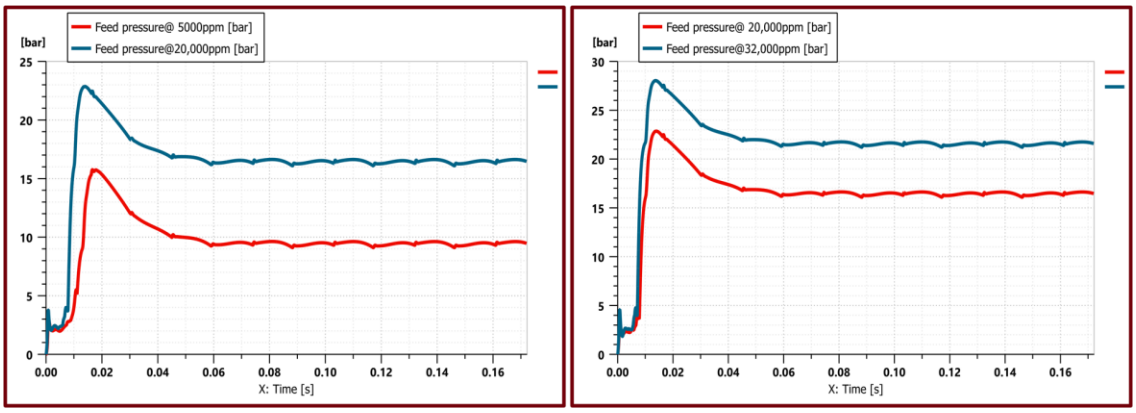

Figure 6.41: Feed Pressure Behavior with Different Salinities.

While The figure at the right shows the Feed pressure behavior with different salinities as one of the simulations was with feedwater salinity of 20,000 ppm and the other was with 32,000 ppm. The red plot represents the feed pressure with feedwater salinity of 20,000 ppm while the blue plot represents the feed pressure with feedwater salinity of 32,000 ppm. This simulation shows that when the water salinity increases, the generated feed pressure increases as the water salinity is an essential factor in the osmotic pressure equation. When the salinity increases, the osmotic pressure increases, and the required feed pressure to head the osmotic pressure and the hydraulic losses increase.

6.4.5.2 Temperature test:

Warmer feed water temperature decreases the saline water viscosity and increases the membrane permeability. Warmer feed water impacts by reducing the osmotic pressure. The feed water temperature impacts both the osmotic pressure and the average solvent flux, which impacts the feed pressure as warmer water requires less feed pressure than colder water. Hot water temperature cannot exceed the higher temperature boundaries of each reverse osmosis membrane-type datasheet.

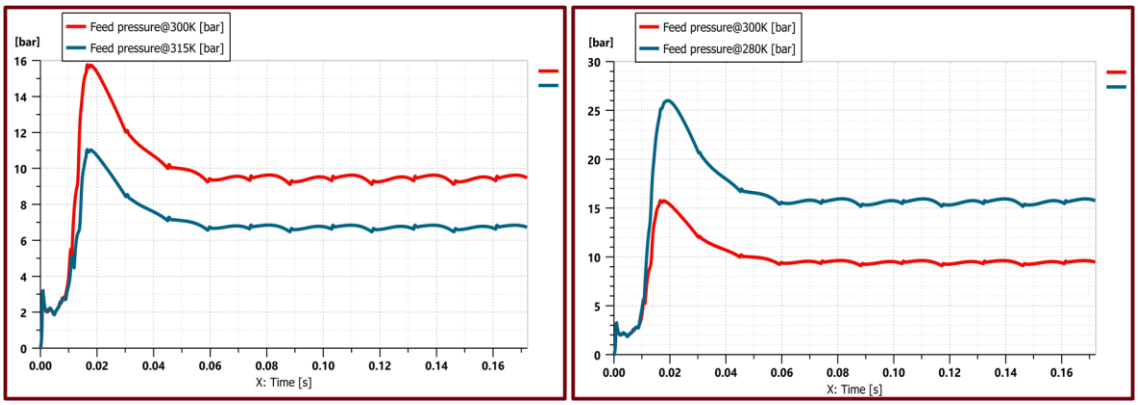

Figure 6.42: Feed Pressure @ Different Temperatures.

The Temperature impacts both ΔΠ and the average solvent flux (Jv), which are essential factors that generate extra feed pressure or reduce it. The rate of permeate flux gain is typically much higher than the rate of deterioration of product water quality. The figure at the left shows the Feed pressure behavior with different temperatures as one of the simulations was with feed water temperature of 300 K. The other was with 315 K. The red plot represents the feed pressure with feed water temperature of 300 K. In contrast, the blue plot represents the feed pressure with a feed water temperature of 315 K. This simulation shows that when the water temperature increases the generated feed pressure decreases as the water temperature is an essential factor of reducing the water viscosity and increases the membrane permeability. When the temperature increases, the feed pressure required to head the osmotic pressure and the hydraulic losses decreases. The figure at the left represents the feed pressure behavior with different temperatures as one of the simulations was with feed water temperature of 300 K. The other was with 280 K. The red plot represents the feed pressure with a feed water temperature of 300 K. In contrast, the blue plot represents the feed pressure with feed water temperature of 280 K. This simulation shows that when the water temperature decreases the generated feed pressure increases as the warmer water temperature is an important factor of reducing the water

viscosity and increases the membrane permeability. When the water temperature decreases, the feed pressure required to head the osmotic pressure and the hydraulic losses increases.

6.4.5.3 Recovery test:

In this section the recovery sensitivity is simulated and discussed, and it is effect on the generated feed pressure. An increase in recovery results in a slow decrease in permeate flux until it reaches the point at which osmotic pressure exceeds the applied pressure.

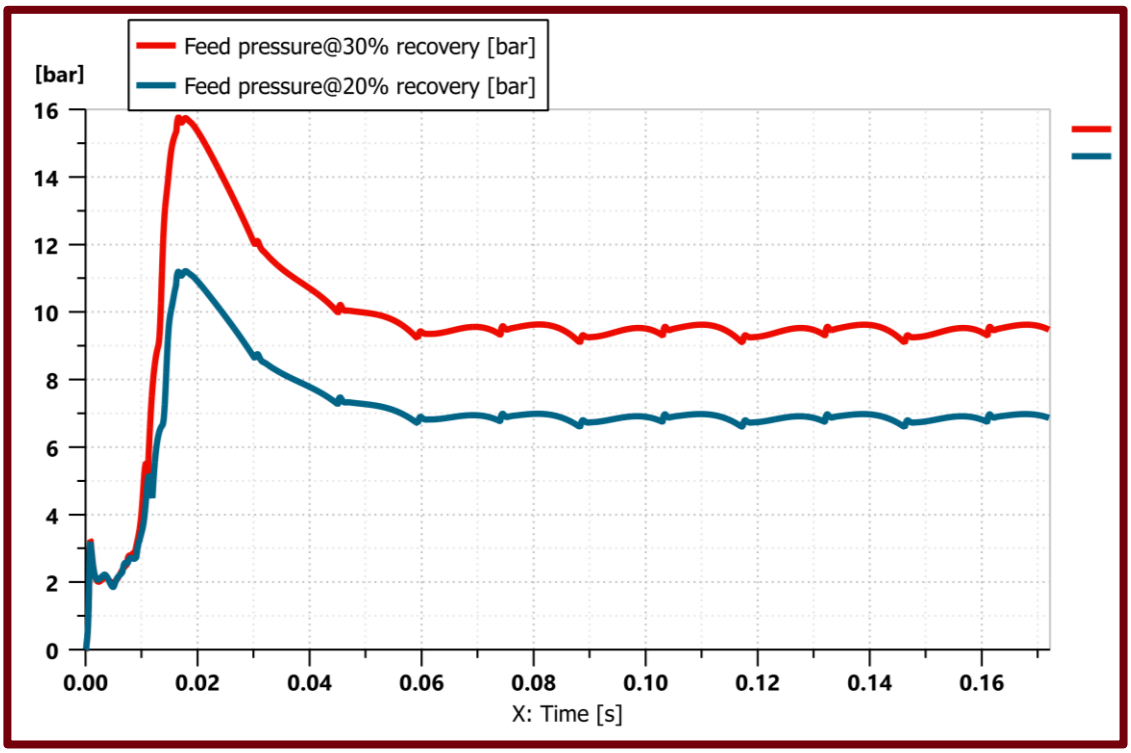

Figure 6.43: Feed Pressure Behavior @ Different Recoveries

The figure above shows the behavior of the feed pressure with different recoveries. The Feed pressure behavior with different recoveries as one of the simulations was with reverse osmosis membrane recovery of 30%, and the other was with 20%. The red plot represents the feed pressure with membrane recovery of 30%, while the blue plot represents the feed pressure with membrane recovery of 20%. This simulation shows that when the

membrane recovery increases, the generated feed pressure increases. The more the membrane recovery is, the more permeate water to be produced, which required more feed pressure to produce more clean water. When the membrane recovery decreases, the feed pressure decreases as lower permeate water is produced. An increase in recovery results in a slight decrease in permeate flux until it reaches the point at which osmotic pressure exceeds the applied pressure, and net drive pressure is inadequate to drive flow through the membrane. At that point, freshwater flow production is discontinued as it is inversely proportional between increasing in the recovery level and decreasing in both salt rejection rate and the permeate flux until it reaches a point and starts being constant. Recovery impacts both the flow rate and the average solvent flux in our equation in permeate flow rate and hydrostatic pressure terms. which generate extra feed pressure or reduce it.

6.4.5.4 Reflection coefficient test:

This section shows the feed pressure sensitivity with the membrane lifetime. As the required feed pressure decrease.

$$J_v = Lm\ (\Delta \mathrm{P} - \boldsymbol{\sigma}\ \Delta\Pi)$$

Where:

- $\boldsymbol{\sigma}$ is the Staverman or reflection coefficient which take value in the interval $0 \leq \boldsymbol{\sigma} \geq 1$.
- The closer the σ to 1 the greater membrane separation.

The figure below shows a simulation for the reflection coefficient and how the membrane health effects the feed pressure.

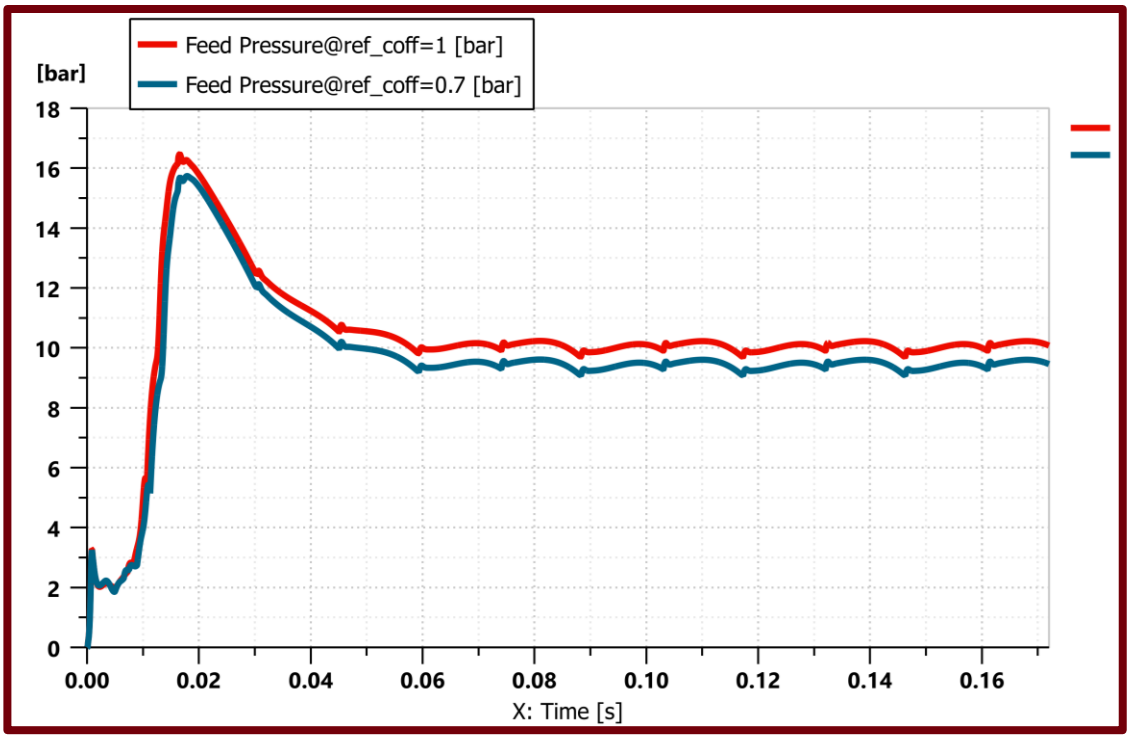

Figure 6.44: Feed Pressure @Different Reflection Coefficients.

The figure above shows the reflection coefficient effect on the feed pressure with time. In contrast, the reflection coefficient takes a value from 0 to 1 ($0 \leq \sigma \geq 1$). The more σ, the more the membrane separation is, and the more membrane lifetime it has. The plot above it simulates that when the membrane was new and its reflection coefficient equals 1, the generated feed pressure from the high-pressure pump will be accurate. When it decreases to zero, the pressure will decrease, which will affect both the membrane recovery and the salt rejection.

6.5.6 Fault detection indication using excessive power consumption:

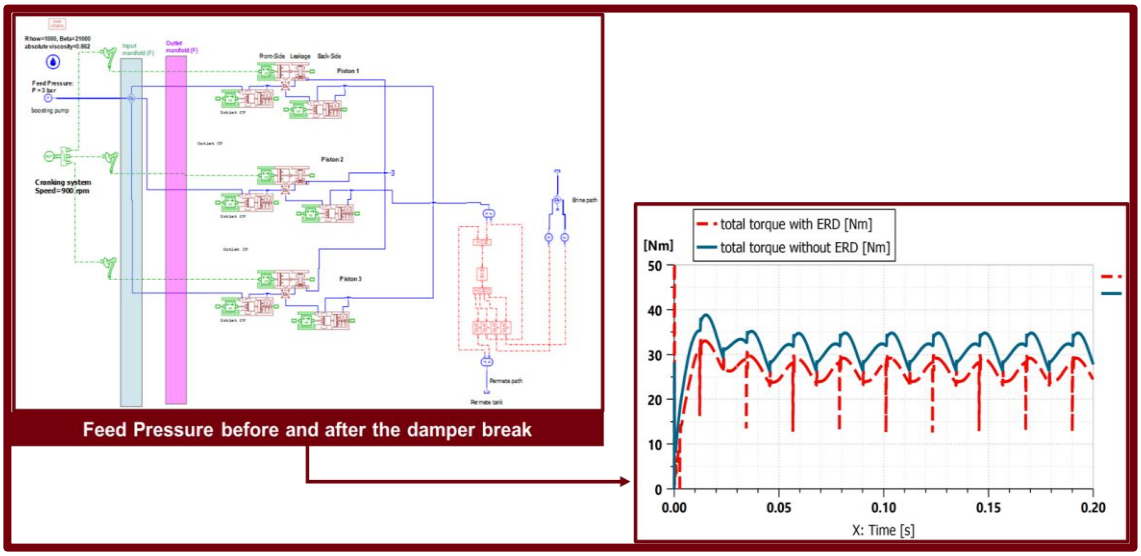

Figure 6.45: Excessive Energy Consumption indication for Fault Detection.

6.6 USING TWO DIFFERENT DIGITAL MODELS FOR FAULT DETECTION CASE STUDY

This section shows a case study for a centrifugal pump that takes place in The British University in Egypt. Several types of faults occur in centrifugal pumps that can be attributed to one or several probable causes. These faults such as Cavitation, bearing, and sealing failures, lubrication, excessive vibration, axial, and radial thrust, and excessive power consumption. In this section, we choose one of the faults, which is the Cavitation as centrifugal pumps. Cavitation is one of the most common faults in centrifugal pumps because of the low suction flow rate and low suction pressure. Cavitation damage is accompanied by four symptoms like erosion, reduction in pumping efficiency, vibration, and noise. There are three main types of Cavitation, classified based on the location of the cavitation inception, the location of the implosion of the vapor bubbles, and the difference in a frequency range which are sheet cavitation, cloud cavitation, and vortex cavitation. Cavitation occurs in two phases the first phase; vapor bubbles are formed around the

pump’s impeller, while the second phase, these vapor bubbles start to collapse with the pump’s impeller.

This section presents two different fault detection digital models one using the saw-tooth model that can express the excitation of the centrifugal pump under cavitation with Fourier expansion and describe the periodic function with combination of sine and cosine waves instead of transfers the real-world data from time domain to frequency domain which made this model more cost and time effective. As the pressure pulses within the diffuser tongue region can be modeled as a sawtooth wave, each pressure pulse acts on the blade's projected area, resulting in a periodic exciting force on the rotating impeller. Each blade projected area has a zero value at both the beginning and the endpoints of the blade-diffuser interaction region. Therefore, it can also be approximated in terms of another saw-tooth wave. The saw-tooth digital model was successfully integrated and tested with the physical system, and it showed its accuracy, as shown in the section below. The second cavitation detection model is a machine learning model that integrated three machine learning algorithms-- the support vector machine, k-nearest neighbors, and logistic regression. The data analysis is based on millions of real-world historical data points that are processed from mounted sensors on the physical system, the data were mainly collected from six different parameters vibration sensors, dynamic and static pressure sensors, and flow rate sensors. Based on this machine learning model, potential cavitation faults are successfully classified and recognized, ensuring 99.5% prediction accuracy after preprocessing and training 80% of these data sets and testing the 20%.

6.6.1 Investigating the Vibration Response of Centrifugal Pumps Under Cavitation Condition:

Models are derived to describe the vibration response of the rotor as well as the casing of feeding centrifugal pump under cavitation condition. Equation (6.1) depicts the forced vibration of the rotor in matrix form:

$$m.X^{\circ\circ}(t) + C.X^{\circ}(t) + K.X(t) = Fb(t), X(o), X^{\circ}(o) = 0 \qquad \text{Eq. 6. 1}$$

Where; $X(t)$ is the state vector that expresses the rotor displacement in horizontal and vertical directions, C is viscous damping matrix, K is the stiffness matrix and $Fb(t)$ is the periodic exiting force vector that results from the cavitation condition. Table 6.1 presents the main specifications of the rotor under consideration [1]. Effectively the periodic exiting force acting on the rotor, results from the summation of all forces acting on each blade of the impeller. Accordingly, the horizontal component and the vertical component of the resultant force vector are given by Equations (6.2) and (6.3) respectively.

Table 6.1: Rotor Main Specifications

Part	**Specification**
Impeller	Mass=0.507 kg
Motor Rotor	Mass=2.264 kg
Motor fan	Mass=.04 kg
Rotor	Length=0.251 m

$$Fbx(t) = Fb(t).cos\,(\omega t) \qquad \text{Eq. 6. 2}$$

$$Fby(t) = Fb(t).sin\,(\omega t) \qquad \text{Eq. 6. 3}$$

Figure 6.47 and Figure 6.48 presents the normalized horizontal and vertical exiting force components on the six impeller blades in time domain and frequency domain respectively.

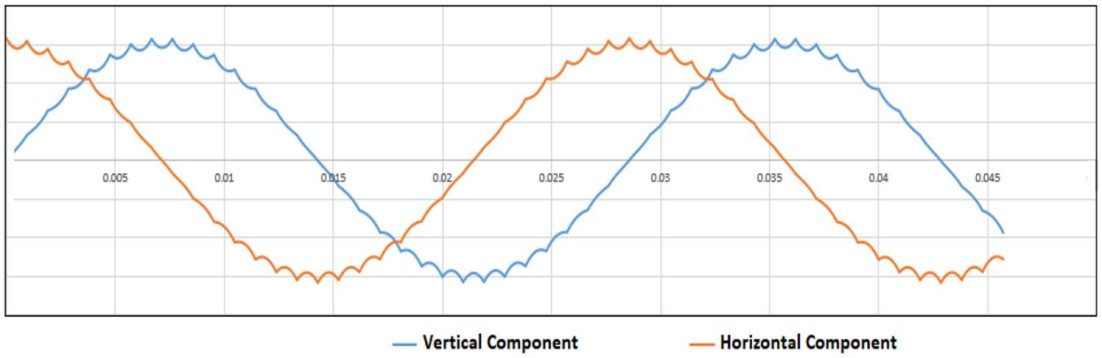

Figure 6.46: Normalized Exiting Force Components of Pump Rotor Under Cavitation Fault.

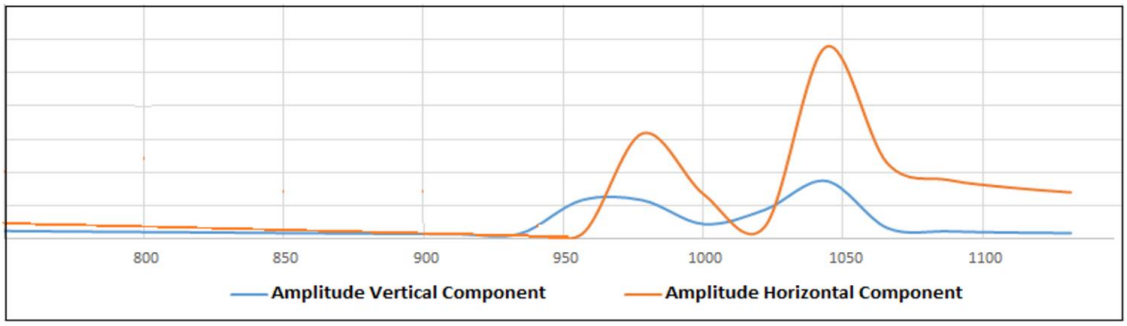

Figure 6.47: Normalized Exiting Force Components of Pump Rotor Under Cavitation Fault.

Figure 6.48 depicts the rotor response to the periodic exiting vertical force component under cavitation condition

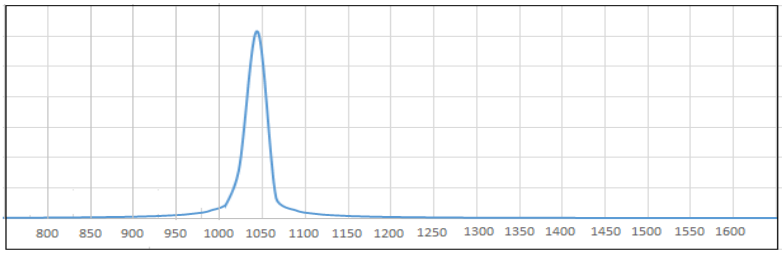

Figure 6.48: Pump Rotor Response to Periodic Pressure Force Vertical Component.

The pump casing can be treated as a pressure vessel subject to periodic internal radial force resulting from the pressure waves of vapor bubbles collapse under the cavitation condition. In this case, the periodic internal force is determined by the pressure pulses times the casing internal surface area. The frequency of this periodic internal force corresponds to the number of impeller blades times the number of diffuser tongues times the synchronous frequency. Physically this frequency expresses the number of pressure pulses resulting from the total number of blade-diffuser tongues interactions per one revolution.

A simple state space model that describes the vibration of the pump casing is given by Equation (6.4).

$$Mc.q^{\circ\circ}(t) + Kc.q(t) = Fc(t), \qquad q(0) = 0\,, q^{\circ}(0) = 0 \qquad \text{Eq. 6. 4}$$

Where, Mc is the mass of the casing, Kc is the stiffness of the casing and $q(t)$ is the displacement. $Fc(t)$ is the periodic internal exiting force that can be determined by multiplying the pressure pulses function of Equations (6.1) and (6.2) by the internal surface area of the casing. To investigate the vibration response of the casing, one approach is to integrate equation (6.4). In this case $Fc(t)$ is expressed in time domain using Fourier expansion where $Fc(t)$ is decomposed into the sum of harmonic functions whose frequencies are multiples of the exiting force frequency. Equation (6.5) despites the Fourier expansion expression of $Fc(t)$.

$$Fc(t) = \frac{a0}{2} + \sum_{i=1}^{\infty}[\, an.\cos(nwot) + bn.sin\,(nwot)] \qquad \text{Eq. 6. 5}$$

$$a0 = 2Ac/Tp\left[\int_0^{\frac{Tp}{2}} 2.Pmax.\frac{tdt}{Tp} + \int_{\frac{Tp}{2}}^{Tp} Pmax\ - 2.Pmax.\left(\frac{t-\frac{Tp}{2}}{Tp}\right)dt\right] \quad \text{Eq. 6. 6}$$

$$an = Ac/Tp\left[\int_0^{\frac{Tp}{2}} 2.Pmax.\cos(nwot)\frac{tdt}{Tp} + \int_{\frac{Tp}{2}}^{Tp} Pmax - 2.Pmax.\cos(nwot)\left(\frac{t-\frac{Tp}{2}}{Tp}\right)dt \quad \text{Eq. 6. 7}$$

$$bn = 0 \qquad (Fc(t) \text{ is an even function}) \quad \text{Eq. 6. 8}$$

Figure 6.49 presents the time domain of the normalized steady state vibration response of pump casing. Figure 6.34 presents the frequency response of the pump casing subjected to the simulated periodic internal force due to cavitation.

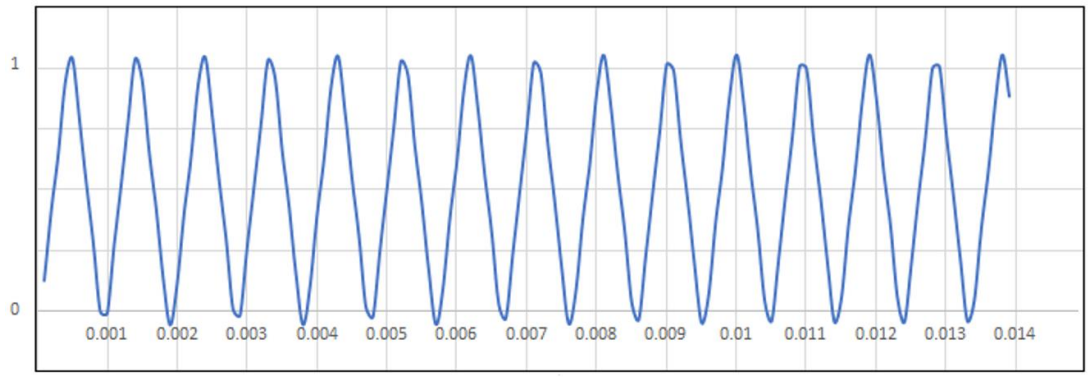

Figure 6.49: Normalized Steady State Vibration of Pump Casing.

The main vibration frequency is 1050 Hz which corresponds to synchronous frequency times the number of blades times the number of diffuser tongues. This result indicates that the developed pump casing model governed by Equations (6.4) through (6.8) has detected the vibration of the casing due to the pressure pulses generated by the cavitation.

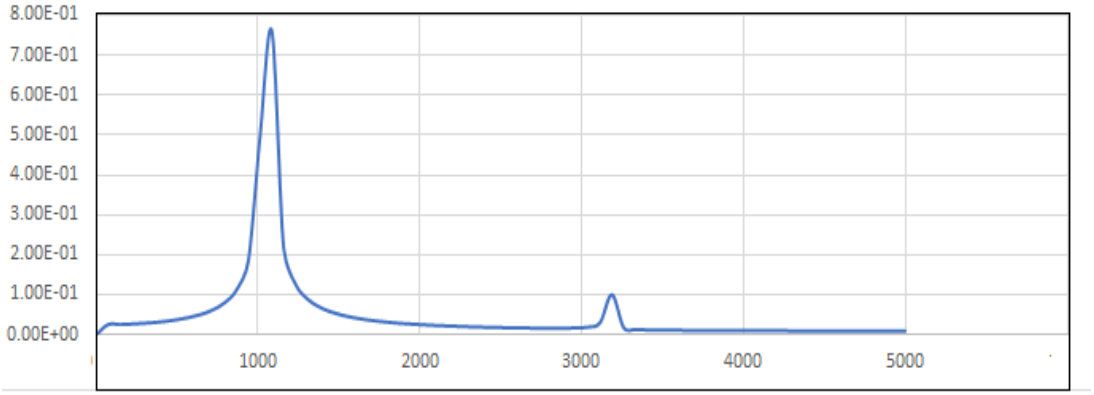

Figure 6.50: Vibration Response of Pump Casing.

The centrifugal pump is a hydraulic turbomachinery that continuously transfers energy to the feed water in a desalination plant. The longevity of centrifugal pumps depends on proper maintenance and early faults detection. In this case study, cavitation in centrifugal pumps is considered. Mathematical models that express pressure pulses as well as the resulting exiting periodic forces were developed. Digital models describing the vibration response of pump rotor and casing under cavitation periodic excitation were tested for a typical small feeding centrifugal pump. Power Spectrum analysis was conducted to present the frequency response characteristics of pump rotor and casing. The dominant detected vibration frequency was 1050 HZ which corresponds to the synchronous frequency times the number of impeller blades times the number of diffusers tongues such results are in agreement with previously published work as well as actual vibration measurements.

6.6.2 Using Machine Learning models in fault detection

Regarding the trendy automatisms and working in an uncertain, evolutionary environment the current industrial plants and systems become more and more mechatronics complex [13]. The classification and detection of the mechanical system faults is an

essential task for a reliable operation. As mentioned above cavitation is one of the most disadvantage problems that occurs frequently in the centrifugal pumps Fault detection using Machine learning algorithms attracted much attention this decade because it is a powerful, fast, computational method that can detect the centrifugal pumps faults efficiently [10][11]. Fault detection using machine learning has been a promising technique of releasing the human labor contribution as it is recognizing the machines health state automatically [14]. The ML model is integrated three machine learning algorithms:

- SVM: is a supervised classification and regression learning algorithm that has strong linear, nonlinear and kernel generalization ability functions. The goal of the algorithm is to create a hyperplane boundary between the possible outputs to separate them into the correct categories. Any new data point can be easily put in the correct category using the hyperplane. SVM algorithm trains different real-world historical data and can efficiently detect cavitation with high accuracy and excellent performance.
- KNN: is a supervised classification learning algorithm and one of the simplest ML algorithms that help in fault detection. KNN algorithm assumes the similarity between the data and puts them into the most similar category to the available categories. KNN has been applied before for different fault detection mechanical use cases, and it showed high accuracy and good scalability.
- Logistic Regression: is a supervised regression analysis method in which the outcome is binary or dichotomous using predictor variables. Logistic regression is also considered a supervised learning classification algorithm used efficiently in predicting the probability of a dependent variable. The model showed a high accuracy to detect the

cavitation as it has been used to build predictive models as a function of predictors and because of the data linearity.

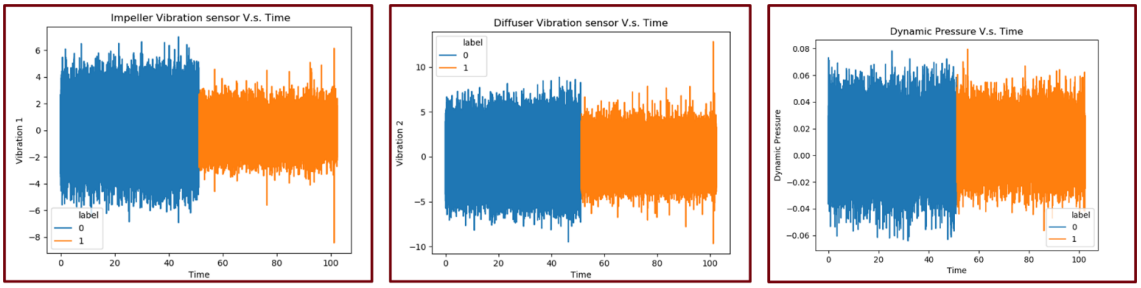

(a) (b) (c)

Figure 6.51: (a) and (b) Collected Vibration Data before and after Cavitation, (c) Collected dynamic pressure data before and after cavitation.

Parts a and b of Figure 12 represents the vibration data that have been collected from two vibration sensors one is mounted to collect the pump's impeller vibration data and the second vibration sensor is mounted to collect the pump's diffuser vibration data. The blue plots represent the data before cavitation exist and takes 0 label, where the orange plots represent the data after cavitation and takes label of 1. The vibration amplitude before cavitation was greater than after cavitation and these real-world collected results can be explained by studying the pressure pulsation data that was collected by using dynamic pressure sensor and represented in part c of the above figure. Part c shows that the dynamic pressure amplitude before the cavitation was greater than after cavitation because of decreasing in the exciting force magnitude affecting the pump's rotor during the cavitation and this decreasing magnitude corresponds to the decrease in $\Delta P = (P_{2\_} P_1)$. Due to the bubble's explosion at this point during cavitation P_1 increase at this BPF frequency the spectral peak does not show any significant decrease from normal to cavitation condition [1].

Figure 13 shows three confusion matrices generated by three different ML algorithms the SVM, the KNN, and the Logistic regression. Confusion matrices represent the detailed algorithm performance in terms of true negatives (TN), true positives (TP), false positives (FP), and false negatives (FN). In the presented use case, 104,963 TP data sets were predicted successfully as cavitated data sets. In contrast, three FN data sets were falsely predicted as healthy data before the cavitation generates. Where 104,652 TN data sets were truly predicted as healthy data sets successfully, while 97 FP data sets were falsely predicted as cavitated data, however, it was not cavitated data sets. This SVM algorithm accuracy is > 99.5% however, the occurrence of 97 falsely predicted as faulty data sets was not acceptable because that can yield to an unplanned/spontaneous decision like shutdown the pump several times, which cause unstable water production and industry disturbance. The KNN algorithm improved the predicted data by decreasing the number of FP data sets; the algorithm is more accurate and efficient than the SVM model as it is more cost and time-efficient in detecting the cavitation faults. However, while the KNN algorithm was working on decreasing the number of FP data sets to 36% of the SVM model, the number of FN data sets increased, which is not acceptable as it means more cavitation data sets will exist without predicting them. Applying the logistic regression algorithm to reduce the two types of errors, the FP and FN detected data sets. The logistic regression algorithm was the most time-efficient model, and it supported the most accurate fault detection result with f1 accuracy of 99.996% because of the data linearity.

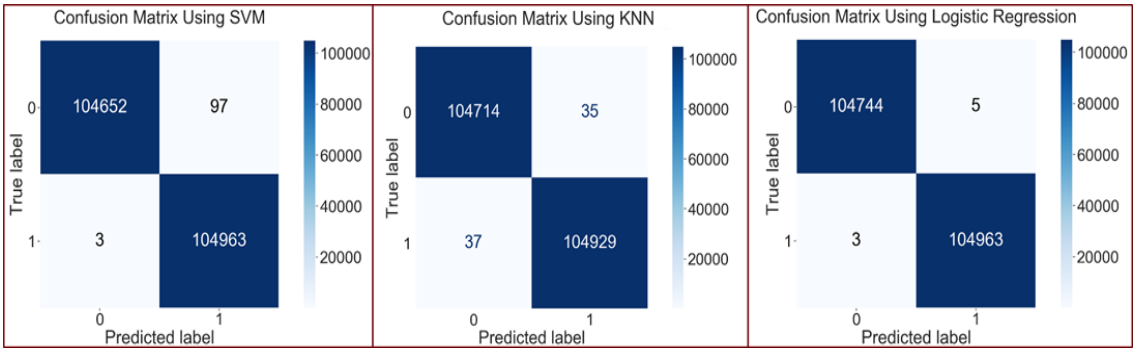

Figure 6.52: Confusion matrix using SVM, KNN & Logistic Regression.

The machine learning models accuracy was calculated using the F1 score method. Different methods can calculate the accuracy of the three models; two methods are recommended for calculating the model accuracy and their equations are listed below. The accuracy method is more recommended when the machine learning models users are more attracted to the True Positives, and True Negatives detected points [16]. In contrast, the F1 score method is more recommended when False Negatives and False Positives are crucial. In most real-life classification problems, the F1 score method is applied because the imbalanced class distribution exists, and it is a better metric to evaluate the model [15]. The aim of using three different ML algorithms and comparing them with each other even with each model's high accuracy, which exceeds 99.5%, is to combining these three models' fault detection before making any decision that can affect the industry. For example, the SVM algorithm is one of the most robust classification algorithms that has been introduced and applied before on several fault detection problems on mechanical, hydraulic, and electrical components. However, SVM showed less efficiency than the KNN model, which was lower than the Logistic regression model in our cavitation detection case. SVM showed the existence of 97 false positives detected points and if the fault detection model depended on just one ML algorithm instead of the three ML models combined with the

saw-tooth physical-based model, several false decisions would occur by the machine operators due to generates false alarms, which could affect the logistics, planning and disrupt the production systems by causing production delay.

$$Accuracy = \frac{TP + TN}{TP + FP + TN + FN}$$

$$F1 - measure = 2 * \frac{Precision * Recall}{Precision * Recall}$$

CHAPTER 7

CONCLUSION

The use case in Section 4 was only applied to two components, a high-pressure pump, and RO membranes, but digital transformation can be applied in stages. The lessons learned, framework, data, and algorithms developed when focusing on a single component can be expanded to cover the system and later the entire plant. Figure 7.1 shows the steps of expanding from high pressure pump to smart plant.

- Step 1: Apply Digital Transformation to three components of a system in the plant such as the high-pressure pump of the reverse osmosis system.
- Step 2: All algorithms, models and techniques developed in Step 1 will be expanded and applied to all the components of the reverse osmosis system.
- Step 3: All algorithms, models, and techniques developed in Step 2 will be expanded and applied to the remaining systems of the plant.
- Step 4: Expand the application of digital transformation to a network of smart plants allowing users to monitor both individual plants and the interactions between plant.

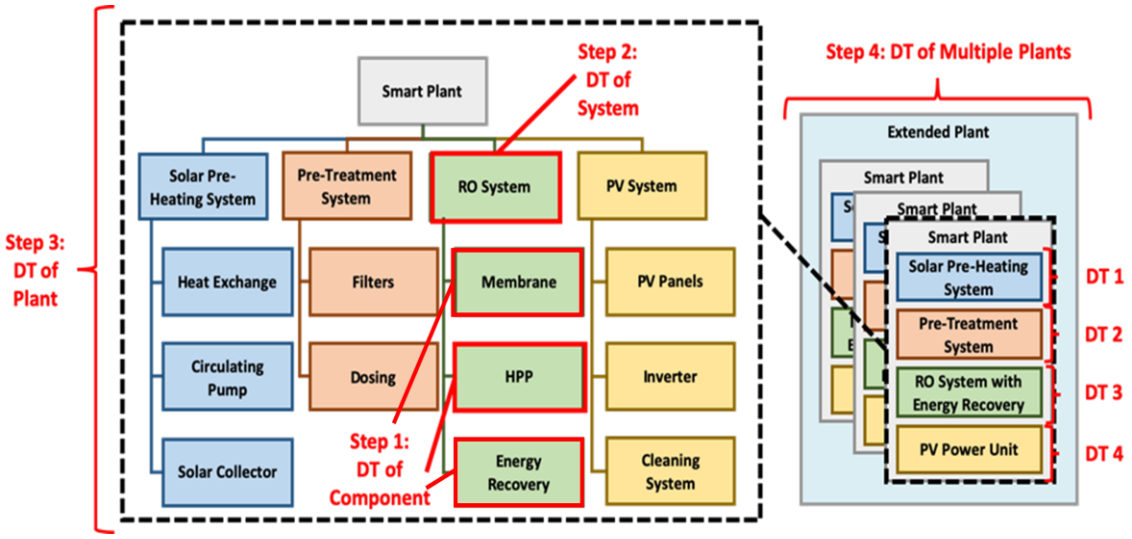

Figure 7.1: Incremental Application of Digital Transformation

7.1 FUTURE WORK

- Modeling the water desalination plants filter and the feeding pump on Amesim and integrate them with the digital water desalination system twin to end up having a whole water desalination plant digital model.
- We started modeling a vane pump using Amesim software and next step is integrating it with three stage reverse osmosis membrane, so it ends up having different types of pumps and using the digital twin of each pump according to which pump is suitable for different kind of environments.

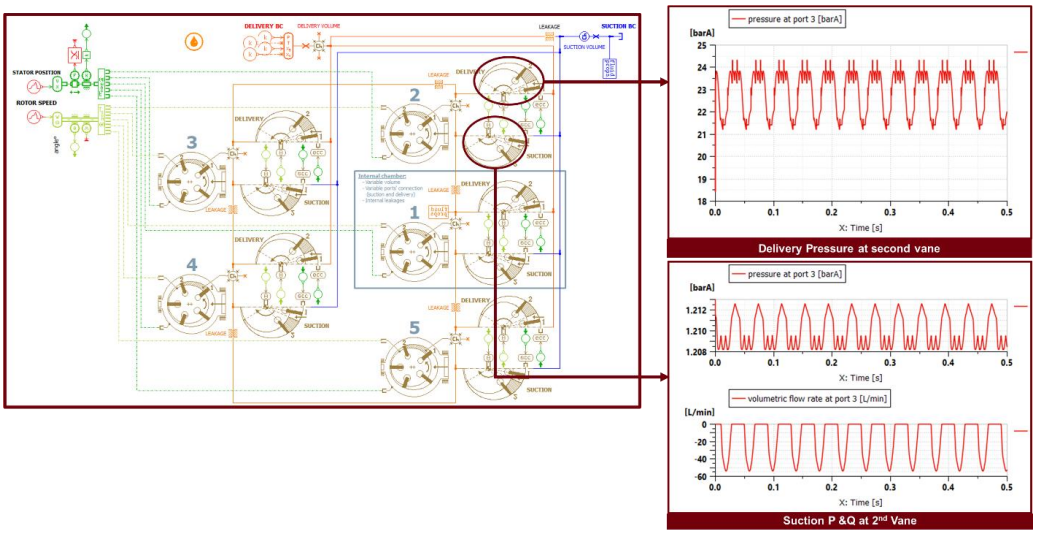

Figure 7.2: Vane Pump modeling and simulations

- Determining the remaining lifetime for the rest of the water desalination system component and start a cost benefit analysis study that can show the cost and time advantage of applying the digital transformation, predictive analytics, and predictive maintenance.

Figure 7.3: Predictive analytics dashboard

- Predictive analytics for the health of the system components and the overall health plant is useful for analyzing if there are frequent failures take place at the same time of the day shift, month, or year. Might be also in certain environmental conditions like certain temperature degrees or a human (operator error).
- Build real time dashboards that allow for all processing, storage, and calculations to be conducted in one location. They also present the necessary information quickly and in an easy-to-understand format so that decisions are made with more knowledge and can yield better results. Once the fault detection models have been implemented, the analysis and results will need to be presented to allow users to quickly understand any problems and inform their decisions. Additional benefits of these dashboards are the ability to enhance training and facilitate knowledge transfer through simulating hands-on experience. A key part of these dashboards is that the information presented is customized and tailored to fit the needs of different users. Three sample views are shown in Figure 7.4. The left side shows a user the health status of the multiple water desalination plants they are overseeing, an executive might use this view to make decisions. The middle dashboard represents the data that a plant manager will be interested in as it shows more specific data regarding to each component in the system. The right side shows the health and status of a specific system and the fault detection analysis for maintainers.

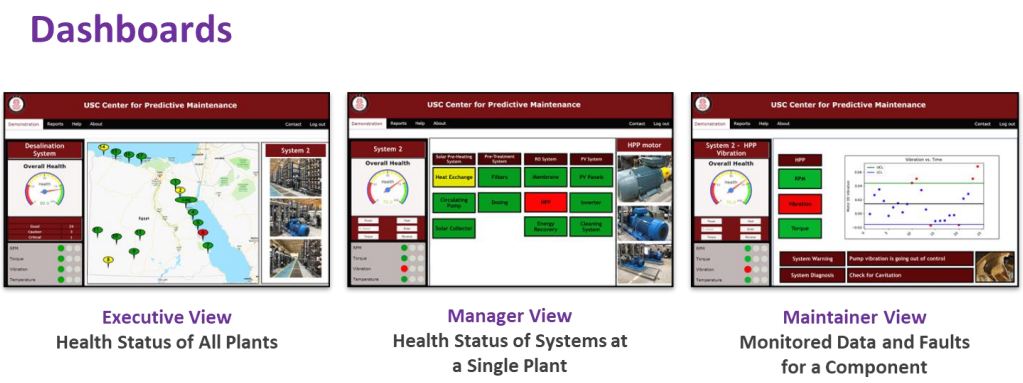

Figure 7.4: Different Dashboards view

REFERENCES

[1] H. Ritchie, "Our World in Data," 01 July 2021. [Online]. Available: https://ourworldindata.org/water-sanitation-2020-update.

[2] M. Zakaria, "Research gate," December 2018. [Online]. Available: https://www.researchgate.net/publication/329144579_Performance_investigation_of_a_solar_desalination_system.

[3] A. GHADHBAN, AN ANALYSIS AND SIMULATION OF SOLAR WATER DESALINATION SYSTEMS, Denver: University of Colorado, 2005.

[4] F. Hazim MohameedQiblawey, "Solar thermal desalination technologies," *Desalination,* vol. Volume 220, no. Issues 1–3, pp. 633-644, 2008.

[5] P. P. M. M. Mohammad Alghoul, "Design and experimental performance of brackish water reverse osmosis desalination unit powered by 2 kW photovoltaic system," *Renewable Energy ,* vol. 93, pp. 101-114, August 2016.

[6] C. B. K. M. E. O. L. T. J. V. J. Bendfeld, "Design of a pv-powered reverse osmosis plant for desalination of brackish water," in *2nd world conference and exhibition on photovolatic solar energy conversion*, Vienna, Austria, 1998.

[7] SoterisKalogirou, "Economic analysis of a solar assisted desalination system," *Renewable Energy*, vol. 12, no. 4, pp. 351-367, December 1997.

[8] D. DomingoZarzo, "Desalination and energy consumption. What can we expect in the near future?," *Desalination,* vol. 427, no. 1, pp. 1-9, February 2018.

[9] G. J. a. P. Battacharya, "Drinking water: sources, sanitation and safeguardaing," The Swedish Research Council Formas, Stockholm, Sweden, 2009.

[10] W. J. P. X. Lu Lin, "Comparative study on pharmaceuticals adsorption in reclaimed water desalination concentrate using biochar: Impact of salts and organic matter," *Science of The Total Environment,* vol. 601–602, pp. 857-864, December 2017.

[11] F. P.-M. C. F.-L. Isabel Martínez-Alcalá, "Pharmaceutical grey water footprint: Accounting, influence of wastewater treatment plants and implications of the reuse," *Water Research,* vol. 135, pp. 278-287, May 2018.

[12] T. M. G. L. Noreddine Ghaffour, "Technical review and evaluation of the economics of water desalination: Current and future challenges for better water supply sustainability," *Desalination,* vol. 309, pp. 197-207, January 2013.

[13] B. A. A. A. O. Mousa S.Mohsen, "Energy Options for Water Desalination in UAE," *Procedia Computer Science,* vol. 83, pp. 894-901, 2016.

[14] H. E. H.T. El-Dessouky, Fundementals of Salt Water Desalination, Kuwait: Department of Chemical Engineering, College of Engineering and Petroleum, Kuwait University, 2002.

[15] S. G. J. G. P. S. D. F. &. M. P. Renou, "Landfill leachate treatment: Review and opportunity," *Journal of hazardous materials,* vol. 150, no. 3, pp. 468-493, 2008.

[16] C. S. A. R. C. &. U. C. G. Slater, "Applications of reverse osmosis to complex industrial wastewater treatment.," *Desalination,* vol. 48, no. 2, pp. 171-187, 1983.

[17] T. Matsuura, Synthetic membranes and membrane separation processes, CRC press, 2020.

[18] R. M. T. G. E. C. &. S. S. Rangarajan, "Predictability of reverse osmosis performance of porous cellulose acetate membranes for mixed uni-univalent electrolytes in aqueous solutions," *ndustrial & Engineering Chemistry Process Design and Development,* vol. 17, pp. 46-56, 1978.

[19] P. B. L. P. a. S. S. Takeshi Matsuura, "Parameters for Prediction of Reverse Osmosis Performance of Aromatic Polyamide-Hydrazide (1:1) Copolymer Membranes," *Industrial & Engineering Chemistry Process Design and Development,* vol. 16, no. 4, pp. 510-516, 1977.

[20] A. D. K. I. K. &. W. J. M. Khawaji, "Advances in seawater desalination technologies," *Desalination,* vol. 221, no. 1-3, pp. 47-69, 2008.

[21] S. e. a. Bou-Hamad, "Comparative performance analysis of two seawater reverse osmosis plants: twin hollow fine fiber and spiral wound membranes," *Desalination,* vol. 120, no. (1-2), pp. 95-106, 1998.

[22] A. L. M. H. M. &. D. A. Abdel Fatah, "Using Digital Models for Condition Based Maintenance of High Pressure Pumps in SWRO Desalination Plants," in *Texas A&M Engineering Experiment Station.,* 2018.

[23] A. A. M. A. H. M. L. a. A. S. D. Abdel Fatah, "Health Monitoring of Centrifugal Pumps Using Digital Models.," *Journal of Dynamic Systems, Measurement, and Control,* vol. 141, no. 9, 2019.

[24] A. K. W. a. K. B. M. Pratesh Jayaswal, "Machine Fault Signature Analysis," *International Journal of Rotating Machinery,* vol. 10, no. Hindawi Publishing Corporation, p. 10, 2008.

[25] V. S. C. P. L. &. P. A. Liagkou, "Challenges and Opportunities in Industry 4.0 for Mechatronics, Artificial Intelligence and Cybernetics," *Electronics,* vol. 10, no. 16, 2021.

[26] N. Voutchkov, Desalination Engineering Planning and design, The McGraw-Hill Companies, 2012.

[27] N. Voutchkov, "Energy use for membrane seawater desalination–current status and trends," *Desalination,* vol. 431, pp. 2-14., 2018.

[28] L. V. N. &. L. O. Birnhack, "Fundamental chemistry and engineering aspects of post-treatment processes for desalinated water," *Desalination,* vol. 273, no. 1, pp. 6- 22, 2011.

[29] N. Voutchkov, Desalination Project Cost Estimating and Management, CRC press, 2018.

[30] R. G. S. L. U. J. &. V. A. Raluy, "Life-cycle assessment of desalination technologies integrated with energy production systems," *Desalination,* vol. 167, pp. 445-458, 2004.

[31] R. G. L. S. J. U. a. A. V. Raluy, "Life cycle assessment of water production technologies-Part 2: reverse osmosis desalination versus the Ebro river water transfer," *The International Journal of Life Cycle Assessment.,* vol. 10, no. 5, pp. 346-354, 2005.

[32] T. F. H. A. Z. &. K. A. Mezher, "Techno-economic assessment and environmental impacts of desalination technologies," *Desalination,* vol. 266, no. 1-3, pp. 263-273, 2011.

[33] H. Krishna, Introduction to desalination technologies, Texas: Water Development, 2004.

[34] Z.-H. L. Z.-X. S. H.-s. X. a. N. X. S.-F. Li, "Performance study on a passive solar seawater desalination system using multi-effect heat recovery," *Applied Energy,* vol. 213, pp. 343-352, 2018.

[35] M. A.-A. H. M. a. Z. A. M. Al-harahsheh, "Solar desalination using solar still enhanced by external solar collector pcm," *Applied thermal engineering,* vol. 128, pp. 1030-1040, 2018.

[36] C. G. Y. &. S. E. Li, "Solar assisted sea water desalination: A review.," *Renewable and Sustainable Energy Reviews,,* vol. 19, pp. 136-163., 2013.

[37] H. S. Aybar, "Analysis of a mechanical vapor compression desalination system.," *Desalination,* vol. 142, no. 2, pp. 181-186., 2002.

[38] N. H. &. E.-F. A. K. Aly, "Mechanical vapor compression desalination systems," *a case study. Desalination,* vol. 158, no. 1-3, pp. 143-150., 2003.

[39] M. W. S. R. Mahmoud Shatat, "Opportunities for solar water desalination worldwide," *Sustainable Cities and Society,* vol. 9, pp. 67-80, December 2013.

[40] M. M. &. A. E. K. M. A. Naim, "Non-conventional solar stills Part 2. Non-conventional solar stills with energy storage element.," *Desalination,* vol. 153, no. 1-3, pp. 71-80, 2003.

[41] K. &. R. A. Rahbar, "Performance enhancement and optimization of solar chimney power plant integrated with transparent photovoltaic cells and desalination method," in *Sustainable Cities and Society*, 2019.

[42] N. S. C. P. T. &. T. J. Voutchkov, Desalination process technology. Cotruvo, J., Voutchkov, N., Fawell, J., Payment, P., Cunliffe, D., Lattemann, S. Desalination Technology–Health and Environmental Impacts. Boca Raton, USA: Taylor and Francis Group, 2010.

[43] A. Kaushal, "Solar stills: A review.," *Renewable and sustainable energy reviews,* vol. 14, pp. 446-453, 2010.

[44] K. W. &. L. D. R. Lawson, "Journal of membrane Science," *Membrane distillation,* vol. 124, no. 1, pp. 1-25, 1997.

[45] H. Strathmann, "Electrodialysis, a mature technology with a multitude of new applications," *Desalination,* vol. 264, no. 3, pp. 268-288, 2010.

[46] Y. Tanaka, "Water dissociation in ion-exchange membrane electrodialysis," *Journal of Membrane Science,* vol. 203, no. 1-2, pp. 227-244, 2002.

[47] O. K. Buros, "The ABCs of desalting," International Desalination Association, Topsfield, MA, 2000.

[48] A. R. R. &. V. N. Chianese, "Treatment of landfill leachate by reverse osmosis," *Water Research,* vol. 33, no. 3, pp. 647-652, 1999.

[49] C. J. S. B. &. Y. P. Delbecq, "Optical Absorption of Cl 2− Molecule-Ions in Irradiated Potassium Chloride," *Physical Review,* vol. 111, no. 5, 1958.

[50] S. Loeb, "The Loeb-Sourirajan membrane," *How it came about.,* pp. 1-9, 1981.

[51] S. Manjikian, "Desalination membranes from organic casting solutions.," *Industrial & Engineering Chemistry Product Research and Development.*, vol. 6, pp. 23-32, 1967.

[52] C. E. &. B. E. J. Reid, "Water and ion flow across cellulosic membranes," *Journal of Applied Polymer Science*, vol. 1, pp. 133-143, 1959.

[53] S. &. S. S. Loeb, "Sea water demineralization by means of an osmotic membrane.," *Saline Water Conversion—II*, vol. 9, pp. 117-132, 1962.

[54] M. A. A. B. A. B. A. E. H. Y. A. Y. .. &. H. H. Mouiya, "Flat ceramic microfiltration membrane based on natural clay and Moroccan phosphate for desalination and industrial wastewater treatment," *Desalination*, vol. 427, pp. 42-50, 2018.

[55] W. J. G. P. S. I. A. F. &. L. S. O. Lau, "Ultrafiltration as a pretreatment for seawater desalination: A review," *Membrane Water Treatment*, vol. 5, no. 1, pp. 15-29, 2014.

[56] C. K. Diawara, "Nanofiltration process efficiency in water desalination.," *Separation & Purification Reviews*, vol. 37, no. 3, pp. 302-324, 2008.

[57] K. S. &. K. O. Spiegler, "Thermodynamics of hyperfiltration (reverse osmosis): criteria for efficient membranes," *Desalination*, vol. 1, no. 4, pp. 311-326, 1966.

[58] N. Voutchkov, Pretreatment for reverse osmosis desalination, Elsevier, 2017.

[59] B. Sauvet-Goichon, "Ashkelon desalination plant—a successful challenge," *Desalination*, vol. 203, no. 1-3, pp. 75-81, 2007.

[60] M. Stewart, Operations, Surface Production, Pump and Compressor Systems: Mechanical Design and Specification, Elsevier, 2018.

[61] T. L. Henshaw, Reciprocating pumps, United States: U.S. Department of Energy, 1987.

[62] Y. H. M. &. B. S. G. Chan, "Model membrane systems and their applications," *Current opinion in chemical biology,* vol. 6, pp. 581-587, 2007.

[63] R. F. K. S. A. a. S. I. Arunthavanathan, "An analysis of process fault diagnosis methods from safety perspectives," in *Computers & Chemical Engineering*, 2020.

[64] B. B. V. &. Č. K. Souček, "Million channel pulse height analyser through pseudorandom digital transformation," *Nuclear Instruments and Methods*, vol. 66, pp. 202-212, 1968.

[65] M. L. M. B. H. P. J. M. S. B. R. C. &. H. W. G. Mendelsohn, "Digital transformation and computer analysis of microscopic images.," *Advances in optical and electron microscopy,* pp. 77-150, 1968.

[66] M. Fitzgerald, "How Starbucks Has Gone Digital," MITSloan Management Review, 2013.

[67] Liu D. et.al, "Resource Fit in Digital Transformation - Lessons Learned from The CBC Bank," *Management Decision,* vol. 49, pp. 1728-1742, 2011.

[68] e. Hess, "Options for Formulating a Digital Transformation Strategy," *MIS Quarterly Executive,* vol. 15, pp. 123-139, 2016.

[69] I. R. J. B. C. M. M. M. K. &. F. N. Sebastian, How big old companies navigate digital transformation, 2017.

[70] E. &. R. M. Hofmann, "Industry 4.0 and the current status as well as future prospects on logistics.," *Computers in Industry,* vol. 89, pp. 23-34, 2017.

[71] K. D. W. S. &. W. T. Thoben, ""“Industrie 4.0” and smart manufacturing-a review of research issues and application examples," *International Journal of Automation Technology,* vol. 11, pp. 4-16, 2017.

[72] M. &. V. J. Grieves, " In Transdisciplinary perspectives on complex system," in *Digital twin: Mitigating unpredictable, undesirable emergent behavior in complex system*, 2017, pp. 85-113.

[73] F. S. A. L. Q. Q. M. Z. B. S. Z. G. S. C.-Y. L. &. A. Y. C. N. Fei Tao, " Digital twin-driven product design framework," *International Journal of Product Research,* 2019.

[74] E. H. a. D. S. Glaessgen, "The Digital Twin Paradigm for Future NASA and US Air Force Vehicles," in *53rd Struct. Dyn. Mater. Conf. Special Session: Digital Twin*, Honolulu, HI, US, 2012.

[75] S. &. A. R. Haag, " Digital twin–Proof of concept," *Manufacturing Letters,* vol. 15, pp. 64-66, 2018.

[76] T. T. M. W. J. W. Z. F. H. L. C. &. H. G. Q. Qu, "System dynamics analysis for internet of things enabled production logistic system," *International journal of production,* vol. 55, pp. 2622-2649., 2017.

[77] D. &. L. J. Culler, "A prototype smart materials warehouse application implemented using custom mobile robots and open source vision technology," *Procedia manufacturing,* pp. 1092-1106, 2016.

[78] B. W. J. S. L. L. P. M. M. &. Y. B. Chen, "Smart factory of industry 4.0: Key technologies, application case, and challenges.," *IEEE* , vol. 6, pp. 6505-6519, 2017.

[79] L. Y. K. H. S. K. Jong Kyeom, "Estimation of probability density functions of damage parameters for valve leakage detection in reciprocating pumps in nuclear power plants," *Nuclear Engineering and Technology*, vol. 48, no. 5, 2016.

[80] N. Y. T. A. P. W. A. S. J. D. &. E. M. Yip, "High performance thin-film composite forward osmosis membrane.," *Environmental science & technology*, vol. 44, no. 10, pp. 3812-3818, 2010.

[81] A. R. Bartman, "Control and Monitoring of Reverse Osmosis Water Desalination," UNIVERSITY OF CALIFORNIA, Los Angeles, 2011.

[82] A. T. R. S. B. B. G. B. D. A. &. B. B. J. Kumar, "Time resolved fluorescence tomography of turbid media based on lifetime contrast.," *Optics express*, vol. 14, no. 25, pp. 12255-12270, 2006.

[83] W. A. R. &. A.-R. K. F. Abdulkarem, "Centrifugal pump impeller crack detection using vibration analysis," in *In 2nd International Conference on Research in Science, Engineering and Technology*, 2014.

[84] S. A. U. C. P. &. N. B. Olabisi, "Application of Reliability Techniques to Evaluate Maintainability of Centrifugal Pump used for Petroleum Product Delivery.," *Journal of Newviews in Engineering and Technology (JNET)*, vol. 2, 2020.

[85] T. p. v. e. o. t. u. a. m. h. b. s. b. A.-R. a. El-Shaikh, "Diagnosis vibration problems of pumping stations: case studies," in *International Water Technology Conference*, 2009.

[86] F. B. A. I. A. &. A. M. M. Zouari, "Observer-based adaptive neural network control for a class of MIMO uncertain nonlinear time-delay non-integer-order systems with asymmetric actuator saturation," *Neural Computing and Applications,* vol. 28, no. 1, pp. 993-1010, 2017.

[87] R. &. A. M. Nordmann, "Fault diagnosis in a centrifugal pump using active magnetic bearings," *International Journal of Rotating Machinery,* vol. 10, no. 3, pp. 183-191, 2004.

[88] C. Kallesøe, " Fault detection and isolation in centrifugal pumps," Department of Control Engineering, Aalborg University., 2005.

[89] A. &. C. F. Hernandez-Solis, "Diagnosis of submersible centrifugal pumps: a motor current and power signature approaches," *EPE Journal,* vol. 20, pp. 58-64, 2010.

[90] N. G. J.-M. F. a. O. A. Lo, "Review of machine learning approaches in fault diagnosis applied to IoT systems," in *In 2019 International Conference on Control, Automation and Diagnosis*, 2019.

[91] M. M. S. &. U. J. Sohaib, "Deep Learning for Data-Driven Predictive Maintenance. In Vision, Sensing and Analytics: Integrative Approaches," *Springer, Cham,* pp. 71-95, 2021.

[92] G. S. T. M. B. a. D. M. Bode, "Real-world application of machine-learning-based fault detection trained with experimental data," *Energy* , vol. 198, 2020.

[93] S. C. S. R. Y. L. K. Y. O. B. L. O. R. S. e. a. Liu, "Automatic early fault detection for rod pump systems," in *In SPE annual technical conference and exhibition. OnePetro*, 2011.

[94] N. U. S. S. V. A. P. S. L. Z. &. W. P. Dutta, "Centrifugal pump cavitation detection using machine learning algorithm technique," in *n 2018 IEEE International Conference on Environment and Electrical Engineering and 2018 IEEE Industrial and Commercial Power Systems Europe*, 2018.

[95] R. P. Smith, Z. Qureshi, R. J. Scaife and H. M. El-Dessouky, "Limitations of processing carbon fibre reinforced plastic/polymer material using automated fibre placement technology," *Journal of Reinforced Plastics & Composites,* vol. 35, no. 21, pp. 1527-1542, 2016.

[96] "Correlated Solutions," VIC 3D, [Online]. Available: http://correlatedsolutions.com/vic-3d/. [Accessed 21 October 2017].

[97] "TenCate," Product Data Sheet, [Online]. Available: https://www.tencatecomposites.com/product-explorer/products/ovl4/TenCate-Cetex-TC1200. [Accessed 21 October 2017].

[98] "Wolfram Language & System, Documentation Center," [Online]. Available: http://reference.wolfram.com/language/ref/Interpolation.html. [Accessed 22 October 2017].

[99] "Notepad++," [Online]. Available: https://notepad-plus-plus.org/resources.html. [Accessed 23 October 2017].

[100] D. Hillel, Salinity Management for Sustainable Irrigation, Washington DC: World Bank Publications, August 2000.

[101] G. J. a. P. Battacharya, "Drinking water from groundwater," The Swedish Research Council Formas, The Swedish Research Council Formas, 2009.

[102] M. W. S. R. Mahmoud Shatat, "Opportunities for solar water desalination worldwide: Review," *Sustainable Cities and Society,* vol. 9, pp. 67-80, 2013.

APPENDIX A

A.1 MATHEMATICAL DYNAMIC MODELING OF SPIRAL-WOUND MODULE:

Spiral wound membrane is the most common commercial used membrane in industry due to its high membrane area to volume ratio (specific surface area), and high permeation rate, and ease of operation [22]. Clean water spirals to the central collection tube through the permeate envelope while the saline water passes along the length of the module. When the feed water portion is passing through the membrane this portion become more concentrated at the end of the brine channel, which yields to an increase in the osmotic pressure. Both the feed and the permeate are transported through the module in fluid-conductive spacer material [23]. To enhance the effective velocities and reduce the void volumes spacers are placed in both brine and permeate channels [24].

- One of the most models that have been used in RO system design for the solvent and solute transport through membrane is the solute diffusion model [26].
- Reverse osmosis membrane is non-porous membrane constructed of flat channels with spacers. [membrane modeling]
- To calculate the concentration polarization, effect the thin film theory is a valid method. [membrane modeling]. The brine flows only along the axial direction the z-axis. While both velocity of the permeate along the z-axis and the perpendicular flow to the bulk flow are negligible.

- The glued area of the membrane is ignored, i.e., $w_{BR} = w_m$ and $l_{BR} = l_m$. [membrane modeling]
- $h_{sp} = h_{BR}$ as the thickness of the feed-spacer is approximated by the height of brine channel. [membrane modeling]
- It is assumed to have immediate mixing between the permeate water which is locally produced and the permeate channel bulk flow
- Pressure drops in permeate side is neglected. [membrane modeling]
- Solute concentration, velocity at brine side vary linearly in axial direction, fluid temperature and wall friction are the factors which yields to Hydraulic pressure drops. Arithmetic mean is used to average those operating variables. [membrane modeling]
- The only considered components are Na+ and Cl-, of the possible dissolved components in the feed water path. Because of that the mass concentration of total dissolved solids (TDS) in the feed path will be assumed to be the same as that of NaCl.
- The effect of feed pH is ignored on the reverse osmosis system performance.
- To calculate the thermodynamic properties for saline fluids in the binary H2O–NaCl system Driesner's correlations [27] are used.
- The saline water properties estimation, i.e., D_{NaCl} and μNaCl have been done by using the empirical equations [28, 29].

The two RO desalination system mathematical derivation models below are used to determine the system(feed) pressure and system flowrates at given actuator conditions. The models were tested, and the simulated dynamics of the digital model system are

modeled based on the use of mass and energy balances with respect to time [19_alex_bartman].

i.First Model:

The permeation of solvent through the membrane is driven by pressure (convection), and can be expressed by the following model:

$$J_w = A(\Delta P - \sigma\Delta\pi) \qquad \text{Eq. A. 1}$$

Where water permeation across the membrane depends on applied hydraulic pressure difference:

- Jw is the mass flux that passes through the membrane (water permeate flux) $[kg \cdot m2 \cdot s - 1]$.
- A is the permeability coefficient (specific for each membrane) $[kg \cdot m - 2 \cdot kPa - 1 \cdot s - 1]$.
- ΔP is the pressure difference between the two sides of the membrane $[kPa]$.
- $\Delta\pi$ is the osmotic pressure difference.

σ is the reflection coefficient, which measures the membrane selectivity (i.e., σ =0, no membrane selectivity; 0< σ <1, not completely semi permeable with solute transport; σ =1, ideal membrane without solute transport). In other words, The Staverman coefficient, σ, is a separation property of the membrane which may take values in the interval 0 ≤ ≤ 1. The closer the σ is to 1, the greater the membrane separation; consequently, σ = 0 identifies a membrane with very small solute refusal, and σ = 1 identifies a membrane with total solute refusal. [5_first_paperamr]

Initially while modeling this model, we assumed σ =1 as the reverse osmosis membrane were new and have the capability of the total solute refusal and new, this

assumption will be helpful as if the real-world data were slightly different from the simulated data that's mean the reverse osmosis membranes starts being affected and its solute refusal become lower and by applying some correlations, we can study the membrane health and predicting the membrane remaining lifetime. This correlation will be part of the future work for this research to study and predict the membrane remaining lifetime and its behavior regards the fatigue and failures that effect it.

The solute mass flux can be described as:

$$J_s = B(C_f - C_p) \qquad \text{Eq. A. 2}$$

Where:

Js is the mass flux of solute through the membrane $[kg \cdot m^2 \cdot s^{-1}]$

B is the solute permeability $[m \cdot s^{-1}]$

C_f & C_p are the concentrations of the feed and permeate solutions respectively $[kg \cdot m^3]$

The solute permeability B can be described as:

$$B = \frac{D_s K_s}{l} \qquad \text{Eq. A. 3}$$

Where:

- D_s is the diffusion coefficient for the solute in the membrane $[m^2 \cdot s^{-1}]$
- K_s is the partition coefficient of the solute
- l is the membrane thickness $[m]$

By submission both the solute flux and the solvent flux the total permeate volumetric flux can be obtained as:

$$J_p = \frac{(J_w + J_s)}{\rho_P} \qquad \text{Eq. A. 4}$$

Where: ρ_p *is the permeate density* $[kg \cdot m^3]$.

The solvent recovery and the solute rejection are two methods to monitor the performance of the reverse osmosis membrane process. The solvent recovery (*Y*) method is described as the fraction of permeate flowrate divided by feed flow rate (Eq. A.5) to shows the percentage of permeate flowrate. Where the second method called solute rejection (*R*) method is described as the fraction of salinity denied by the membrane (Eq. A.6). The solute rejection method is often labeled by the reverse osmosis membrane manufactures to define the rejection properties of the membrane. Typically, reverse osmosis membranes achieve NaCl rejections of 98–99.8% [40].

$$Y(\%) = \frac{Q_p}{Q_f} x100 \qquad \text{Eq. A. 5}$$

Q_P & Q_f are the permeate and feed volumetric flowrates respectively$[m^3 \cdot s^{-1}]$

$$R(\%) = \left(1 - \frac{C_p}{C_f}\right) \qquad \text{Eq. A. 6}$$

C_P and C_f are the permeate and feed concentrations respectively$[kg.m^{-3}]$

Sea water reverse osmosis module defining the solute concentration, specific internal energy, and solute density dynamic equations based on the energy and mass conservation laws:

$$V_{BR} \frac{d\rho_{b,t}}{dt} = Q_{f,t}\, \rho_{f,t} - Q_{r,t}\, \rho_{r,t} - Q_{p,t}\, \rho_{p,t} \qquad \text{Eq. A. 7}$$

$$V_{BR} \frac{dC_{b,t}}{dt} = Q_{f,t}\, C_{f,t} - Q_{r,t}\, C_{r,t} - Q_{p,t}\, C_{p,t} \qquad \text{Eq. A. 8}$$

$$V_{BR} \frac{d\rho_{b,t}\, \widehat{U}_{b,t}}{dt} = Q_{f,t}\, \rho_{f,t}\, \hat{h}_{f,t} - Q_{r,t}\, \rho_{r,t} \hat{h}_{r,t} - Q_{p,t}\, \rho_{p,t} \hat{h}_{p,t} \qquad \text{Eq. A. 9}$$

$$V_{BR} = n_1\, w_{BR}\, h_{BR} l_{BR} \emptyset_{BR} \qquad \text{Eq. A. 10}$$

Equations (11) and (12) express the axial velocities to the volumetric flowrates at brine side as follow:

$$V_{zf,t} = \frac{Q_{f,t}}{n_1 \, w_{BR} \, h_{BR} \emptyset_{BR}} \quad at \; z = 0 \qquad \text{Eq. A. 11}$$

$$V_{zr,t} = \frac{Q_{r,t}}{n_1 \, w_{BR} \, h_{BR} \emptyset_{BR}} \quad at \; z = l_{BR} \qquad \text{Eq. A. 12}$$

(Q_p) The volumetric flow rate of the permeate water depends on the local solvent flux (J_{vz}): $Q_p = 2 \, n_1 w_{BR} \int_0^{lbr} J_{vz} dz$ According to the classical solution-diffusion model, the average solvent flux (Q_p) and solute flux of species i (Eq. A.13, Eq. A.13.1) through the membrane are given as follows [22, 25, 30].

$$\bar{J}_V = L_v \left(\Delta p - \sum_i \Delta \pi \right) \qquad at \; z = \frac{l_{BR}}{2}, \forall i \in \{Na^+, Cl^-\} \qquad \text{Eq. A. 13}$$

$$\bar{J}_V = (Permeate \; flow \; rate / membrane \; area) = \frac{Qp}{A_{mem}} \qquad \text{Eq. A. 13.1}$$

$$\bar{J}_{s,i} = \bar{J}_V \frac{C_{p,i}}{MW_i} = L_{s,i} \left(\frac{C_{m,i} - C_{p,i}}{MW_i} \right) \quad at \; z = \frac{l_{BR}}{2}, \forall i \in \{Na^+, Cl^-\} \qquad \text{Eq. A. 13.2}$$

Eq. A. 15 shows the relationship between both the average solute and solvent fluxes.

Subject to

$$L_v = L_{v0}\, exp\, \left[\frac{\alpha_1(T_b-293)}{293} - \alpha_2 p_f\right] \left(1 - \frac{A_s}{A_m}\right) \quad \text{Eq. A. 14}$$

$$L_{s,i} = L_{s0,i}\, exp\, \left[\frac{\beta_1(T_b - 293)}{293}\right], \forall i \in \{Na^+, Cl^-\} \quad \text{Eq. A. 15}$$

$$\Delta p = P_f - P_p - \frac{\Delta P_{Hydro}}{2} \quad at\ z = \frac{l_{BR}}{2} \quad \text{Eq. A. 15}$$

$$\Delta \pi_i = \left(\frac{\bar{c}_{m,i} - \bar{c}_{p,i}}{MW_i}\right) RT, \forall i \in \{Na^+, Cl^-\} \quad \text{Eq. A. 16}$$

Where: R is ideal gas constant, T is the temperature.

- Eq. A. 17 (Δp) applied hydraulic pressure difference.
- $(\sum \Delta \pi i)$ the sum of the osmotic pressures difference of dissolved solids in NaCl aqueous solution.
- $\Delta phydr$ is the Hydraulic pressure loss along a spiral wound element due to wall friction. Shown in Eq. A.16, is summarized below [31].

  Eq. A13.2 shows Δp is proportional to the solute transport across the membrane regarding to that to get purer permeate water the higher Δp should be applied. Also, there is a direct proportional between osmotic pressure and the solute concentration [33-35]. The phenomenon of concentration polarization builds a high osmotic pressure difference across the membrane. resulting in the difference between the solute concentration in the bulk phase and at the membrane surface. According to Fick's law for diffusion and the thin-film theory, the concentration at the membrane surface can be defined as follows [36-39].

$$\frac{C_m - C_p}{C_b - C_p} = \exp\left(\frac{J_v}{K_{NaCl}}\right) \quad \text{Eq. A. 18}$$

Hydraulic pressure loss along a spiral-wound element:

Due to wall friction along the spiral-wound element there is a hydraulic pressure drop and can be described as:

$$\Delta p_{\text{hydro}} = \frac{\lambda^* \rho_b^* v_{zb}^2}{2\, d_h} \quad \text{Eq. A. 24}$$

$$\lambda = 6.23\ \text{Re}_b^{-0.3} \quad \text{Eq. A. 25}$$

$$\text{Re}_b = \frac{\rho_b\ v_{zb}\ d_h}{\mu_{NaCl}} \quad \text{Eq. A. 26}$$

$$v_{zb} = \frac{v_{zf} + v_{zr}}{2} \quad \text{Eq. A. 27}$$

From Eq A.13.1 to A.14.1:

$$\bar{J}_V = L_v\,(\Delta p - \textstyle\sum_i \Delta\pi) \ \ \& since\ \bar{J}_V = \frac{Qp}{A_{mem}}$$

$$so\ \frac{Qp}{A_{mem}} = L_v \left(\Delta p - \sum_i \Delta\pi\right) \quad \text{Eq. A. 28}$$

Substitute from Eq. A. 19 to Eq. A. 20:

$$\frac{Qp}{A_{mem}} = L_v \left(P_f - P_p - \frac{\Delta P_{Hydro}}{2} - \sum_i \Delta\pi\right) \quad \text{Eq. A. 29}$$

Multiply by 'A_{mem}' for both sides in equation Eq. A. 21:

$$Qp = A_{mem} * L_v * P_f - A_{mem} * L_v * P_p - A_{mem} * L_v * (\Delta \text{P}_{\text{hydro}/2}) - A_{mem} * L_v{}^*\Delta\pi \quad \text{Eq. A. 30}$$

Assume the permeate pressure is equal to zero to simplify the equation for now:

$$Qp = A_{mem} * L_v * Pf - A_{mem} * L_v * (\Delta \text{P}_{\text{hydro}/2}) - A_{mem} * L_v{}^*\Delta\pi$$

$$vf = \frac{Qf}{n_l\, w_b\, h_b \emptyset_b} \qquad vr = \frac{Qr}{n_l\, w_b\, h_b \emptyset_b}$$

By substitution Eq. A. 22 into equation Eq. A. 23: Eq. A. 31

$$Q_f = Q_r + Q_p \quad \text{Eq. A. 32}$$

Q_f is the feed flowrate, Q_r is the brine flowrate and Q_p is the permeate flowrate. Eq. A. 33

$$Q_p = Q_r + Q_f * recovery$$

$$Q_f = Q_r + Q_f * Y$$

$$\text{So } Q_r = Q_f(1 - Y)$$

From Eq. 34 to 30 Eq. A. 34

$$vr = \frac{Q_f(1-Y)}{n_l\, w_b\, h_b \emptyset_b} \quad \text{Eq. A. 35}$$

Then from Eq. 29 & 35 into 24: Eq. A. 36

$$v_{zb} = \left(\frac{\left(\frac{Qf}{n_l\, w_b\, h_b \emptyset_b}\right)}{2} - \frac{\left(\frac{Q_f(1-Y)}{n_l\, w_b\, h_b \emptyset_b}\right)}{2} \right) = \left(\frac{(2 - rec) * Qf}{2\, n_l\, w_b\, h_b \emptyset_b} \right)$$

$from\ Eq.37\ into\ 21$: Eq. A. 37

$$\Delta p_{\text{hydro}} = \frac{\lambda * \rho_b}{2\, d_h} * \left[\frac{(2 - rec) * Qf}{2\, n_l\, w_b\, h_b \emptyset_b}\right]^2$$

From Eq.38 into 28: Eq. A. 38

$$A_{mem} * L_v * P_f = Qp + 0.5 * A_{mem} * L_v * \frac{\lambda * \rho_b}{2\, d_h} * \left[\frac{(2 - rec) * Qf}{2\, n_l\, w_b\, h_b \emptyset_b}\right]^2$$

$$+ A_{mem} * L_v * \Delta\pi$$

Eq. A. 39

$$P_f = (Qp + 0.5 * A_{mem} * L_v * \frac{\lambda * \rho_b}{2\, d_h} * \left[\frac{(2 - rec) * Qf}{2\, n_l\, w_b\, h_b \emptyset_b}\right]^2 + A_{mem} * L_v * \Delta\pi)$$

$$/A_{mem} * L_v$$

Eq. A. 40